NUMERICAL MODELING OF AN UNCONFINED AQUIFER DEWATERING AND A SOIL VAPOR EXTRACTION SYSTEM: A CASE STUDY

by

Emin Çiftçi

B.S., in C.E., Boğaziçi University, 2004

Submitted to the Institute for Graduate Studies in
Science and Engineering in partial fulfillment of
the requirements for the degree of
Master of Science

Graduate Program in Civil Engineering

Boğaziçi University

2006

NUMERICAL MODELING OF AN UNCONFINED AQUIFER DEWATERING AND A SOIL VAPOR EXTRACTION SYSTEM: A CASE STUDY

APPROVED BY:

Prof. Cem Avcı (Thesis Supervisor)	.....
Assoc. Prof. Osman Börekçi	.....
Assoc. Prof. Nadim Copty	.....

DATE OF APPROVAL: 15.09.2006

ACKNOWLEDGEMENTS

I would like to express my sincere gratitude to my thesis supervisor, Dr. Cem Avcı for his guidance, support and encouragement throughout the preparation of this thesis.

I would also like to thank Dr. Osman Börekçi and Dr. Nadim Copty for their valuable advises for this study.

I am also thankful to my friends, Ufuk Şahin, Yavuz Tokmak, Bilge Alıcıoğlu and Cenk Güngör for their generous help.

I am grateful to my parents and my dear sister Zeynep for the endless support they have given me throughout my life and I would like to express my gratefulness to my dear wife, Seda, without whom probably I would have never done this work.

ABSTRACT

NUMERICAL MODELING OF AN UNCONFINED AQUIFER DEWATERING AND A SOIL VAPOR EXTRACTION SYSTEM: A CASE STUDY

Contamination of soil and groundwater with volatile organic compounds has become a serious environmental issue. Soil vapor extraction (SVE) can be considered as one of the most commonly utilized techniques to remove these organic compounds from the soil. A soil vapor extraction system operates on the basis two main processes; volatilization of the residual organic compounds and transport of the organic vapor in the unsaturated zone. In this study a numerical model is developed for simulating soil vapor extraction process and the developed model is implemented for a case study. A gasoline station site, contaminated with four different volatile organic compounds, is the subject of the case study. Another dimension of this case study is the ongoing metro tunnel construction work executed underneath that gas station. The construction work is being executed at a level below groundwater table, therefore, due to leakage through tunnel walls the groundwater table is expected to drop with time. The impact of tunnels on the groundwater table is investigated in this work.

The transient groundwater flow equation, derived by combining continuity equation with Darcy's approach, is utilized while unconfined aquifer dewatering is being modeled. The developed numerical model for soil vapor extraction is based on solving vapor flow and advective-diffusive vapor transport equations successively. For both models, finite difference techniques are implemented.

The aquifer dewatering simulation, performed over a four-month period, indicates that, at some locations the groundwater table drops to the level of the tunnels. With the soil vapor extraction simulation 5% of the organic mass is found to be removed from the soil after an extraction period of one month.

ÖZET

SERBEST YÜZEYLİ BİR AKİFERDE YERALTI SU YÜZEYİ ALÇALMASININ VE BİR TOPRAK BUHARI EKSTRAKSİYON SİSTEMİNİN SAYISAL OLARAK MODELLENMESİ: ÖRNEK İNCELEME

Toprak ve yeraltı suyunun uçucu organik bileşikler tarafından kirletilmesi önemli bir çevre sorunu haline gelmiştir. Toprak buharı ekstraksiyonu, bu bileşikleri topraktan temizlemek için sıklıkla uygulanan yöntemlerden biridir. Toprak buharı ekstraksiyon sisteminin işleyişi, artık organik bileşiklerin buharlaşması ve organik buharın toprağın doymamış bölümündeki taşınımı esaslarına dayanır. Bu çalışmada, bir toprak buharı ektraksyon sistemi sayısal olarak modellenmiş ve geliştirilen model örnek bir olay için uygulanmıştır. İncelenen olay dört farklı organik bileşik tarafından kirletilmiş olan bir benzin istasyon sahasında gerçekleşmektedir. Bu örnek inceleme ile ilgili başka bir boyut ise, benzin istasyonun altında yürütülmekte olan metro tüneli yapım çalışmasıdır. Bu çalışma yeraltı su yüzeyinden daha alçak bir seviyede yürütülmektedir, bu nedenle yeraltı su yüzeyinde, tünele olacak sızıntıdan kaynaklanan bir alçalma beklenmektedir. Tünellerin yeraltı su yüzeyine olan etkisi bu çalışmada incelenmektedir.

Serbest yüzeyli akiferdeki su seviyesi düşüşü modellenirken, süreklilik denkleminin Darcy kanunu ile birleştirilmeyle elde edilen zamana bağlı yeraltı suyu akım denkleminden yararlanılmaktadır. Geliştirilen buhar ekstraksiyon modeli ise, gaz akımı ve adveksiyonel-difüzyonel gaz taşınımı denklemlerinin arka arkaya çözülmesi esasına dayanmaktadır. Her iki sayısal model için de sonlu farklar yöntemi kullanılmaktadır.

Dört aylık bir zaman dilimi için gerçekleştirilen yeraltı su yüzeyi alçalması simülasyonu, su yüzeyinin bazı noktalarda tünel seviyesine kadar alçaldığını göstermektedir. Toprak buharı ekstraksiyonu simülasyonu ile, bir aylık ekstraksiyon süresi sonunda topraktaki uçucu organik bileşiklerin %5'nin temizlendiği sonucuna ulaşılmaktadır.

TABLE OF CONTENTS

LIST OF FIGURES

LIST OF TABLES

LIST OF SYMBOLS/ABBREVIATIONS

A_1, A_2, A_3	Antoine's vapor pressure constants
B	Initial saturated thickness of an unconfined aquifer
C	Concentration of the organic compound in the gas phase
C_{eq}	Equilibrium vapor concentration
$C^n_{eq_{i,j,k}}$	Equilibrium vapor concentration at the cell *i, j, k* at time step *n*
$C^n_{i,j,k}$	Concentration of the gas at the cell *i, j, k* at time step *n*
C_l	Concentration of the organic compound in the liquid phase
D_{eff}	Effective diffusion coefficient
D_m	Diffusion coefficient
D_{xx}	Dispersion coefficient in *x*-direction
$D^n_{xx_{i,j,m}}$	Dispersion coefficient in *x*-direction at the cell *i, j, k* at time step *n*
D_{yy}	Dispersion coefficient in *y*-direction
$D^n_{yy_{i,j,m}}$	Dispersion coefficient in *y*-direction at the cell *i, j, k* at time step *n*
D_{zz}	Dispersion coefficient in *z*-direction
$D^n_{zz_{i,j,m}}$	Dispersion coefficient in *z*-direction at the cell *i, j, k* at time step *n*
$d_{i,j,k}$	Depth of the finite difference cell with the index *i*, *j*, *k*
H	Vertical thickness of the domain
H_t	The depth of the tunnel below groundwater table
h	Hydraulic head
h_g	Thickness of the grouted zone
$h^n_{i,j,k}$	Hydraulic head at the cell *i, j, k* at time step *n*
J_x	The mass flux in *x*-direction
K	Hydraulic conductivity
K_0	Zero order modified Bessel function of the second kind
K_1	First order modified Bessel function of the second kind

K_d	Distribution coefficient
K_{eq}	Equivalent hydraulic conductivity
K_H	Henry's law constant
$K_L a$	Overall mass transfer coefficient in free atmosphere
K_{xx}	Hydraulic conductivity in *x*-direction
$K_{xx_{i,j,k}}$	Hydraulic conductivity in *x*-direction at the cell *i, j, k*
K_{yy}	Hydraulic conductivity in *y*-direction
$K_{yy_{i,j,k}}$	Hydraulic conductivity in *y*-direction at the cell *i, j, k*
K_{zz}	Hydraulic conductivity in *z*-direction
$K_{zz_{i,j,k}}$	Hydraulic conductivity in *z*-direction at the cell *i, j, k*
k	Intrinsic permeability
k^*	Relative permeability
k_h	Horizontal air permeability
$k^{*n}_{i,j,k}$	Relative permeability at the cell *i, j, k* at time step *n*
k_v	Vertical air permeability
k_{xx}	Intrinsic permeability in *x*-direction
$k_{xx_{i,j,k}}$	Intrinsic permeability in *x*-direction at the cell *i, j, k*
k_{yy}	Intrinsic permeability in *y*-direction
$k_{yy_{i,j,k}}$	Intrinsic permeability in *y*-direction at the cell *i, j, k*
k_{zz}	Intrinsic permeability in *z*-direction
$k_{zz_{i,j,k}}$	Intrinsic permeability in *z*-direction at the cell *i, j, k*
l_b	The depth from ground surface to the bottom of the well screen
$l_{i,j,k}$	Length of the finite difference cell with the index *i*, *j*, *k*
l_t	The depth from ground surface to the top of the well screen
M	Molecular weight
m	Mass of the point source
$m^n_{l_{i,j,k}}$	Mass of the residual organic liquid at the cell *i, j, k* at time step *n*

P	Pressure
$P^n_{i,j,k}$	Pressure at the cell *i, j, k* at time step *n*
P_o	Vapor pressure of the pure liquid
P_v	Vapor pressure of the liquid
Q_{leak}	Leakage rate through tunnel walls
Q_m	Constant mass flow rate due to extraction
q_x	Specific discharge in *x*-direction
$q^n_{x_{i,j,k}}$	Specific discharge in *x*-direction at the cell *i, j, k* at time step *n*
q_y	Specific discharge in *y*-direction
$q^n_{y_{i,j,k}}$	Specific discharge in *y*-direction at the cell *i, j, k* at time step *n*
q_z	Specific discharge in *z*-direction
$q^n_{z_{i,j,k}}$	Specific discharge in *z*-direction at the cell *i, j, k* at time step *n*
qc	The source flow due to the volatilization of organic compounds
$qc^n_{i,j,k}$	The source flow due to the volatilization at the cell *i, j, k* at time step *n*
R	Universal gas constant
r	Radial distance from the well
r_t	Equivalent tunnel radius
r_w	Radius of the extraction well
S	Storativity of the aquifer
S_s	Specific storage of the aquifer
S_y	Specific yield of the aquifer
s_c	Drawdown for a confined aquifer
s_u	Drawdown for an unconfined aquifer
T	System temperature
T_r	Transmissivity of the aquifer
t	Time
Δt	Time interval
v_x	Actual velocity in *x*-direction

$v^n_{x_{i,j,k}}$	Actual velocity in *x*-direction at the cell *i, j, k* at time step *n*
v_y	Actual velocity in *y*-direction
$v^n_{y_{i,j,k}}$	Actual velocity in *y*-direction at the cell *i, j, k* at time step *n*
v_z	Actual velocity in *z*-direction
$v^n_{z_{i,j,k}}$	Actual velocity in *z*-direction at the cell *i, j, k* at time step *n*
W	A source or a sink component for the fluid flow
$W^n_{i,j,k}$	A source or a sink at the cell *i, j, k* at time step *n*
$w_{i,j,k}$	Width of the finite difference cell with the index *i*, *j*, *k*
x, y, z	Cartesian coordinates
Δx	The spacing between the centers of two adjacent cells in *x*-direction
x_i	Molar fraction of the organic constituent
Δy	The spacing between the centers of two adjacent cells in *y*-direction
Δz	The spacing between the centers of two adjacent cells in *z*-direction
α	Overall mass transfer coefficient in porous medium
α_L	Longitudinal dispersivity
α_{TH}	Horizontal transverse dispersivity
α_{TV}	Vertical transverse dispersivity
β_l	Shape factor
λ	Pore size distribution
μ	Dynamic viscosity of the fluid
θ	Total porosity
θ_e	Effecive liquid saturation
θ_g	Gas-filled porosity
$\theta^n_{g_{i,j,k}}$	Gas-filled porosity at the cell *i, j, k* at time step *n*
θ_l	Liquid-filled porosity
θ_r	Irreducable moisture content
ρ	Density of the fluid

ρ_b	Bulk density of the soil
τ	Tortuosity
ω	Successive over relaxation parameter
ψ	Capacity factor

AME	Absolute mean error
bgs	Below ground surface
DMW	Deep monitoring well
E	East
GW	Groundwater
MW	Monitoring well
N	North
NATM	New Austrian tunneling method
RMSE	Root mean square error
S	South
SOR	Successive over relaxation
SVE	Soil vapor extraction
VOCs	Volatile organic compounds
W	West

1. INTRODUCTION

1.1. The Objectives of this Study

Contamination of soil and groundwater with volatile organic compounds (VOCs) has become a major environmental problem. The cause of this problem is usually due to leakages from underground storage tanks or accidental surface disposals. Immediately after the spill, the liquid begins to move through the unsaturated zone. A portion of this liquid may reach the groundwater table, while the remaining portion becomes trapped in the soil matrix. The amount of organic liquid retained in the unsaturated portion of the soil is defined as residual liquid.

The organic vapor produced as a result of volatilization of this residual liquid migrates both in the lateral and vertical directions in the vadose zone and leads to the contamination of soil moisture. During recharge events or seasonal groundwater movements, this contaminated soil moisture can reach the groundwater system. Therefore residual organic liquids act as a long term source for groundwater contamination. Taking this fact into consideration, it is quite important to take actions in order to remove VOCs from the vadose zone for protecting the groundwater.

Soil vapor extraction (SVE) is one of the most commonly utilized methods for the remediation of contaminated soils. The working principle of a soil vapor extraction system is based on the volatilization and the transport of the organic vapors in the unsaturated zone, which can be represented mathematically by a series of equations. The objective of this study is to develop a numerical model for simulating the soil vapor extraction process and to apply this method to a case study which involves a spill from a gasoline station, in Istanbul, Turkey. Another dimension of this case study is the ongoing metro tunnel construction process executed underneath the gas station mentioned above. The impact of the tunnels on the groundwater table is as well investigated in this study.

1.2. Problem Definition

An oil spill accident occurred when a gasoline station in Istanbul was seriously damaged by the Marmara earthquake, in 1999. Recently conducted investigations indicated that residual organic contaminants were present in the unsaturated portion of the soil around the station.

In order to conduct hydrogeological site investigations and to perform soil vapor extraction, monitoring and extraction wells have been installed around the gas station. At the same time the tunnels are being constructed underneath the gas station. Figure 1.1 shows the location of the gasoline station and the operating wells.

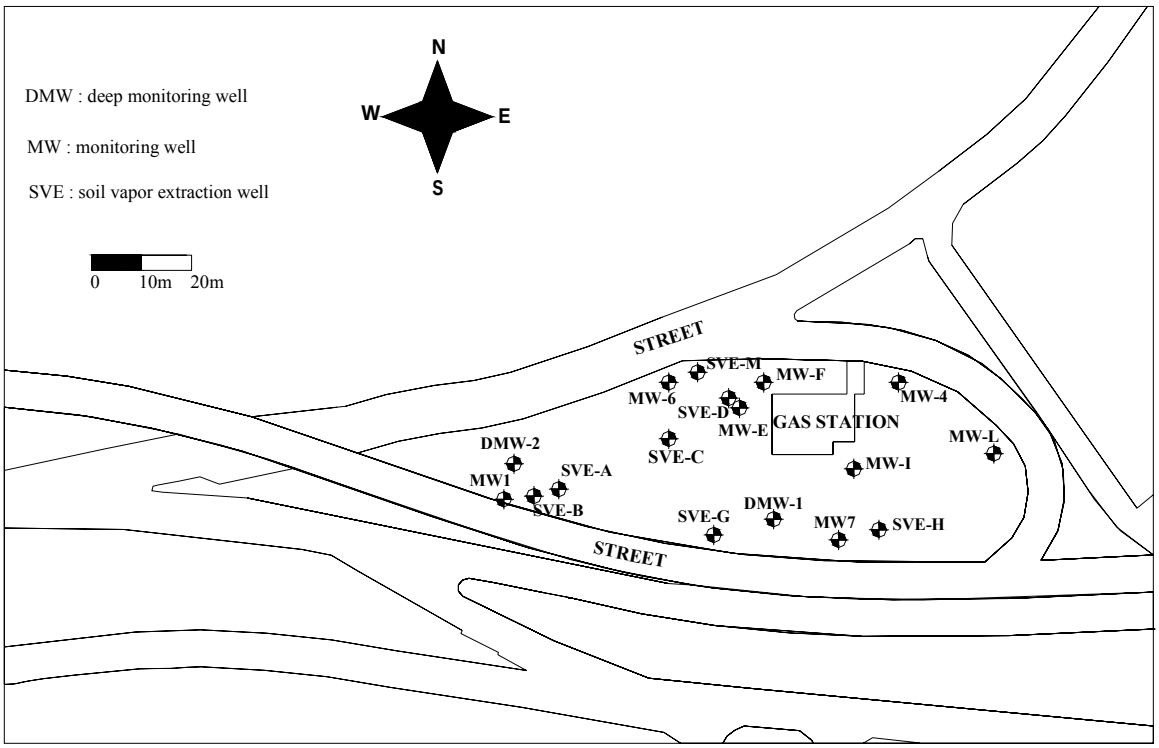

Figure 1.1 Location of the gasoline station and the operating wells

The three-dimensional view of the site, illustrating the wells, groundwater table and the tunnels, is presented in Figure 1.2.

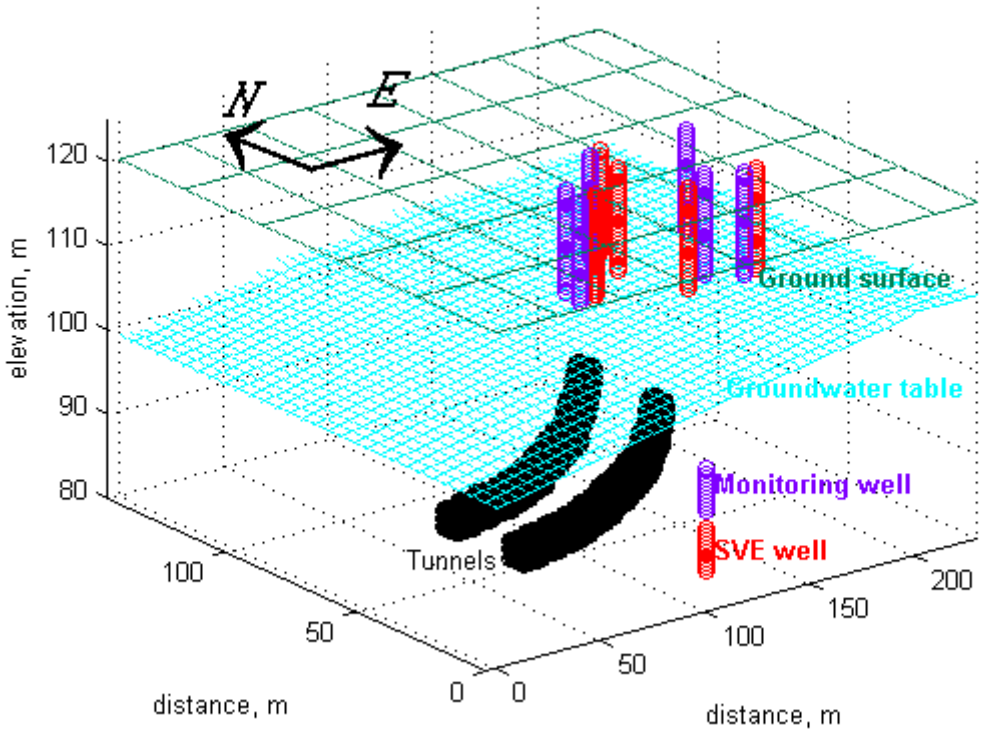

Figure 1.2. The 3D illustration of the site

1.2.1. Geology

Based on the soil investigations, the geology of the site is found to be characterized by three different formations, namely; fill material, weathered greywacke and fractured greywacke.

The main component of the fill material is highly plastic silty clay, which has a very low permeability. The thickness of this layer was observed to vary between 2 and 4 meters.

The fill material is underlain by the Trakya Formation which is carboniferous aged greywacke. The portion of the formation closer to ground surface is highly weathered with some clay content. The thickness of the weathered greywacke varies between 1-2 m to 7-8 m from East to West. According to a pumping test conducted in January 2002, the hydraulic conductivity of the weathered section is about 1.24×10^{-6} m/s.

The deepest geological unit of the site is the fractured section of the greywacke. As depth increases, the greywacke is observed to be less fractured and permeable. According to packer test results, the hydraulic conductivity of this section is found to be $3\times10^{-7}\,\mathrm{m/s}$ at 10 m below ground surface while it decreases to $3\times10^{-8}\,\mathrm{m/s}$ at 22 m below ground surface. The well logs obtained according to the collected samples are provided in Figure 1.3.

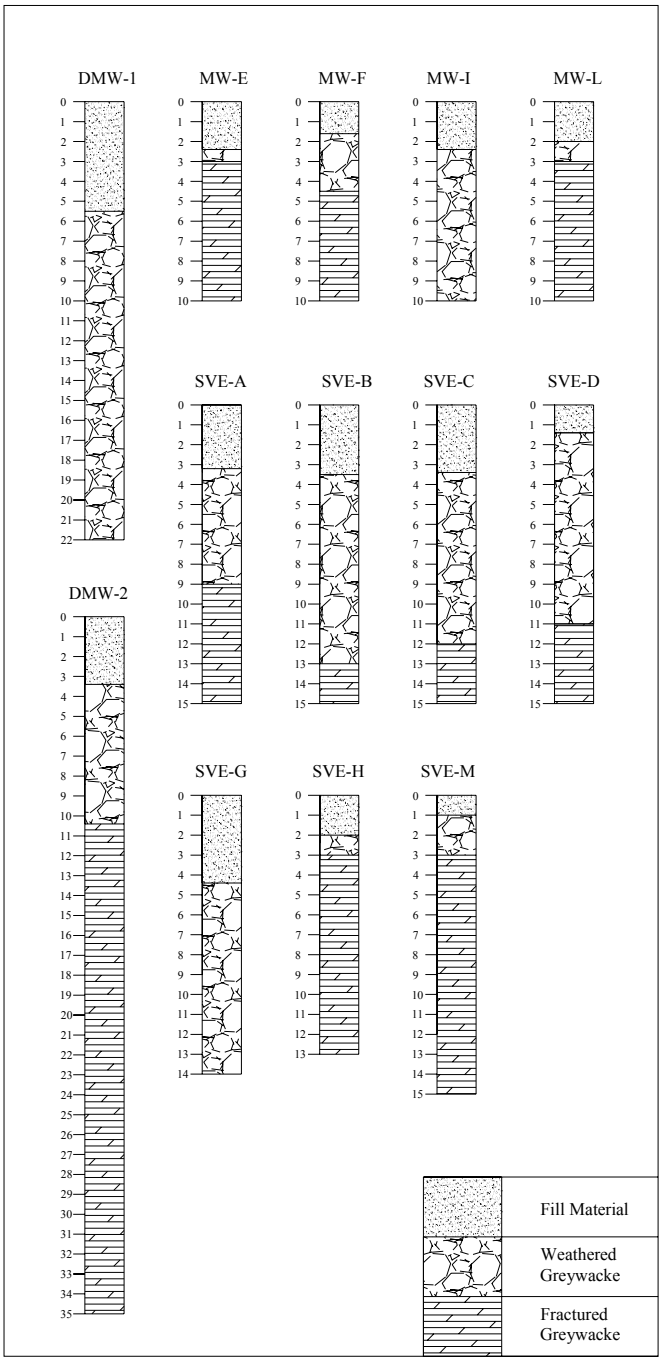

Figure 1.3. The well logs from the site

1.2.2. Groundwater Conditions

The depth to the groundwater table varies between 10m and 20m below ground surface, which corresponds to 100m and 110m, respectively, above sea level. The dominant factor affecting the direction of the flow is the topography of the land surface. The direction of the flow is monitored to be from East to West. According to the measurements acquired from pumping tests performed in January 2002, the aquifer behaves like an unconfined aquifer. Its conductivity decreases with depth. Calculated storativity values vary between 6.6×10^{-3} and 9.2×10^{-3} with a mean of 7.8×10^{-3}.

North-West portion of the site is observed to be a no-flow region due to the existence of an impervious geological formation.

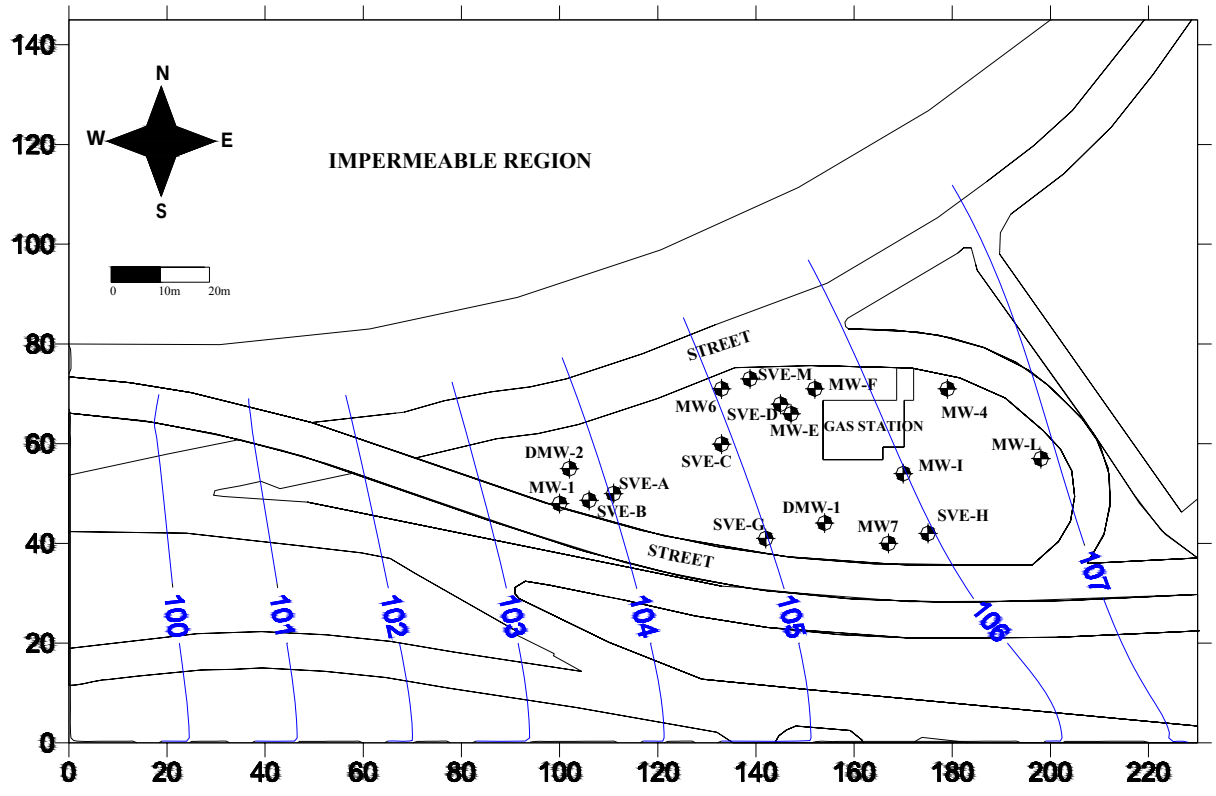

Figure 1.4. Contour of equipotential lines for the groundwater flow

1.2.3. Soil Contamination

According to data from tested soil samples, the gas station site is found to be contaminated with four different volatile organic compounds. These detected organic compounds, which are benzene, toulene, ethylbenzene and xylene, exist in the form of residual non-aqueous phase liquids (NAPL). The residual xylene concentration is measured to be the highest among these VOCs. The concentration of each residual component changes with depth. The plots which illustrate the concentration distribution of each volatile organic compound at 5 m below ground surface are presented in Figure 1.5 through.Figure 1.8.

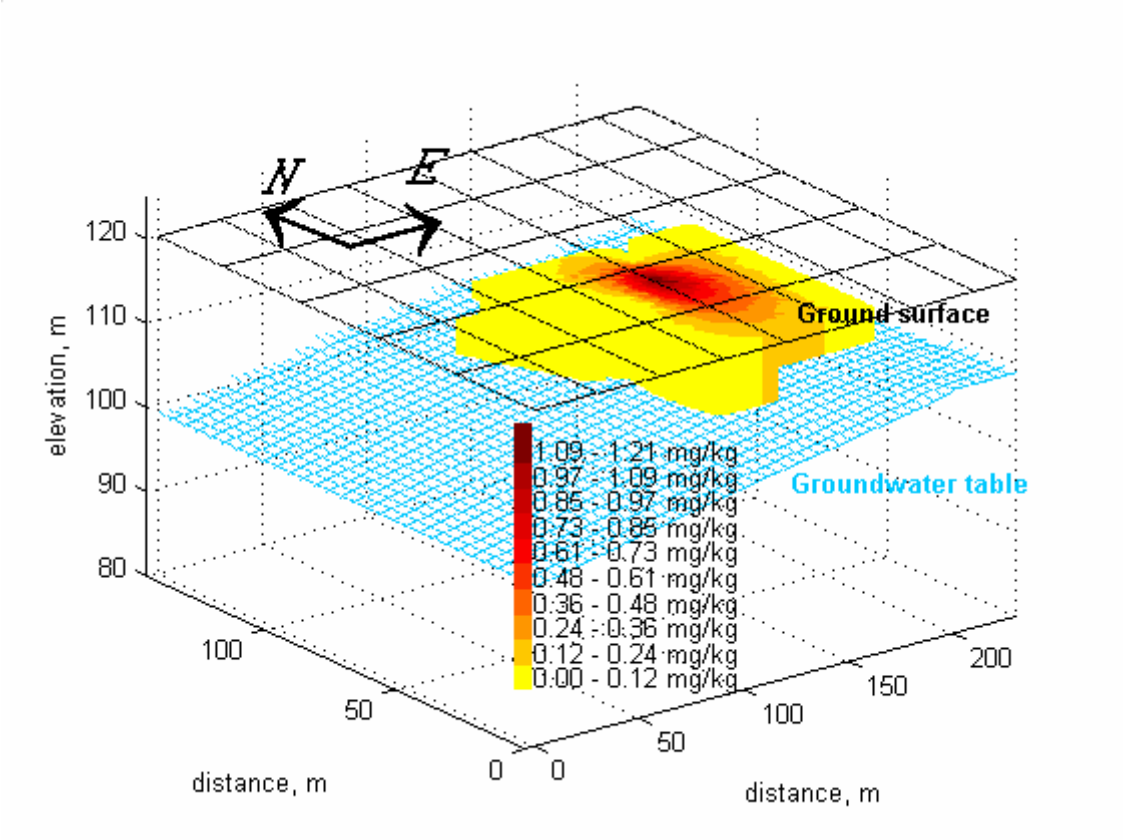

Figure 1.5. Residual benzene concentration in the vadose zone

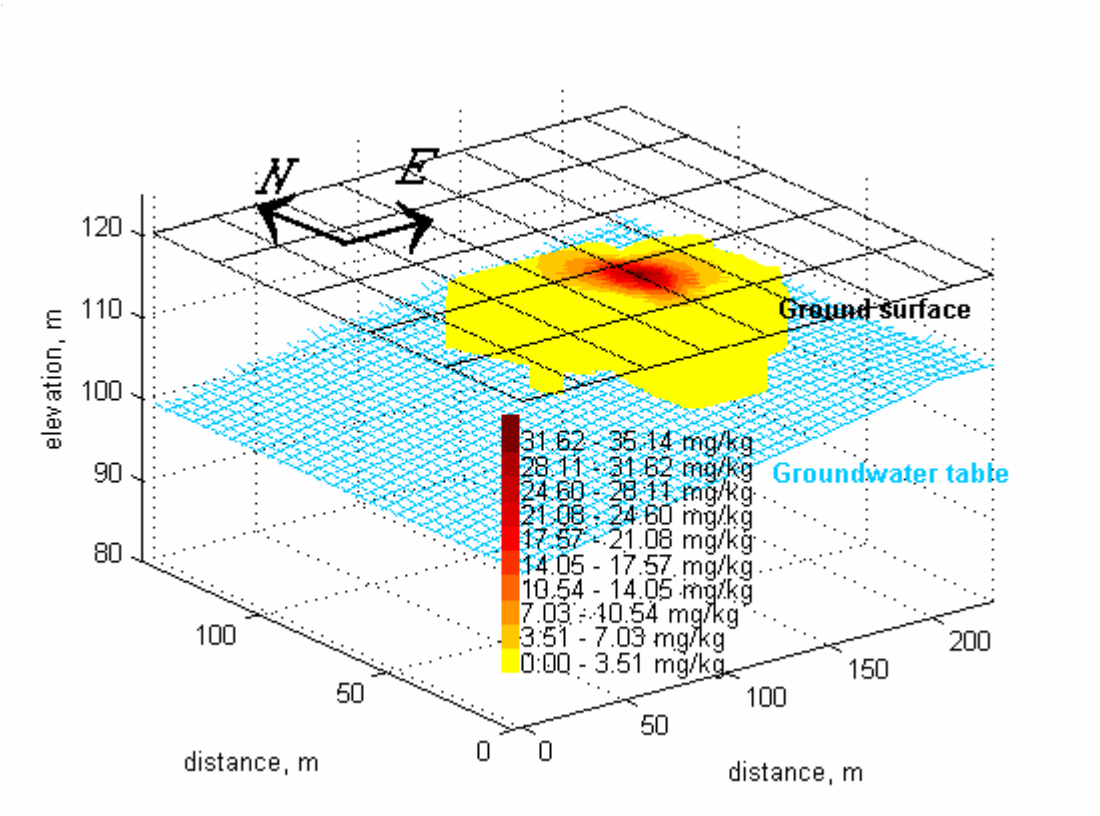

Figure 1.6. Residual toulene concentration in the vadose zone

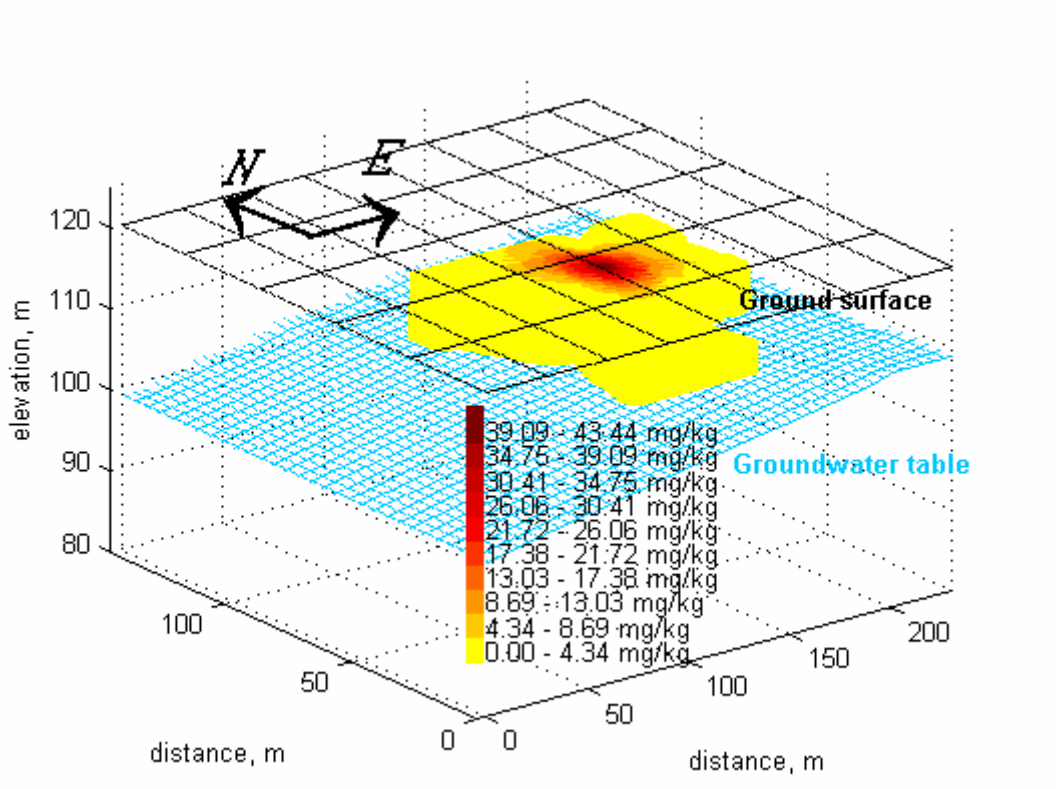

Figure 1.7. Residual ethylbenzene concentration in the vadose zone

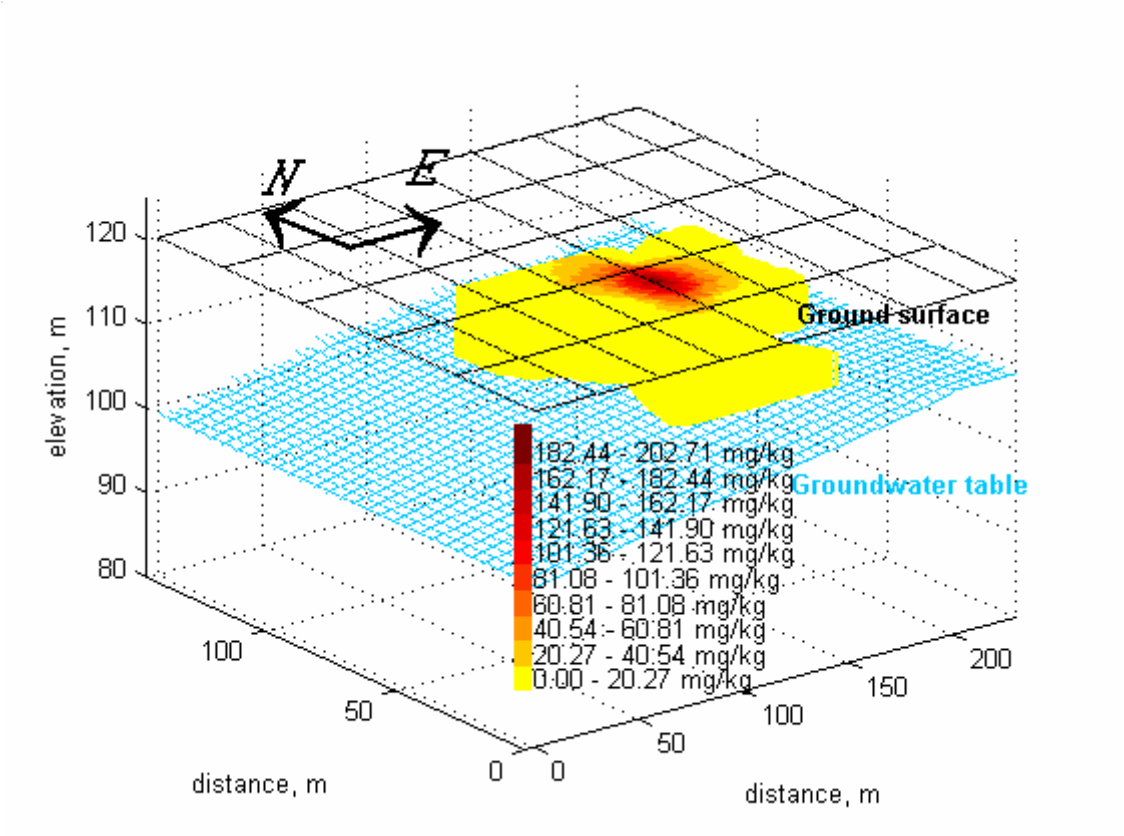

Figure 1.8. Residual xylene concentration in the vadose zone

1.2.4. Metro Tunnel Construction

Construction work of two metro tunnels is being executed, underneath the gas station site. The construction work is expected to have significant influence on the hydrogeology of the region, basically due to the fact that the tunnels under construction lie below the groundwater table. Hence, it is highly probable that dewatering of groundwater will take place on account of seepage through tunnel walls.

These two tunnels are located 18 m apart from each other; each one being constructed at a level between 34 m and 28 m below ground surface Construction work is executed by means of New Austrian Tunneling method (NATM) in which the processes of shot-crete and deployment of rock bolts are applied in order to stabilize the overburden.

As displayed in Figure 1.9, the portion of the tunnels passing underneath the gas station site is estimated to be completed in four months. In the first two months, the South tunnel is going to be constructed, to be followed by the construction of the North tunnel soon afterwards.

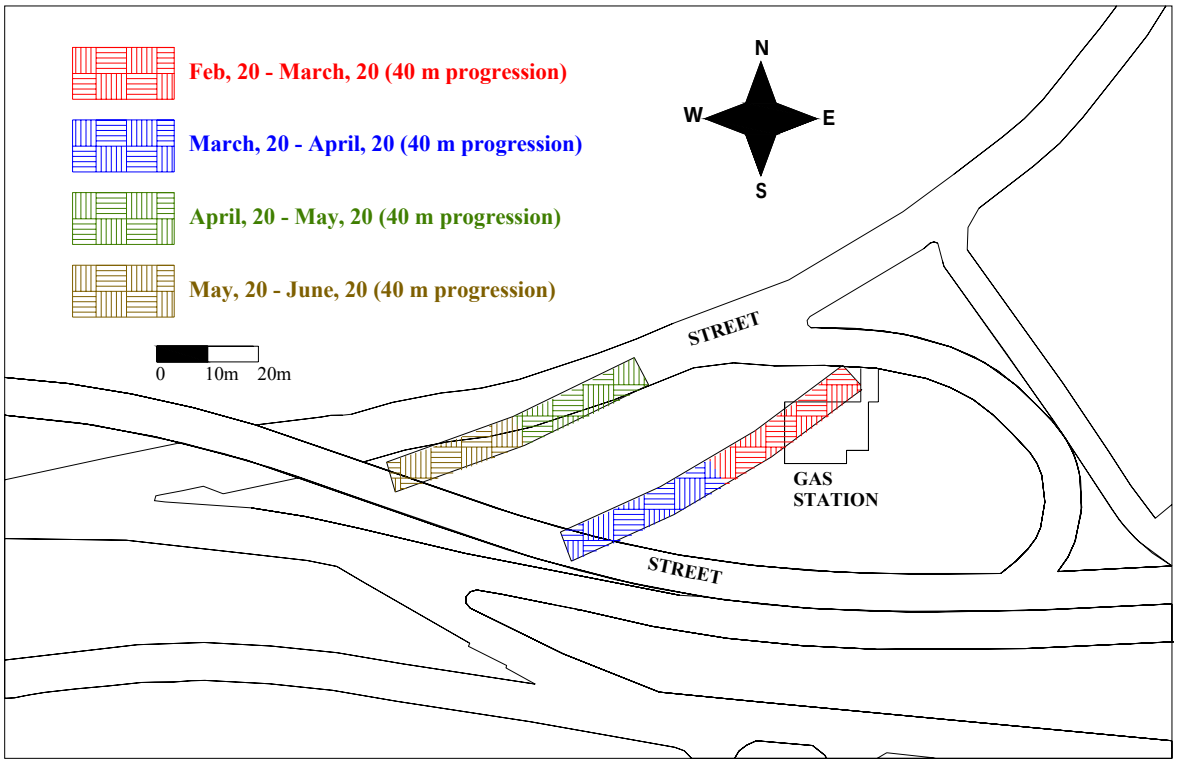

Figure 1.9. The time schedule for the tunnel construction work underneath the gas station site

2. LITERATURE REVIEW

2.1. Unconfined Groundwater Flow

The first significant contribution to the research on unconfined flow phenomenon was made by Dupuit (1863). This approximation is based on the assumption that the vertical component of the unconfined flow is negligible so that the two dimensional flow is reduced to a one dimensional problem. It is possible to obtain reasonable results with this technique on condition that the flow is shallow, the slope of the free surface is small and the aquifer is homogeneous. Steady state one dimensional unconfined flow in horizontal *x*-direction under the Dupuit assumptions can be represented by the expression given in Eq.(2.1)

$$\frac{K}{2}\frac{d^2h^2}{dx^2} + W = 0 \tag{2.1}$$

where h is the hydraulic head, K is the hydraulic conductivity and W represents the recharge component. This expression can be expanded by introducing the horizontal *y*-component of the flow, as:

$$\frac{K}{2}\left(\frac{\partial^2 h^2}{\partial x^2} + \frac{\partial^2 h^2}{\partial y^2}\right) + W = 0 \tag{2.2}$$

Theis (1935) developed an expression for unsteady-state confined flow to a pumping well. With this equation, given in Eq.(2.3), time and storativity parameters began to be used in groundwater problems.

$$s_c(r,t) = \frac{Q}{4\pi T_r}\int_u^\infty \frac{e^{-u}}{u}\,du \tag{2.3}$$

due to the equation above, Q is the pumping rate, T_r is the transmissivity of the confined aquifer, r is the radial distance from the well, t is the time parameter and u is defined as:

$$u = \frac{r^2 S}{4T_r t} \tag{2.4}$$

where S is the storativity of the aquifer.

The Theis solution is based on the assumption that all of the pumped water comes from the storage due to the compression of soil matrix and expansion of water. However for unconfined aquifers, as the groundwater level drops around the well, slow gravity drainage becomes the dominant factor responsible for the release of water. Therefore for unconfined aquifers direct application of Theis Solution may be misleading. Jacob(1950) showed that, when the drawdown in an unconfined aquifer is very small compared to the saturated thickness of the aquifer, the Theis solution can be utilized by replacing the storativity term with the specific yield of the unconfined aquifer. A corrective operation is required when the maximum drawdown is larger than 5% of the original saturated thickness. The response of an unconfined aquifer to pumping can be estimated by utilizing this approach as;

$$s_u = B - \left(B^2 - 2s_c B\right)^{1/2} \tag{2.5}$$

where s_u is the drawdown for the unconfined aquifer, s_c is the drawdown for the equivalent confined aquifer and B is initial saturated thickness of the aquifer (Schwartz and Zhang, 2002).

Immediately after an unconfined aquifer is started to be pumped, for a short period the aquifer behaves like a confined aquifer. Following this early stage, due to gravity drainage the downward movement of the water table is delayed for a while, and finally when the flow in the aquifer becomes horizontal again, the drawdown curve looks like the Theis curve as it does in the early stage. The time-drawdown response of an unconfined aquifer is illustrated in Figure 2.1.

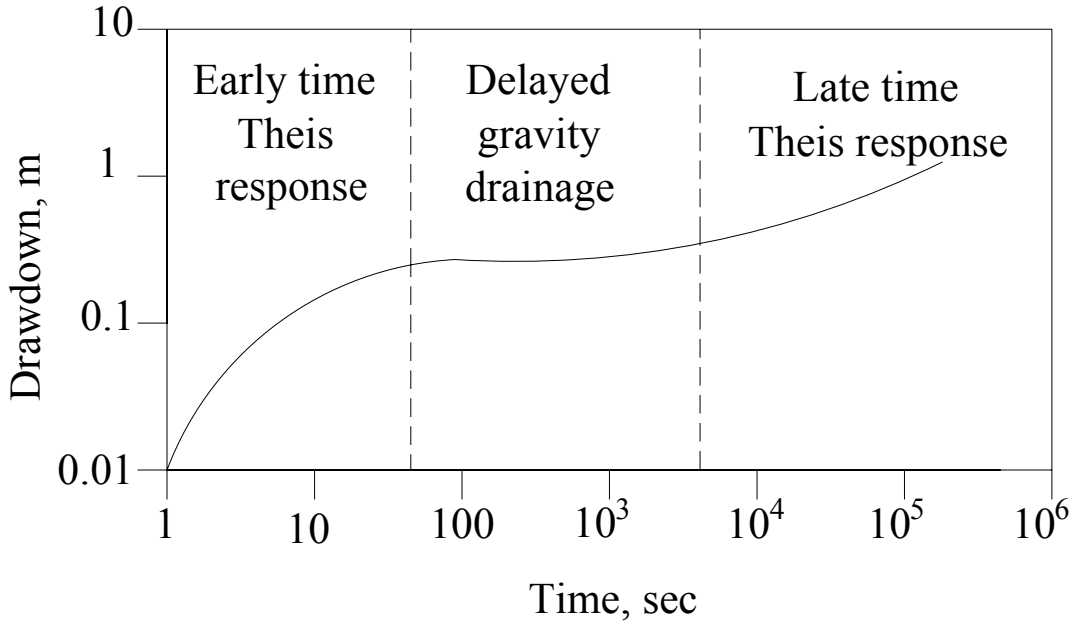

Figure 2.1. The response of an unconfined aquifer to pumping

Boulton (1963), Prickett (1965), and Neuman (1975) developed well functions regarding the concept of delayed water table response. The analytical solution proposed by Neuman (1975) is presented as;

$$s_u = \frac{Q}{4\pi T} W\left(u_A, u_B, \eta\right) \tag{2.6}$$

where $W(u_A, u_B, \eta)$ is the unconfined well function which depends on the variables described as;

$$u_A = \frac{r^2 S}{4 T_r t} \tag{2.7}$$

$$u_B = \frac{r^2 S_y}{4 T_r t} \tag{2.8}$$

$$\eta = \frac{r^2 K'}{B^2 K} \tag{2.9}$$

where K and K' are the horizontal and the vertical conductivities respectively, S is the storativity, S_y is the specific yield and B is the initial saturated thickness. The curves representing the values of the well function, $W(u_A, u_B, \eta)$, are presented in Figure 2.2.

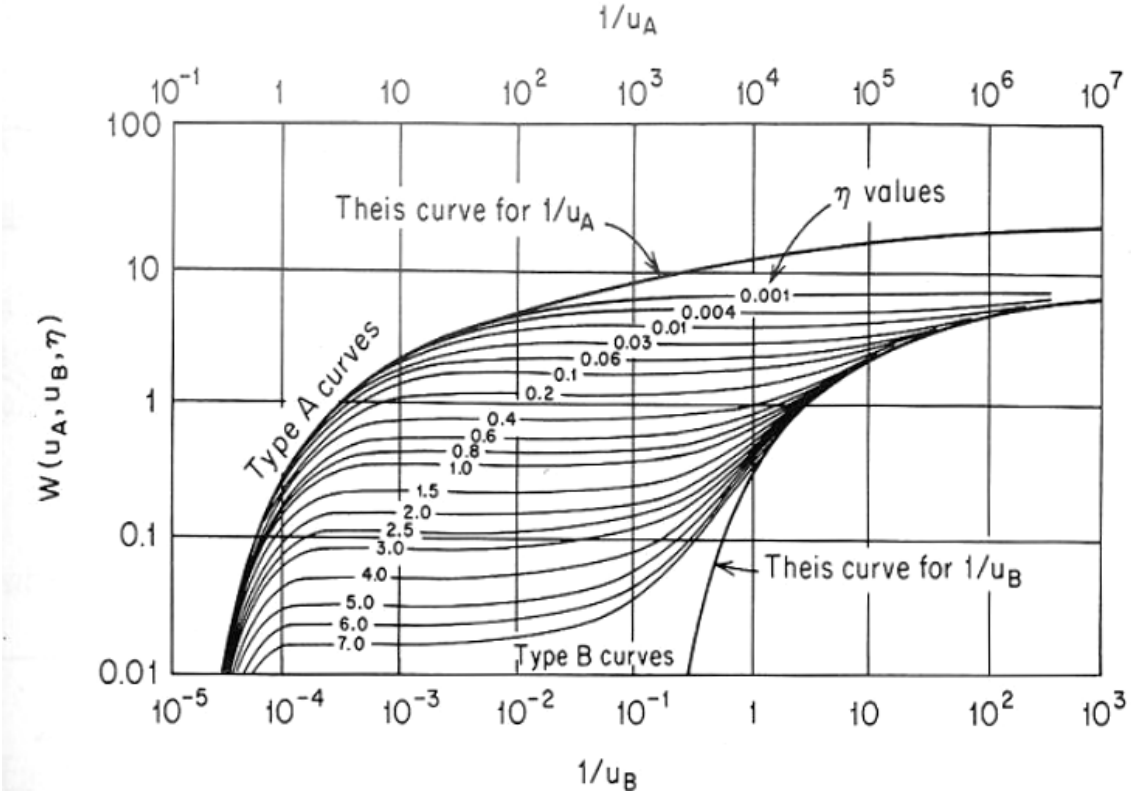

Figure 2.2. Type curves for drawdown in an unconfined aquifer with fully penetrating wells (after Neuman, 1975)

Moench (1995) analyzed unconfined flow to a well by utilizing an improved Laplace transform solution instead of Neuman's time domain solution. When compared to Neuman's solution, the Laplace transform solution is easier to evaluate due to the fact that fewer parameters are used in this solution.

2.2. Aquifer Dewatering Due to Tunnel Construction

Deawatering of an unconfined aquifer due to leakage into a tunnel has been the topic of numerous research studies.

Kim and Lee (2003) investigated the effect of the subway construction on the groundwater table in Seoul. The subway network, consisting of 8 subway lines was traced to drain groundwater at a rate of approximately 200,000 m^3/day which in turn led to the decline of water table along the subway route.

Karlsrud (2002) state that the measured leakege into a non-grouted tunnel ranges from 15 to 80 litre/min per 100m tunnel. The leakage is observed to be concentrated in fractured zones. Such concentrated leaks are measured to yield up to 60-80 l/min per 100 m tunnel.

The leakage into a rock tunnel can be calculated according to the expression proposed by Karlsrud (2002), and given in Eq.(2.10)

$$Q_{leak} = \pi K H_t \frac{2}{\ln\left(2\frac{H_t}{r_t} - 1\right)} \tag{2.10}$$

where K is the hydraulic conductivity of the rock, H_t is the depth of the tunnel below water table and r_t is the equivalent radius of the tunnel, that is the radius of the circle with an area equal to the area of the tunnel. This expression is based on the assumptions that the deeply embedded tunnel lies in an homogenious aquifer and that the groundwater table is not influenced by the leakage.

When the tunnel surface is grouted, the hydraulic conductivity at the tunnel face is reduced by an order of ten and the leakage into the tunnel for such situations can be calculated as;

$$Q_{leak} = \pi K_g H_t \frac{2}{\ln\left(\frac{r_t + h_g}{r_t}\right)} \tag{2.11}$$

where K_g is the hydraulic conductivity of the grouted rock zone and h_g is the thickness of the grouted zone.

2.3. Volatilization of Organic Compounds

The extent of volatilization of residual volatile organic compound is significant in determining the overall removal rate of compound from the porous medium. Any substance in nature possesses a vapor pressure that can be considered as a measure of the tendency of that substance to evaporate. As defined by Weast (1981), vapor pressure is the force per unit area exerted by the vapor of the chemical in equilibrium with its pure solid or liquid form.

The tendency of a substance to volatilize increases with its rising vapor pressure. Chemicals with vapor pressures of less than 10^{-7} mm Hg are not supposed to volatilize to a significant extent (Dragun, 1988).

The vapor pressure of a compound is strongly influenced by the temperature. An increase in temperature leads to an increase in vapor pressure. Vapor pressure can be approximated by an equation developed by Jury et al. (1987), as given in Eq.(2.12)

$$P_v = Ae^{-B/T} \tag{2.12}$$

where T is the temperature and, A and B are the substance-specific constants.

Henry's law determines the degree of volatilization of a residual compound dissolved in water. According to this law, the concentration of a volatile organic compound in water is proportional to its partial pressure at low concentrations. The proportionality constant which describes this relationship is known as Henry's law constant and can be obtained by Eq.(2.13)

$$K_H = \frac{C}{C_l} \tag{2.13}$$

where K_H is the Henry's law constant, C is the concentration of the compound in the gas phase and C_l is the concentration of the compound in the liquid phase. Munz and Roberts (1987) state that each rise of $10\,^{o}\mathrm{C}$ in temperature leads to a 1.6 times increase in the Henry's constant.

For a compound which exists as a free product in the unsaturated zone, the vapor pressure can be estimated by utilizing Raoult's law, as given in Eq.(2.14)

$$P_v = x_i P_o \tag{2.14}$$

where x_i is the molar fraction of the residual organic compound, of which the value is less than one, when there exist more than one component. Eq.(2.15) can be used to calculate the molar fraction of the i^{th} residual component.

$$x_i = \frac{W_i / M_i}{\sum_{j=1}^{n} (W_i / M_i)} \tag{2.15}$$

where W_i and M_i are the mass and molecular weight of the i^{th} residual component respectively and n is the number of components. P_o in Eq.(2.15) is the vapor pressure of the pure liquid constituent and can be computed by Antoine's vapor pressure equation given in Eq.(2.16);

$$P_o = 10^{\left(A_1 - \frac{A_2}{A_3 + T}\right)} \tag{2.16}$$

where A_1, A_2 and A_3 are the constituent specific constants and T is the system temperature (Reid et al., 1987).

Equilibrium vapor concentration can be obtained by employing the ideal gas law, as given in Eq.(2.17)

$$C_{eq} = \frac{P_v M}{RT} \tag{2.17}$$

where M is the molecular weight of the compound and R is the universal gas constant.

Coats and Smith (1964), proposed a first order type rate equation to account for mass exchange between liquid and gas phases, as presented in Eq.(2.18);

$$qc = \alpha\left(C - C_{eq}\right) \tag{2.18}$$

where qc represents the rate of mass exchange between liquid and gas phases, and α denotes overall mass transfer coefficient.

An expression proposed by Zaman (1993) can be used to estimate the overall mass transfer coefficient, α, as given in Eq.(2.19);

$$\alpha = \beta_1\left(K_L a\right)\theta_l^{0.67} \tag{2.19}$$

where $K_L a$ is the overall mass transfer coefficient of the liquid in free atmosphere, β_1 is a shape factor which depends on the pore geometry and the residual liquid distribution in the media. θ_l is the volumetric liquid content of the residual liquid. Zaman proposed specific values of $\beta_1(K_L a)$ for different organic compounds. For the current study these proposed values are used to obtain the overall mass transfer coefficient for each constituent. The overall mass transfer coefficient acts as a time dependent parameter due to the change in volumetric liquid content with time.

2.4. Transport of Organic Vapors in the Vadose Zone

2.4.1. Molecular Diffusion

Molecular diffusion in natural systems is the mass transport caused by the random thermal motion of molecules and atoms from locations of higher concentration towards those with lower concentration. The diffusion of a compound in one dimensional porous systems can be described by Fick's First law which is given in Eq.(2.20)

$$J_x = -D_{eff} \frac{dC}{dx} \tag{2.20}$$

where J_x is the mass flux, D_{eff} is the effective diffusion coefficient of the compound in the gas phase and $\frac{dC}{dx}$ is the concentration gradient along the *x*-axis. The effective diffusion coefficient can be obtained by the equation given as;

$$D_{eff} = \theta_g \tau D_m \tag{2.21}$$

where D_m is the molecular diffusion of the compound in free atmosphere, θ_g is the effective gas filled porosity of the medium and τ is the tortuosity of the medium. Several empirical relationships have been developed to estimate tortuosity on the basis of the gas filled porosity, θ_g and total porosity, θ. The first proposed equation to be utilized for estimating the tortuosity of the medium was developed by Penman (1940) and is given in Eq.(2.22)

$$\tau = 0.66\theta_g \tag{2.22}$$

Marshall (1959) developed a different empirical equation for the tortuosity estimation as shown in Eq.(2.23)

$$\tau = \theta_g^{3/2} \tag{2.23}$$

According to the empirical relationship developed by Milington and Quirk (1961), tortuosity of the medium can be estimated as;

$$\tau = \frac{\theta_g^{10/3}}{\theta^2} \tag{2.24}$$

Another empirical relationship proposed by Moldrup et al.(1997) can be expressed as;

$$\tau = 0.66\frac{\theta_g^{2}}{\theta} \tag{2.25}$$

For a three-phase system, consisting of soil solids, air and water, based on Fick's second law, Grathwohl (1998) developed a transient solution which is presented as;

$$\frac{\partial C}{\partial t} = \frac{D_{eff}}{\psi}\frac{\partial^2 C}{\partial x^2} \tag{2.26}$$

where ψ is the capacity factor and can be computed by Eq.(2.27);

$$\psi = \theta_g + \frac{\theta_w}{K_H} + \frac{K_d \rho_b}{K_H} \tag{2.27}$$

where θ_w is the water filled porosity, ρ_b denotes the dry bulk density of the soil and K_d is the distribution coefficient which describes the water-solid partitioning of hydrophobic organic compounds.

Eq.(2.26) is based on the assumption that the partial pressures of the volatile species are low when compared to other gases such as nitrogen or oxygen. Baehr and Bruell (1990) employed Stefan-Maxwell equation in order to develop the diffusion equation for situations where volatile organic compounds constitute a substantial fraction of the total gas concentration.

2.4.2. Vapor Flow Due to Pressure Gradient

The movement of the gases in the unsaturated zone is subject to the influence of many factors. The pressure gradient induced by a vacuum well can be interpreted as the dominant factor which leads to the advective flow of the vapor especially in the vicinity of that well.

Gas flow through porous media can be obtained by using continuity equation as;

$$\frac{\partial}{\partial t}(\rho\theta_g)+\nabla.(\rho q)=0 \tag{2.28}$$

where q is specific discharge of gas, ρ is the density of the gas, θ_g is the gas filled porosity of the soil and t represents time (Baehr and Hult, 1991). The specific discharge of the gas can found by utilizing Darcy's law as;

$$q=-\frac{kk^*}{\mu}\nabla P \tag{2.29}$$

where k and k^* are the intrinsic and relative permeabilities of the porous medium respectively, μ is the viscosity of the gas and P is the pressure. Brooks and Corey (1964) suggested a semiemprical equation to predict the relative permeability of the gas, k*, which is given by:

$$k^*=(1-\theta_e)^2(1-\theta_e^{\frac{2+\lambda}{\lambda}}) \tag{2.30}$$

where λ is the dimensionless pore size distribution and θ_e is the effective liquid saturation to be obtained by Eq.(2.31):

$$\theta_e=\frac{\theta_l-\theta_r}{\theta-\theta_r} \tag{2.31}$$

where θ_l is the liquid content in the soil while θ_r is the irreducable moisture content and θ is the total porosity of the soil.

According to the ideal gas law the density of the gas can be computed as:

$$\rho = \frac{MP}{RT} \tag{2.32}$$

where M is the molecular weight of the gas, R is the universal gas constant and T accounts for the system temperature. Combining Eq.(2.28), Eq.(2.29) and Eq.(2.32) the air flow equation becomes;

$$\nabla\left(-\frac{MP}{RT}\left(\frac{kk^*}{\mu}\nabla P\right)\right) + W = -\theta_g \frac{\partial}{\partial t}\left(\frac{MP}{RT}\right) \tag{2.33}$$

where W is the mass flow rate based on the existence of a sink or source component.

2.5. Soil Vapor Extraction System

Soil vapor extraction is one of the techniques utilized to remove volatile organic compounds from the vadose zone. In this process screened wells, which are installed into the contaminated region apply vacuum to create a pressure gradient. The induced air enhances the volatilization of organic compound and the generated organic vapor is then collected by the extraction wells. An illustration of a soil vapor extraction system is presented in Figure 2.3.

The air permeability of the soil is a significant parameter to be considered while evaluating the efficieny of the SVE and designing the system. The effectiveness of the system is limited at sites with low permeability.

Rathfelder et al.(1995) and Hutzler et al.(1989) state that under normal conditions, the SVE system effectively removes organic compounds with vapor pressures above

0.5 mm Hg. Rhodes et al.(1993) show that SVE does not economically remove heavier, less volatile organic compounds such as diesel, kerosene and fuel oil.

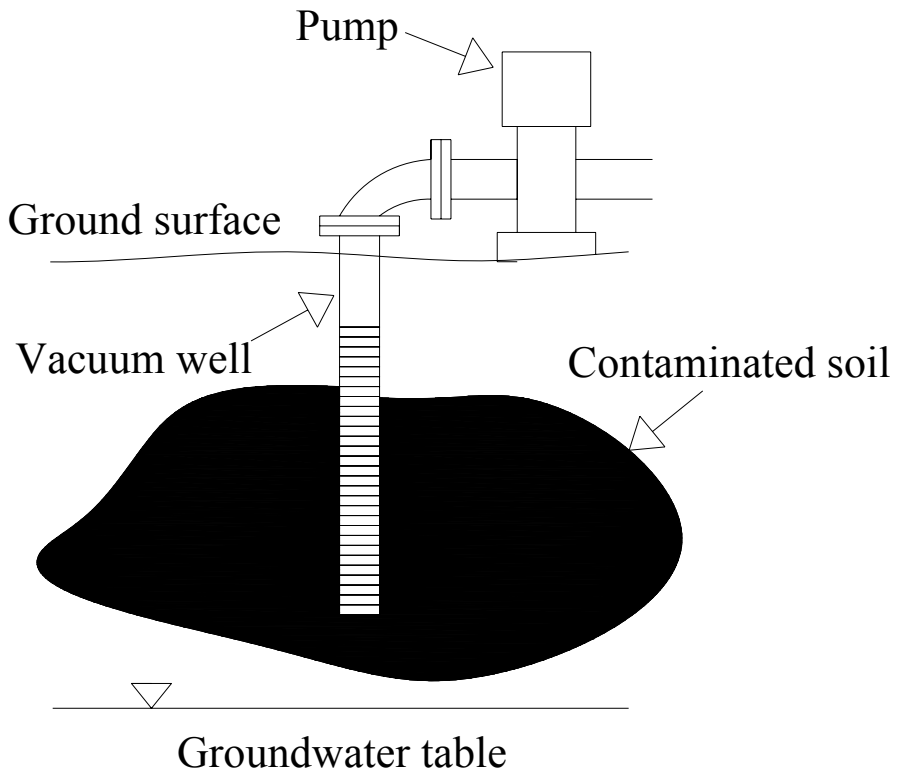

Figure 2.3. Illustration of a soil vapor extraction system

The temperature of the subsurface environment has an important effect on SVE process. Steam injection or soil heating processes enhance volatilization of organic compounds, so that these applications increase the efficiency of soil vapor extraction system. (Hunt et al, 1986).

3. NUMERICAL MODEL DEVELOPMENT

3.1. Basic Aspects of the Finite Difference Method

The finite difference method is one of the methods utilized for solving groundwater flow and transport equations. The governing equations include derivatives of time and space dependent variables. The finite difference method is based on the principle that these derivatives can be approximately represented by discrete linear changes over discrete space or time intervals, so that the governing differential equation is replaced by a system of algebraic equations.

In the finite difference method, the continuous domain is discretized by a grid and the algebraic finite difference equation is solved for each grid block.

The finite difference representations of derivatives can be derived from Taylor's series expansion. When we define a continuous function of *x*, namely $f(x)$, then the value of *f* at location $x+\Delta x$ can be estimated from a Taylor series expanded about point *x*, as given in Eq.(3.1):

$$f(x+\Delta x) = f(x) + \frac{\partial f}{\partial x}\Delta x + \frac{\partial^2 f}{\partial x^2}\frac{(\Delta x)^2}{2} + \cdots \frac{\partial^n f}{\partial x^n}\frac{(\Delta x)^n}{n!} + \cdots \tag{3.1}$$

The first term on the right hand side of Eq. (3.1) is the value of the function at *x*. By introducing the second term, the slope of the curve at point *x* is taken into account. The third term represents the curvature at $f(x)$. To obtain more accurate value for $f(x+\Delta x)$, additional higher order terms should be included and for the exact representation of $f(x+\Delta x)$ an infinite number of terms is required. When the first two terms on the right hand side of Eq.(3.1) are taken, neglecting the remaining terms, an approximate representation of $f(x+\Delta x)$ can be obtained, as given in Eq.(3.2)

$$\frac{\partial f}{\partial x} = \frac{f(x+\Delta x) - f(x)}{\Delta x} + O(\Delta x) \tag{3.2}$$

where $O(\Delta x)$ represents the truncation error of order Δx. The finite difference expression in Eq.(3.2) is called a *first-order forward difference.*

Similarly, the value of f at location $x - \Delta x$ can be estimated from a Taylor series expanded about point x, as;

$$f(x-\Delta x) = f(x) - \frac{\partial f}{\partial x}\Delta x + \frac{\partial^2 f}{\partial x^2}\frac{(\Delta x)^2}{2} - \cdots \frac{\partial^n f}{\partial x^n}\frac{(\Delta x)^n}{n!} + \cdots \tag{3.3}$$

When the first two terms on the right hand side of Eq.(3.3) are taken, *the first order backward difference* expression is obtained which is given in Eq.(3.4)

$$\frac{\partial f}{\partial x} = \frac{f(x) - f(x-\Delta x)}{\Delta x} + O(\Delta x) \tag{3.4}$$

By substracting Eq.(3.3) from Eq.(3.1), the *second order central difference* is obtained as given in Eq.(3.5)

$$\frac{\partial f}{\partial x} = \frac{f(x+\Delta x) - f(x-\Delta x)}{2\Delta x} + O(\Delta x)^2 \tag{3.5}$$

When the Taylor series expansions given by Eq.(3.1) and Eq.(3.3) are summed up, considering the first three terms on the RHS of the resultant sum, *second order central second difference* is obtained, as given in Eq.(3.6)

$$\frac{\partial^2 f}{\partial x^2} = \frac{f(x+\Delta x) - 2f(x) + f(x-\Delta x)}{(\Delta x)^2} + O(\Delta x)^2 \tag{3.6}$$

Methods for solving the above algebraic equations can be categorized as direct and iterative. In direct methods, the algebraic equation is solved by performing matrix

operations. The iterative methods involve making some initial guesses of the unknowns and improving these guesses through a set of repeated calculations until an error criterion is reached.

The finite difference approach has some advantages when compared to other numerical techniques. This technique is conceptually straightforward and does not require advanced training in applied mathematics. However, the method has some limitations while working on flow and transport equation due to the fact that, it works best only for rectangular or prismatic aquifers, and does not allow a flexible mesh geometry. Moreover, the accuracy of solutions to contaminant transport solutions is lower than might be obtained by other numerical techniques, such as finite element method (Istok, 1989).

3.2. Model Development

3.2.1. Development of the Groundwater Flow Model

The transient groundwater flow equation, derived by combining continuity equation with Darcy's law, is presented in Eq.(3.7);

$$\frac{\partial}{\partial x}\left(K_{xx}\frac{\partial h}{\partial x}\right)+\frac{\partial}{\partial y}\left(K_{yy}\frac{\partial h}{\partial y}\right)+\frac{\partial}{\partial z}\left(K_{zz}\frac{\partial h}{\partial z}\right)+W=S_s\frac{\partial h}{\partial t} \tag{3.7}$$

where K_{xx}, K_{yy}, K_{zz} account for the hydraulic conductivity in x, y and z directions respectively. h is the hydraulic head, t is the time parameter and S_s is the specific storage. W represents a source or a sink element (Bear, 1972).

The finite difference form of the groundwater flow equation can be derived by directly expressing the derivatives of the above governing equation in difference form. Another alternative to construct the finite difference form is to make use of the continuity equation which states that the sum of flows into and out of any control volume is equal to the change of storage plus the sink or the source component. While developing

MODFLOW, McDonald and Harbough (1988) followed this second approach which is given mathematically in Eq.(3.8)

$$\sum Q_i = S_s \frac{\Delta h}{\Delta t} \Delta V \tag{3.8}$$

where Δh is the change in head over a time interval Δt and ΔV is the volume of the brick shaped cell which is illustrated in Figure 3.1.

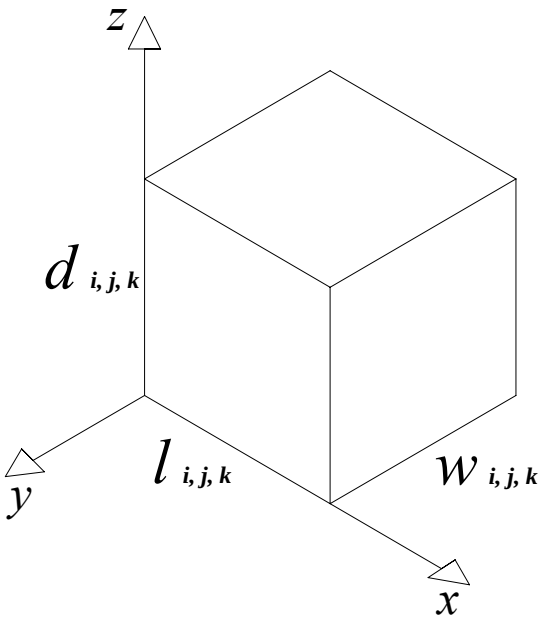

Figure 3.1. The cell with the index *i, j, k*

The indices *i, j* and *k* run in *x, y* and *z* directions respectively.

The volumetric flowrate through the left surface of the cell can be obtained by Darcy equation as;

$$Q_{ls} = -K_{eq} A_{ls} \frac{\Delta h}{\Delta x} \tag{3.9}$$

where

$$K_{eq} = \frac{\frac{l_{i,j,k}}{2} + \frac{l_{i-1,j,k}}{2}}{\frac{l_{i,j,k}}{2K_{xx_{i,j,k}}} + \frac{l_{i-1,j,k}}{2K_{xx_{i-1,j,k}}}} \tag{3.10}$$

$$A_{ls} = w_{i,j,m} \times d_{i,j,m} \tag{3.11}$$

$$\frac{\Delta h}{\Delta x} = \frac{h_{i,j,k} - h_{i-1,j,k}}{\frac{l_{i,j,k}}{2} + \frac{l_{i-1,j,k}}{2}} \tag{3.12}$$

Combining Eq.(3.9), Eq.(3.10), Eq.(3.11) and Eq.(3.12) the flow through the left surface of the cell from the adjacent cell can be found as:

$$Q_{ls} = \frac{w_{i,j,k} d_{i,j,k}}{\frac{l_{i,j,k}}{2K_{xx_{i,j,k}}} + \frac{l_{i-1,j,k}}{2K_{xx_{i-1,j,k}}}} (h_{i-1,j,k} - h_{i,j,k}) \tag{3.13}$$

This approach can be used in order to calculate the flowrates through the other surfaces;

$$Q_{rs} = \frac{w_{i,j,k} d_{i,j,k}}{\frac{l_{i,j,k}}{2K_{xx_{i,j,k}}} + \frac{l_{i+1,j,k}}{2K_{xx_{i+1,j,k}}}} (h_{i+1,j,k} - h_{i,j,k}) \tag{3.14}$$

$$Q_{fs} = \frac{l_{i,j,k} d_{i,j,k}}{\frac{w_{i,j,m}}{2K_{yy_{i,j,m}}} + \frac{w_{i,j+1,m}}{2K_{yy_{i,j+1,m}}}} (h_{i,j+1,k} - h_{i,j,k}) \tag{3.15}$$

$$Q_{bs} = \frac{l_{i,j,k} d_{i,j,k}}{\frac{w_{i,j,k}}{2K_{yy_{i,j,k}}} + \frac{w_{i,j-1,k}}{2K_{yy_{i,j-1,k}}}} (h_{i,j-1,k} - h_{i,j,k}) \tag{3.16}$$

$$Q_{ts} = \frac{l_{i,j,k} w_{i,j,k}}{\frac{d_{i,j,k}}{2K_{zz_{i,j,k}}} + \frac{d_{i,j,k-1}}{2K_{zz_{i,j,k-1}}}} (h_{i,j,k-1} - h_{i,j,k}) \tag{3.17}$$

$$Q_{bots} = \frac{l_{i,j,k} w_{i,j,k}}{\frac{d_{i,j,k}}{2K_{zz_{i,j,k}}} + \frac{d_{i,j,k+1}}{2K_{zz_{i,j,k+1}}}} (h_{i,j,k+1} - h_{i,j,k}) \tag{3.18}$$

where $Q_{rs}, Q_{fs}, Q_{bs}, Q_{ts}, Q_{bots}$ are the flowrates through the right, front, back, top and bottom surfaces respectively.

Now the finite difference form of Eq.(3.8) can be written as:

$$Q_{ls} + Q_{rs} + Q_{fs} + Q_{bs} + Q_{ts} + Q_{bots} + W = \left(l_{i,j,k} w_{i,j,k} d_{i,j,k}\right) S_s \frac{h_{i,j,k}^{n+1} - h_{i,j,k}^{n}}{\Delta t} \tag{3.19}$$

By applying the *successive over relaxation* (SOR) method to this expression with the parameter ω, and dividing both sides with the term $\left(l_{i,j,k} w_{i,j,k} d_{i,j,k}\right)$ the equation becomes:

$$S_s \frac{h_{i,j,k}^{n+1} - h_{i,j,k}^{n}}{\Delta t} = (1-\omega) A^{n} + \omega A^{n+1} + \frac{W_{i,j,k}}{l_{i,j,k} w_{i,j,k} d_{i,j,k}} \tag{3.20}$$

where

$$A^n = \frac{h^n_{i-1,j,k} - h^n_{i,j,k}}{\left(\frac{l_{i,j,k}}{2K_{xx_{i,j,k}}} + \frac{l_{i-1,j,k}}{2K_{xx_{i-1,j,k}}}\right) l_{i,j,k}} + \frac{h^n_{i+1,j,k} - h^n_{i,j,k}}{\left(\frac{l_{i,j,k}}{2K_{xx_{i,j,k}}} + \frac{l_{i+1,j,k}}{2K_{xx_{i+1,j,k}}}\right) l_{i,j,k}}$$
$$+ \frac{h^n_{i,j-1,k} - h^n_{i,j,k}}{\left(\frac{w_{i,j,k}}{2K_{yy_{i,j,k}}} + \frac{w_{i,j-1,k}}{2K_{yy_{i,j-1,k}}}\right) w_{i,j,k}} + \frac{h^n_{i,j+1,k} - h^n_{i,j,k}}{\left(\frac{w_{i,j,k}}{2K_{yy_{i,j,k}}} + \frac{w_{i,j+1,k}}{2K_{yy_{i,j+1,k}}}\right) w_{i,j,k}} \tag{3.21}$$
$$+ \frac{h^n_{i,j,k-1} - h^n_{i,j,k}}{\left(\frac{d_{i,j,k}}{2K_{zz_{i,j,k}}} + \frac{d_{i,j,k-1}}{2K_{zz_{i,j,k-1}}}\right) d_{i,j,k}} + \frac{h^n_{i,j,k+1} - h^n_{i,j,k}}{\left(\frac{d_{i,j,k}}{2K_{zz_{i,j,k}}} + \frac{d_{i,j,k+1}}{2K_{zz_{i,j,k+1}}}\right) d_{i,j,k}}$$

$$A^{n+1} = \frac{h^{n+1}_{i-1,j,k} - h^{n+1}_{i,j,k}}{\left(\frac{l_{i,j,k}}{2K_{xx_{i,j,k}}} + \frac{l_{i-1,j,k}}{2K_{xx_{i-1,j,k}}}\right) l_{i,j,k}} + \frac{h^{n+1}_{i+1,j,k} - h^{n+1}_{i,j,k}}{\left(\frac{l_{i,j,k}}{2K_{xx_{i,j,k}}} + \frac{l_{i+1,j,k}}{2K_{xx_{i+1,j,k}}}\right) l_{i,j,k}}$$
$$+ \frac{h^{n+1}_{i,j-1,k} - h^{n+1}_{i,j,k}}{\left(\frac{w_{i,j,k}}{2K_{yy_{i,j,k}}} + \frac{w_{i,j-1,k}}{2K_{yy_{i,j-1,k}}}\right) w_{i,j,k}} + \frac{h^{n+1}_{i,j+1,k} - h^{n+1}_{i,j,k}}{\left(\frac{w_{i,j,k}}{2K_{yy_{i,j,k}}} + \frac{w_{i,j+1,k}}{2K_{yy_{i,j+1,k}}}\right) w_{i,j,k}} \tag{3.22}$$
$$+ \frac{h^{n+1}_{i,j,k-1} - h^{n+1}_{i,j,k}}{\left(\frac{d_{i,j,k}}{2K_{zz_{i,j,k}}} + \frac{d_{i,j,k-1}}{2K_{zz_{i,j,k-1}}}\right) d_{i,j,k}} + \frac{h^{n+1}_{i,j,k+1} - h^{n+1}_{i,j,k}}{\left(\frac{d_{i,j,k}}{2K_{zz_{i,j,k}}} + \frac{d_{i,j,k+1}}{2K_{zz_{i,j,k+1}}}\right) d_{i,j,k}}$$

For an unconfined cell, the specific storage, S_s is replaced by the specific yield, S_y term and the change in volume storage with time, $\frac{d\forall}{dt}$ becomes:

$$\frac{d\forall}{dt} = S_y A \frac{\partial h}{\partial t} \tag{3.23}$$

where A is the base area of the cell. The finite difference form of the groundwater flow equation for an unconfined cell becomes:

$$S_y \frac{h_{i,j,k}^{n+1} - h_{i,j,k}^{n}}{\Delta t} = (1-\omega)B^n + \omega B^{n+1} + \frac{W_{i,j,k}}{l_{i,j,k} w_{i,j,k}} \tag{3.24}$$

where

$$\begin{aligned} B^n = & \frac{\left(h_{i-1,j,m}^{n} - h_{i,j,m}^{n}\right) d_{i,j,k}}{\left(\frac{l_{i,j,k}}{2K_{xx_{i,j,k}}} + \frac{l_{i-1,j,k}}{2K_{xx_{i-1,j,k}}}\right) l_{i,j,k}} + \frac{\left(h_{i+1,j,k}^{n} - h_{i,j,k}^{n}\right) d_{i,j,k}}{\left(\frac{l_{i,j,k}}{2K_{xx_{i,j,k}}} + \frac{l_{i+1,j,k}}{2K_{xx_{i+1,j,k}}}\right) l_{i,j,k}} \\ & + \frac{\left(h_{i,j-1,k}^{n} - h_{i,j,k}^{n}\right) d_{i,j,k}}{\left(\frac{w_{i,j,k}}{2K_{yy_{i,j,k}}} + \frac{w_{i,j-1,k}}{2K_{yy_{i,j-1,k}}}\right) w_{i,j,k}} + \frac{\left(h_{i,j+1,k}^{n} - h_{i,j,k}^{n}\right) d_{i,j,k}}{\left(\frac{w_{i,j,k}}{2K_{yy_{i,j,k}}} + \frac{w_{i,j+1,k}}{2K_{yy_{i,j+1,k}}}\right) w_{i,j,k}} \\ & + \frac{h_{i,j,k-1}^{n} - h_{i,j,k}^{n}}{\left(\frac{d_{i,j,k}}{2K_{zz_{i,j,k}}} + \frac{d_{i,j,k-1}}{2K_{zz_{i,j,k-1}}}\right)} + \frac{h_{i,j,k+1}^{n} - h_{i,j,k}^{n}}{\left(\frac{d_{i,j,k}}{2K_{zz_{i,j,k}}} + \frac{d_{i,j,k+1}}{2K_{zz_{i,j,k+1}}}\right)} \end{aligned} \tag{3.25}$$

$$\begin{aligned} B^{n+1} = & \frac{\left(h_{i-1,j,k}^{n+1} - h_{i,j,k}^{n+1}\right) d_{i,j,k}}{\left(\frac{l_{i,j,k}}{2K_{xx_{i,j,k}}} + \frac{l_{i-1,j,k}}{2K_{xx_{i-1,j,k}}}\right) l_{i,j,k}} + \frac{\left(h_{i+1,j,k}^{n+1} - h_{i,j,k}^{n+1}\right) d_{i,j,k}}{\left(\frac{l_{i,j,k}}{2K_{xx_{i,j,k}}} + \frac{l_{i+1,j,k}}{2K_{xx_{i+1,j,k}}}\right) l_{i,j,k}} \\ & + \frac{\left(h_{i,j-1,k}^{n+1} - h_{i,j,k}^{n+1}\right) d_{i,j,k}}{\left(\frac{w_{i,j,k}}{2K_{yy_{i,j,k}}} + \frac{w_{i,j-1,k}}{2K_{yy_{i,j-1,k}}}\right) w_{i,j,k}} + \frac{\left(h_{i,j+1,k}^{n+1} - h_{i,j,k}^{n+1}\right) d_{i,j,k}}{\left(\frac{w_{i,j,k}}{2K_{yy_{i,j,k}}} + \frac{w_{i,j+1,k}}{2K_{yy_{i,j+1,k}}}\right) w_{i,j,k}} \\ & + \frac{h_{i,j,k-1}^{n+1} - h_{i,j,k}^{n+1}}{\left(\frac{d_{i,j,k}}{2K_{zz_{i,j,k}}} + \frac{d_{i,j,k-1}}{2K_{zz_{i,j,k-1}}}\right)} + \frac{h_{i,j,k+1}^{n+1} - h_{i,j,k}^{n+1}}{\left(\frac{d_{i,j,k}}{2K_{zz_{i,j,k}}} + \frac{d_{i,j,k+1}}{2K_{zz_{i,j,k+1}}}\right)} \end{aligned} \tag{3.26}$$

Figure 3.2 explains under what conditions a cell is confined or unconfined and how it becomes dry.

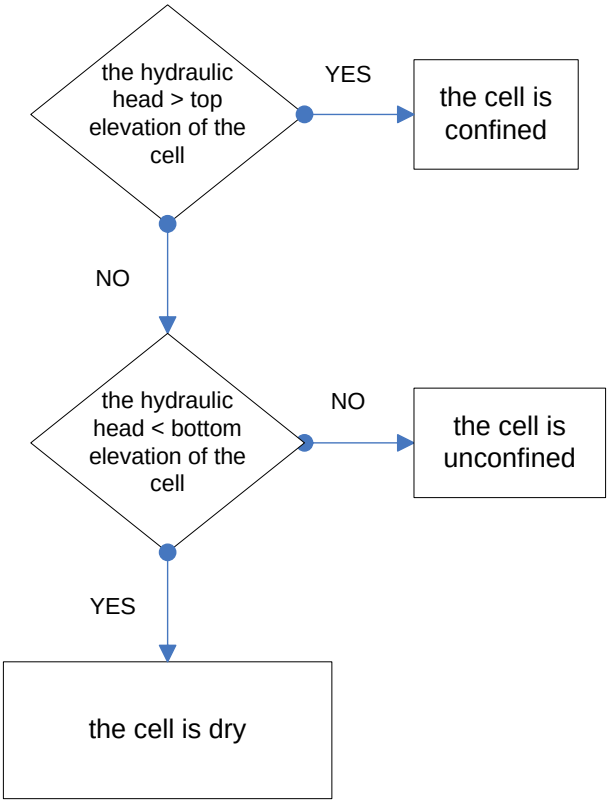

Figure 3.2. The flow-chart utilized to determine the nature of the cell

3.2.2. Modeling Vapor Flow Due to Local Pressure Gradient

The movement of the soil vapor in the vadose zone results from two main factors, i.e. vapor flow due to local pressure gradient and advective-diffusive transport. These transport mechanisms are governed by two equations. The soil vapor extraction system can be modeled by solving these two governing equations consecutively.

The governing equation which represents vapor flow due to pressure gradient is presented in Eq.(3.27)

$$\nabla\left(-\frac{MP}{RT}\left(\frac{kk^{*}}{\mu}\nabla P\right)\right)+W=-\theta_{g}\frac{\partial}{\partial t}\left(\frac{MP}{RT}\right) \tag{3.27}$$

When both RHS and LHS of Eq.(3.27) is divided by the term $\frac{M}{RT}$, the equation becomes;

$$\frac{\partial}{\partial x}\left(k_{xx}k^{*}P\frac{\partial P}{\partial x}\right)+\frac{\partial}{\partial y}\left(k_{yy}k^{*}P\frac{\partial P}{\partial y}\right)+\frac{\partial}{\partial z}\left(k_{zz}k^{*}P\frac{\partial P}{\partial z}\right)+\frac{RT}{M}W=\theta_{g}\mu\frac{\partial P}{\partial t} \tag{3.28}$$

A new variable is defined to be used instead of P^2;

$$\phi=P^{2} \tag{3.29}$$

The following equations can be obtained through basic derivative operations;

$$P\frac{\partial P}{\partial x}=\frac{1}{2}\frac{\partial P^{2}}{\partial x}=\frac{1}{2}\frac{\partial\phi}{\partial x} \tag{3.30}$$

$$\frac{\partial P}{\partial t}=\frac{\partial\sqrt{\phi}}{\partial t}=\frac{1}{2\sqrt{\phi}}\frac{\partial\phi}{\partial t} \tag{3.31}$$

By substituting Eq.(3.30) and Eq.(3.31) into Eq. (3.28) the flow equation becomes.

$$\frac{\partial}{\partial x}\left(\frac{k_{xx}k^{*}}{2}\frac{\partial\phi}{\partial x}\right)+\frac{\partial}{\partial y}\left(\frac{k_{yy}k^{*}}{2}\frac{\partial\phi}{\partial y}\right)+\frac{\partial}{\partial z}\left(\frac{k_{zz}k^{*}}{2}\frac{\partial\phi}{\partial z}\right)+\frac{RT}{M}W=\frac{\theta_{g}\mu}{2\sqrt{\phi}}\frac{\partial\phi}{\partial t} \tag{3.32}$$

Eq.(3.32) can be expanded as:

$$\begin{aligned}\frac{\theta_{g}\mu}{\sqrt{\phi}}\frac{\partial\phi}{\partial t}=&\left(k_{xx}k^{*}\frac{\partial^{2}\phi}{\partial x^{2}}+\frac{\partial\phi}{\partial x}\frac{\partial(k_{xx}k^{*})}{\partial x}\right)+\left(k_{yy}k^{*}\frac{\partial^{2}\phi}{\partial y^{2}}+\frac{\partial\phi}{\partial y}\frac{\partial(k_{yy}k^{*})}{\partial y}\right)\\&+\left(k_{zz}k^{*}\frac{\partial^{2}\phi}{\partial z^{2}}+\frac{\partial\phi}{\partial z}\frac{\partial(k_{zz}k^{*})}{\partial z}\right)+\frac{RT}{M}W\end{aligned} \tag{3.33}$$

The finite difference form of the above equation with the Crank-Nicolson scheme can be written as:

$$\frac{1}{2}\left(C^n + D^n\right) + \frac{1}{2}\left(C^{n+1} + D^{n+1}\right) + \frac{M}{RT}W = \frac{\theta^n_{g_{i,j,k}}\mu}{\sqrt{\phi}}\frac{\left(\phi^{n+1}_{i,j,k} - \phi^n_{i,j,k}\right)}{\Delta t} \tag{3.34}$$

where

$$\begin{aligned} C^n = {} & k_{xx_{i,j,k}} k^{*n}{}_{i,j,k}\left(\frac{\phi^n_{i+1,j,k} - 2\phi^n_{i,j,k} + \phi^n_{i-1,j,k}}{\Delta x^2}\right) \\ & + k_{yy_{i,j,k}} k^{*n}{}_{i,j,k}\left(\frac{\phi^n_{i,j+1,k} - 2\phi^n_{i,j,k} + \phi^n_{i,j-1,k}}{\Delta y^2}\right) \\ & + k_{zz_{i,j,k}} k^{*n}{}_{i,j,k}\left(\frac{\phi^n_{i,j,k+1} - 2\phi^n_{i,j,k} + \phi^n_{i,j,k-1}}{\Delta z^2}\right) \end{aligned} \tag{3.35}$$

$$\begin{aligned} D^n = {} & \left(\frac{\phi^n_{i+1,j,k} - \phi^n_{i-1,j,k}}{2\Delta x}\right)\left(\frac{k_{xx_{i+1,j,k}} k^{*n}{}_{i+1,j,k} - k_{xx_{i-1,j,k}} k^{*n}{}_{i-1,j,k}}{2\Delta x}\right) \\ & + \left(\frac{\phi^n_{i,j+1,k} - \phi^n_{i,j-1,k}}{2\Delta y}\right)\left(\frac{k_{yy_{i,j+1,k}} k^{*n}{}_{i,j+1,k} - k_{yy_{i,j-1,k}} k^{*n}{}_{i,j-1,k}}{2\Delta y}\right) \\ & + \left(\frac{\phi^n_{i,j,k+1} - \phi^n_{i,j,k-1}}{2\Delta z}\right)\left(\frac{k_{zz_{i,j,k+1}} k^{*n}{}_{i,j,k+1} - k_{zz_{i,j,k-1}} k^{*n}{}_{i,j,k-1}}{2\Delta z}\right) \end{aligned} \tag{3.36}$$

$$\begin{aligned} C^{n+1} = {} & k_{xx_{i,j,k}} k^{*n+1}{}_{i,j,k}\left(\frac{\phi^{n+1}_{i+1,j,k} - 2\phi^{n+1}_{i,j,k} + \phi^{n+1}_{i-1,j,k}}{\Delta x^2}\right) \\ & + k_{yy_{i,j,k}} k^{*n+1}{}_{i,j,k}\left(\frac{\phi^{n+1}_{i,j+1,k} - 2\phi^{n+1}_{i,j,k} + \phi^{n+1}_{i,j-1,k}}{\Delta y^2}\right) \\ & + k_{zz_{i,j,k}} k^{*n+1}{}_{i,j,k}\left(\frac{\phi^{n+1}_{i,j,k+1} - 2\phi^{n+1}_{i,j,k} + \phi^{n+1}_{i,j,k-1}}{\Delta z^2}\right) \end{aligned} \tag{3.37}$$

$$D^{n+1} = \left(\frac{\phi^{n+1}_{i+1,j,k} - \phi^{n+1}_{i-1,j,k}}{2\Delta x} \right) \left(\frac{k_{xx_{i+1,j,k}} k^{*n+1}_{i+1,j,k} - k_{xx_{i-1,j,k}} k^{*n+1}_{i-1,j,k}}{2\Delta x} \right) + \left(\frac{\phi^{n+1}_{i,j+1,k} - \phi^{n+1}_{i,j-1,k}}{2\Delta y} \right) \left(\frac{k_{yy_{i,j+1,k}} k^{*n+1}_{i,j+1,k} - k_{yy_{i,j-1,k}} k^{*n+1}_{i,j-1,k}}{2\Delta y} \right) + \left(\frac{\phi^{n+1}_{i,j,k+1} - \phi^{t+1}_{i,j,k-1}}{2\Delta z} \right) \left(\frac{k_{zz_{i,j,k+1}} k^{*n+1}_{i,j,k+1} - k_{zz_{i,j,k-1}} k^{*n+1}_{i,j,k-1}}{2\Delta z} \right) \tag{3.38}$$

$$\sqrt{\phi} = P^{n}_{i,j,k} \tag{3.39}$$

$$\Delta x = \frac{\left(l_{i,j,k} + \left(l_{i+1,j,k} + l_{i-1,j,k} \right) / 2 \right)}{2} \tag{3.40}$$

$$\Delta y = \frac{\left(w_{i,j,k} + \left(w_{i,j+1,k} + w_{i,j-1,k} \right) / 2 \right)}{2} \tag{3.41}$$

$$\Delta z = \frac{\left(d_{i,j,k} + \left(d_{i,j,k+1} + d_{i,j,k-1} \right) / 2 \right)}{2} \tag{3.42}$$

Specific discharge of the gas in porous medium is given as;

$$q = -\frac{kk^{*}}{\mu} \nabla P \tag{3.43}$$

The x, y and z components of the discharge vector are:

$$q_x = -\frac{k_{xx} k^{*}}{\mu} \frac{\partial P}{\partial x} \tag{3.44}$$

$$q_y = -\frac{k_{yy} k^{*}}{\mu} \frac{\partial P}{\partial y} \tag{3.45}$$

$$q_z = -\frac{k_{zz}k^*}{\mu}\frac{\partial P}{\partial z} \tag{3.46}$$

The finite difference form of the velocity components can be written as:

$$q_{x_{i,j,m}}^{\ n} = -\frac{k_{xx_{i,j,k}}k_{i,j,k}^{*n}}{\mu}\frac{\left(P_{i+1,j,k}^n - P_{i-1,j,k}^n\right)}{2\Delta x} \tag{3.47}$$

$$q_{y_{i,j,k}}^{\ n} = -\frac{k_{yy_{i,j,k}}k_{i,j,k}^{*n}}{\mu}\frac{\left(P_{i,j+1,k}^n - P_{i,j-1,k}^n\right)}{2\Delta y} \tag{3.48}$$

$$q_{z_{i,j,k}}^{\ n} = -\frac{k_{zz_{i,j,k}}k_{i,j,k}^{*n}}{\mu}\frac{\left(P_{i,j,k+1}^n - P_{i,j,k-1}^n\right)}{2\Delta z} \tag{3.49}$$

Actual velocity components can be expressed as:

$$v_{x_{i,j,k}}^{\ n} = q_{x_{i,j,k}}^{\ n} / \theta_{g_{i,j,k}}^n \tag{3.50}$$

$$v_{y_{i,j,k}}^{\ n} = q_{y_{i,j,k}}^{\ n} / \theta_{g_{i,j,k}}^n \tag{3.51}$$

$$v_{z_{i,j,k}}^{\ n} = q_{z_{i,j,k}}^{\ n} / \theta_{g_{i,j,k}}^n \tag{3.52}$$

3.2.3. Modeling Advective-Dispersive Vapor Transport

The governing equation which can be utilized to solve vapor transport problem is described as:

$$\begin{aligned}\frac{\partial(\theta_g C)}{\partial t} = {} & \frac{\partial}{\partial x}\left(\theta_g D_{xx}\frac{\partial C}{\partial x}\right) + \frac{\partial}{\partial y}\left(\theta_g D_{yy}\frac{\partial C}{\partial y}\right) + \frac{\partial}{\partial z}\left(\theta_g D_{zz}\frac{\partial C}{\partial z}\right) \\ & - \frac{\partial\left(q_x C\right)}{\partial x} - \frac{\partial\left(q_y C\right)}{\partial y} - \frac{\partial\left(q_z C\right)}{\partial z} + qc\end{aligned} \tag{3.53}$$

where C is the concentration of the vapor, D_{xx}, D_{yy} and D_{zz} are the dispersion coefficients along x, y and z directions respectively (Bear, 1972). *qc* is the source term due to the volatilization of the residual VOCs and can be computed by using Eq.(2.18). The dispersion coefficients can be calculated by the equations given in Eq.(3.54) through Eq.(3.56) (Burnett and Frind, 1987);

$$D_{xx} = \alpha_L \frac{v_x^2}{|v|} + \alpha_{TH} \frac{v_y^2}{|v|} + \alpha_{TV} \frac{v_x^2}{|v|} + \tau D_m \tag{3.54}$$

$$D_{yy} = \alpha_L \frac{v_y^2}{|v|} + \alpha_{TH} \frac{v_x^2}{|v|} + \alpha_{TV} \frac{v_z^2}{|v|} + \tau D_m \tag{3.55}$$

$$D_{zz} = \alpha_L \frac{v_z^2}{|v|} + \alpha_{TV} \frac{v_x^2}{|v|} + \alpha_{TV} \frac{v_y^2}{|v|} + \tau D_m \tag{3.56}$$

where α_L is the longitudinal dispersivity, while α_{TH} and α_{TV} are the transverse dispersivities in horizontal and vertical directions respectively. D_m is the molecular diffusion coefficient of the vapor in air. τ is the tortuosity which can be estimated by the equation proposed by Millinton and Quirk, given in Eq.(2.24). $|v|$ is the absolute value of the actual gas velocity and can be computed as;

$$|v| = \sqrt{v_x^2 + v_y^2 + v_z^2} \tag{3.57}$$

The vapor transport equation given in Eq.(3.53) can be expanded as:

$$\begin{aligned}\frac{\partial\left(\theta_g C\right)}{\partial t} &= \theta_g D_{xx}\frac{\partial^2 C}{\partial x^2}+\frac{\partial\left(\theta_g D_{xx}\right)}{\partial x}\frac{\partial C}{\partial x}-\frac{\partial\left(q_x C\right)}{\partial x}+\\ &+\theta_g D_{yy}\frac{\partial^2 C}{\partial y^2}+\frac{\partial\left(\theta_g D_{yy}\right)}{\partial y}\frac{\partial C}{\partial y}-\frac{\partial\left(q_y C\right)}{\partial y}+\\ &+\theta_g D_{zz}\frac{\partial^2 C}{\partial^2 z}+\frac{\partial\left(\theta_g D_{zz}\right)}{\partial z}\frac{\partial C}{\partial z}-\frac{\partial\left(q_z C\right)}{\partial z}+qc\end{aligned} \tag{3.58}$$

The finite difference form of Eq.(3.58) with Crank-Nicolson scheme is given as:

$$\frac{\theta^{n+1}_{g_{i,j,k}} C^{n+1}_{i,j,k}-\theta^{n}_{g_{i,j,k}} C^{n}_{i,j,k}}{\Delta t}=\frac{1}{2}\left(K^n+L^n-M^n+qc^n_{i,j,k}\right)+\frac{1}{2}\left(A^{n+1}+B^{n+1}-M^{n+1}+qc^{n+1}_{i,j,k}\right) \tag{3.59}$$

where

$$\begin{aligned}K^n &= \theta^n_{g_{i,j,k}} D^n_{xx_{i,j,k}}\frac{C^n_{i+1,j,k}-2C^n_{i,j,k}+C^n_{i-1,j,k}}{\Delta x^2}\\ &+\theta^n_{g_{i,j,k}} D^n_{yy_{i,j,k}}\frac{C^n_{i,j+1,k}-2C^n_{i,j,k}+C^n_{i,j-1,k}}{\Delta y^2}\\ &+\theta^n_{g_{i,j,k}} D^n_{zz_{i,j,k}}\frac{C^n_{i,j,k+1}-2C^n_{i,j,k}+C^n_{i,j,k-1}}{\Delta z^2}\end{aligned} \tag{3.60}$$

$$\begin{aligned}L^n &= \frac{\left(\theta^n_{g_{i+1,j,k}} D^n_{xx_{i+1,j,k}}-\theta^n_{g_{i-1,j,k}} D^n_{xx_{i-1,j,k}}\right)}{2\Delta x}\frac{\left(C^n_{i+1,j,k}-C^n_{i-1,j,k}\right)}{2\Delta x}\\ &+\frac{\left(\theta^n_{g_{i,j+1,k}} D^n_{yy_{i,j+1,k}}-\theta^n_{g_{i,j-1,k}} D^n_{yy_{i,j-1,k}}\right)}{2\Delta y}\frac{\left(C^n_{i,j+1,k}-C^n_{i,j-1,k}\right)}{2\Delta y}\\ &+\frac{\left(\theta^n_{g_{i,j,k+1}} D^n_{zz_{i,j,k+1}}-\theta^n_{g_{i,j,k-1}} D^n_{zz_{i,j,k-1}}\right)}{2\Delta z}\frac{\left(C^n_{i,j,k+1}-C^n_{i,j,k-1}\right)}{2\Delta z}\end{aligned} \tag{3.61}$$

$$M^{n} = \frac{q^{n}_{x\ i+1,j,k} C^{n}_{i+1,j,k} - q^{n}_{x\ i-1,j,k} C^{n}_{i-1,j,k}}{2\Delta x} + \frac{q^{n}_{y\ i,j+1,k} C^{n}_{i,j+1,k} - q^{n}_{y\ i,j-1,k} C^{n}_{i,j-1,k}}{2\Delta y} + \frac{q^{n}_{z\ i,j,k+1} C^{n}_{i,j,k+1} - q^{n}_{y\ i,j,k-1} C^{n}_{i,j,k-1}}{2\Delta z} \tag{3.62}$$

$$K^{n+1} = \theta^{n+1}_{g_{i,j,k}} D^{n+1}_{xx_{i,j,k}} \frac{C^{n+1}_{i+1,j,k} - 2C^{n+1}_{i,j,k} + C^{n+1}_{i-1,j,k}}{\Delta x^{2}} + \theta^{n+1}_{g_{i,j,k}} D^{n+1}_{yy_{i,j,k}} \frac{C^{n+1}_{i,j+1,k} - 2C^{n+1}_{i,j,k} + C^{n+1}_{i,j-1,k}}{\Delta y^{2}} + \theta^{n+1}_{g_{i,j,k}} D^{n+1}_{zz_{i,j,k}} \frac{C^{n+1}_{i,j,k+1} - 2C^{n+1}_{i,j,k} + C^{n+1}_{i,j,k-1}}{\Delta z^{2}} \tag{3.63}$$

$$L^{n+1} = \frac{\left(\theta^{n+1}_{g_{i+1,j,k}} D^{n+1}_{xx_{i+1,j,k}} - \theta^{n+1}_{g_{i-1,j,k}} D^{n+1}_{xx_{i-1,j,k}}\right)}{2\Delta x} \frac{\left(C^{n+1}_{i+1,j,k} - C^{n+1}_{i-1,j,k}\right)}{2\Delta x} + \frac{\left(\theta^{n+1}_{g_{i,j+1,k}} D^{n+1}_{yy_{i,j+1,k}} - \theta^{n+1}_{g_{i,j-1,k}} D^{n+1}_{yy_{i,j-1,k}}\right)}{2\Delta y} \frac{\left(C^{n+1}_{i,j+1,k} - C^{n+1}_{i,j-1,k}\right)}{2\Delta y} + \frac{\left(\theta^{n+1}_{g_{i,j,k+1}} D^{n+1}_{zz_{i,j,k+1}} - \theta^{n+1}_{g_{i,j,k-1}} D^{n+1}_{zz_{i,j,k-1}}\right)}{2\Delta z} \frac{\left(C^{n+1}_{i,j,k+1} - C^{n+1}_{i,j,k-1}\right)}{2\Delta z} \tag{3.64}$$

$$M^{n+1} = \frac{q^{n+1}_{x\ i+1,j,k} C^{n+1}_{i+1,j,k} - q^{n+1}_{x\ i-1,j,k} C^{n+1}_{i-1,j,k}}{2\Delta x} + \frac{q^{n+1}_{y\ i,j+1,k} C^{n+1}_{i,j+1,k} - q^{n+1}_{y\ i,j-1,k} C^{n+1}_{i,j-1,k}}{2\Delta y} + \frac{q^{n+1}_{z\ i,j,k+1} C^{n+1}_{i,j,k+1} - q^{n+1}_{y\ i,j,k-1} C^{n+1}_{i,j,k-1}}{2\Delta z} \tag{3.65}$$

The mass of the removed (volatilized) residual organic liquid from a cell in each time step can be approximated as;

$$m_{l_{i,j,k}}^{n} - m_{l_{i,j,k}}^{n+1} = \Delta t \frac{\left(qc_{i,j,k}^{n} + qc_{i,j,k}^{n+1}\right)}{2} \Delta x \Delta y \Delta z \tag{3.66}$$

where m_l is the mass of the residual organic liquid in a cell and the source term, *qc*, in each time step can be calculated as;

$$qc_{i,j,k}^{n} = \alpha_{i,j,k}^{n} \left(C_{i,j,k}^{n} - C_{eq_{i,j,k}}^{n}\right) \tag{3.67}$$

where the overall mass transfer coefficient can be computed as;

$$\alpha_{i,j,k}^{n} = \beta_1 \left(K_L a\right) \left(\theta_{l_{i,j,k}}^{n}\right)^{0.67} \tag{3.68}$$

where $\beta_1 (K_L a)$ is constant throughout the simulation, whereas, the volumetric liquid content θ_l is a time dependent parameter

The equilibrium concentration, C_{eq}, in Eq.(3.67) is also time dependent on account of the change in molar fraction of each constituent with time.

3.3. Validation of the Model

3.3.1. Testing the Unconfined Groundwater Flow Model

Prior to the application of the model to the real case, validity of the model should be checked. The testing operation can be carried out by simulating a simple case for which an analytical solution exists.

Some analytical solutions have been developed for the purpose of estimating the response of an unconfined aquifer to pumping. One of these solution techniques, proposed by Jacob, is based on the assumption that the unconfined aquifer behaves like a confined aquifer, so that it becomes possible to utilize transient solution developed by Theis. If the calculated drawdown is larger than 5% of the original saturated thickness, the drawdown

value should be corrected. The corrected drawdown in an unconfined aquifer can obtained by the expression presented in Eq.(2.5)

A simple fictional problem is created to be solved both numerically by the proposed model and analytically by utilizing Eq.(2.5). According to the created scenario, a fully penetrating well discharges 10 m^3/day of water from a homogeneous unconfined aquifer having a thickness of 10m. The hydraulic conductivity and the specific yield of the aquifer are assumed to be 1m/day and 0.1 respectively.

For the numerical solution, a square shaped domain with each side having a length of 300 m is taken. The pumping well is assumed to be located at the center of the domain. The horizontal plane of the domain is divided into 300 columns and 300 rows along *x* and *y* directions respectively. Grid spacings in both directions are taken as 1 m. The domain is vertically divided into 5 layers, each having a thickness of 2 m. The time length of the simulation and the time step are taken as 100 days and 3600 seconds respectively.

Throughout the numerical simulation, the head values along the lateral surfaces of the domain are kept constant on the basis of the assumption that the domain is surrounded by a source. In order to represent this source, imaginary recharge wells are used while applying the analytical solution (Ferris et al., 1962). The locations of the imaginary cells are illustrated in Figure 3.3.

The analytically and numerically obtained results are compared in Figure 3.4 and Figure 3.5. The accuracy of the numerical results with respect to the analytical ones are checked by utilizing the mean absolute error and the root mean squared error criteria, which are presented as;

$$Mean\ Absolute\ Error\ (MAE) = \frac{1}{n}\sum_{i=1}^{n}\left|\left(y_a - y_s\right)_i\right| \tag{3.69}$$

$$Root\ Mean\ Squared\ Error\ (RMSE) = \left[\ \frac{1}{n}\sum_{i=1}^{n}\left(y_a - y_s\right)_i^2\ \right]^{0.5} \tag{3.70}$$

where y_a and y_s are the analytically and the numerically obtained parameter values respectively for the i^{th} component of a comparison set and n is the number of points where the comparisons are made (Anderson and Woessner, 1992).

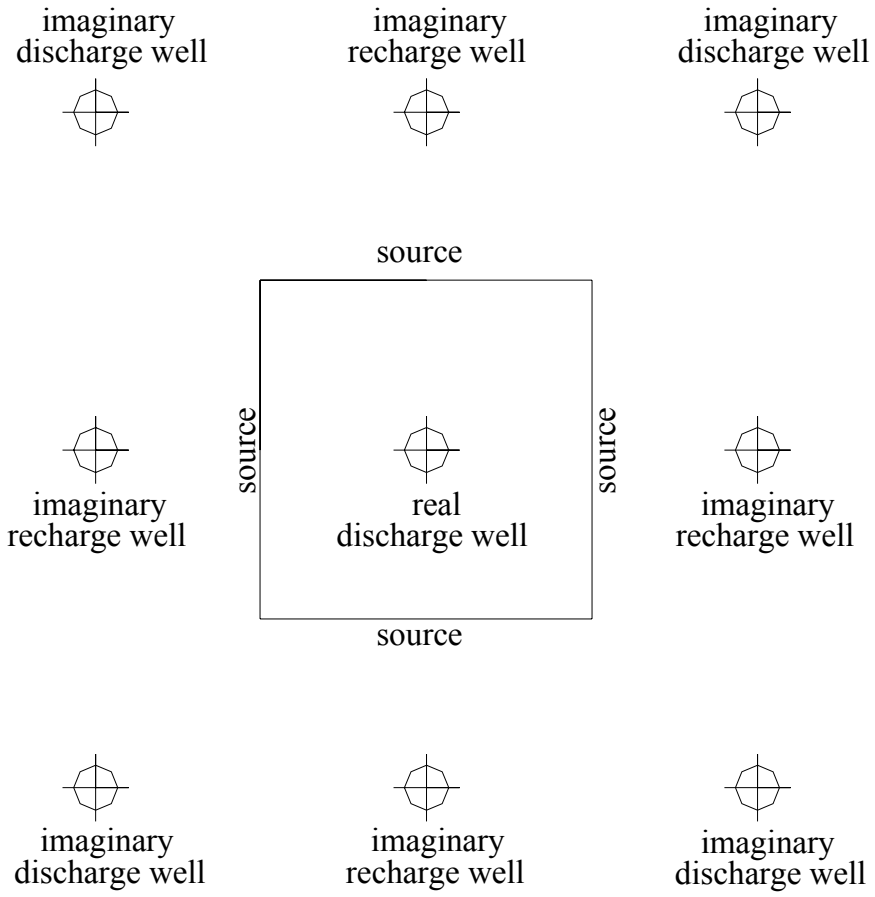

Figure 3.3. The imaginary wells used in analytical solution

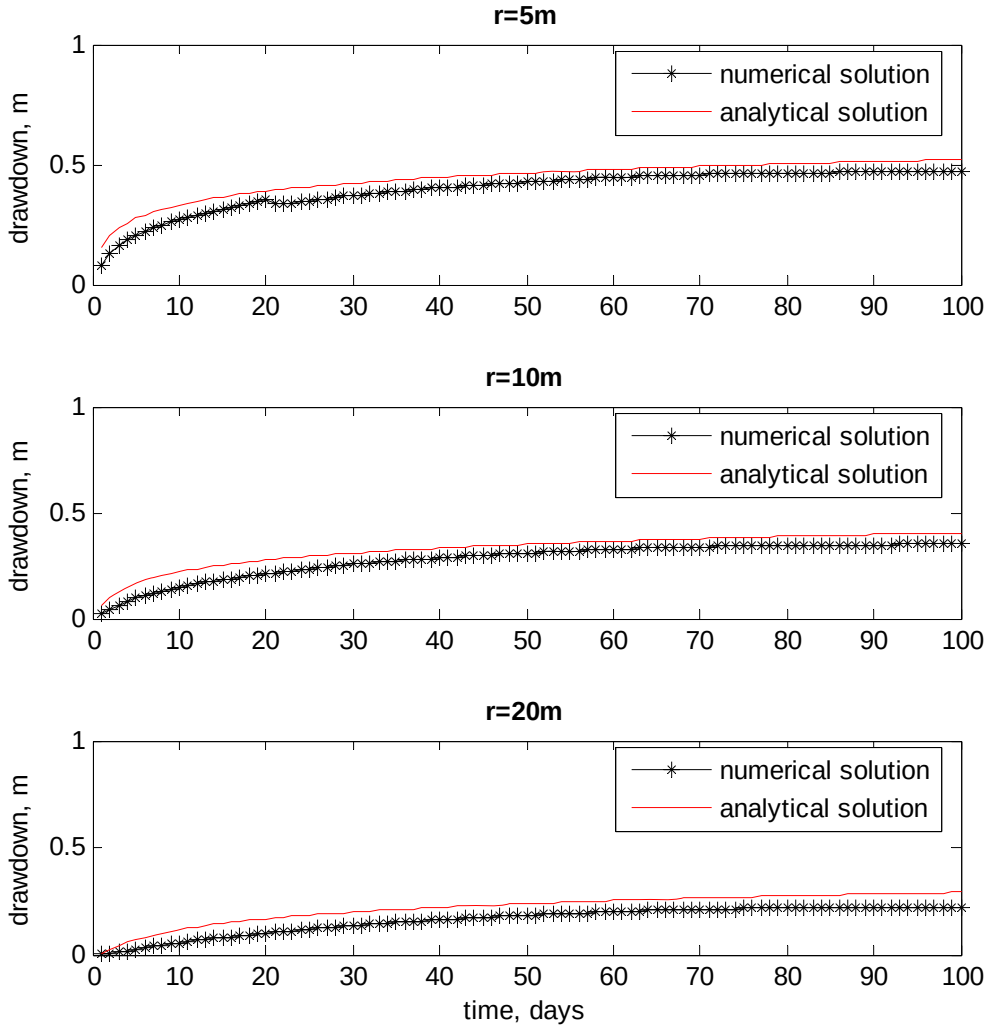

Figure 3.4. The change in drawdown values with time at 5 m, 10 m and 20 m from the pumping well.

Table 3.1. MAE and RMSE values for the time vs. drawdown curves at three different locations

	at r:5 m	at r:10 m	at r:20 m	Unit
Mean Absolute Error (MAE)	0.0223	0.0276	0.0361	m
Root Mean Squared Error (RMSE)	0.0249	0.0299	0.0368	m

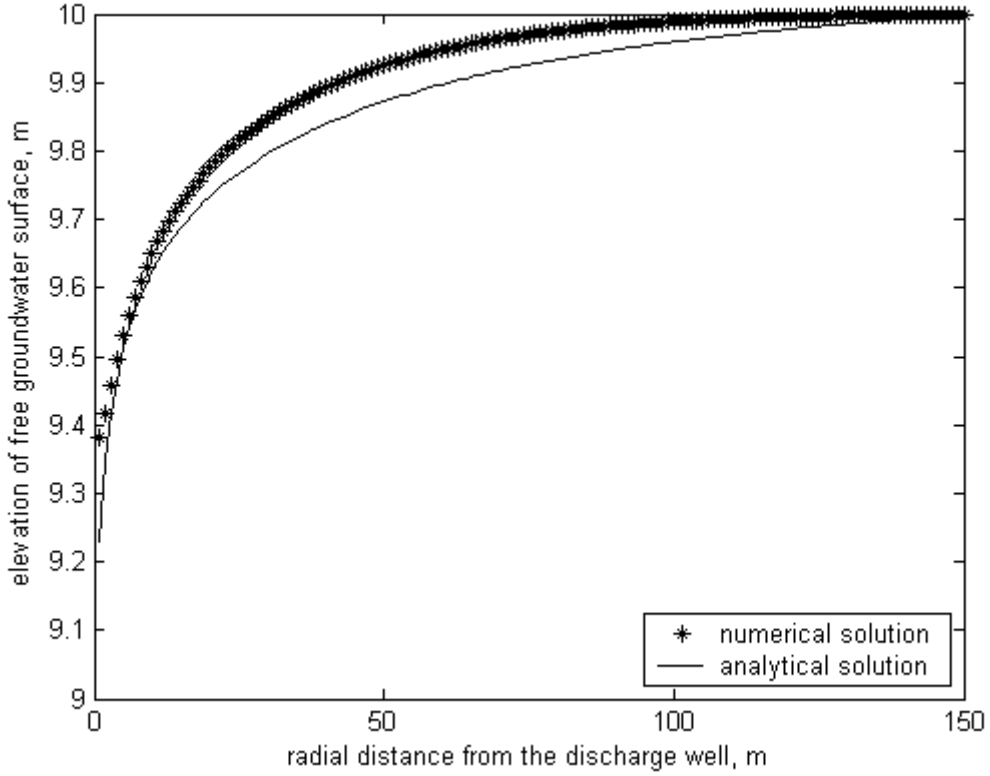

Figure 3.5. The change in groundwater surface elevation for the region extending 150 m from well at the end of 150 days.

The MAE and RMSE values for the curves presented in Figure 3.5 are found to be 0.0344 and 0.0394 m respectively.

In line with these results, the numerical solution is found to be consistent with the analytical one.

3.3.2. Testing the Air Flow Model

An analytical solution has been developed by Baehr and Joss (1995) to be used for estimating steady state air flow resulting from a partially penetrating extraction well. According to this proposed solution, given in Eq.(3.71), the top of the domain is assumed to be directly connected to the atmosphere, while the bottom boundary is considered to be impervious.

$$P = \sqrt{P_{air} + \frac{2aQ_m \mu RT}{M\pi^2 k_h (l_b - l_t) r_w} \left\{ \sum_{\hbar=1}^{\infty} \frac{1}{\hbar - \frac{1}{2}} \left[\frac{\cos(\sigma l_t) - \cos(\sigma l_b)}{\sigma K_1(\sigma \frac{r_w}{a})} \right] K_0\left(\sigma \frac{r}{a}\right) \sin(\sigma Z) \right\}} \quad (3.71)$$

where P is the air pressure at a point which has a radial distance of r from the well center line and has a vertical distance of Z from the land surface. Q_m is the constant mass flow rate due to extraction. r_w is the radius of the well. K_0 and K_1 are zero order and first order modified Bessel functions of the second kind respectively. k_h is horizontal air permeability, k_v is vertical air permeability and a is the square root of anisotropy ratio which is defined as $\sqrt{k_h / k_v}$. μ is the dynamic viscosity of the air phase, while R, T and M are universal gas constant, absolute temperature and average molecular weight of air phase respectively. l_t is the distance from the land surface to the top of the well screen while l_b represents the distance from the land surface to the bottom of the well screen. σ is defined as;

$$\sigma = \frac{\left(\hbar - \frac{1}{2}\right)\pi}{H} \quad (3.72)$$

where H is the vertical thickness of the domain.

In order to check the validity of the air flow model, a simulation is performed over a square shaped domain having a depth of 150 cm. The length and the width of the domain are taken as 810 cm. A well, located at the center of the domain, extracts air at a rate of 5 g/sec. The radius of the well is taken as 5 cm. The top and the bottom of the well screen are located at 60 cm and 120 cm below land surface respectively. The horizontal air permeability of the domain is 10^{-9} cm^2 and the vertical air permeability is 5×10^{-10} cm^2. The dynamic viscosity and the average molecular weight of the air phase are assumed to be 1.86×10^{-4} g / cm.sec and 29 g / mole respectively.

The plan view of the model grid is shown in Figure 3.6

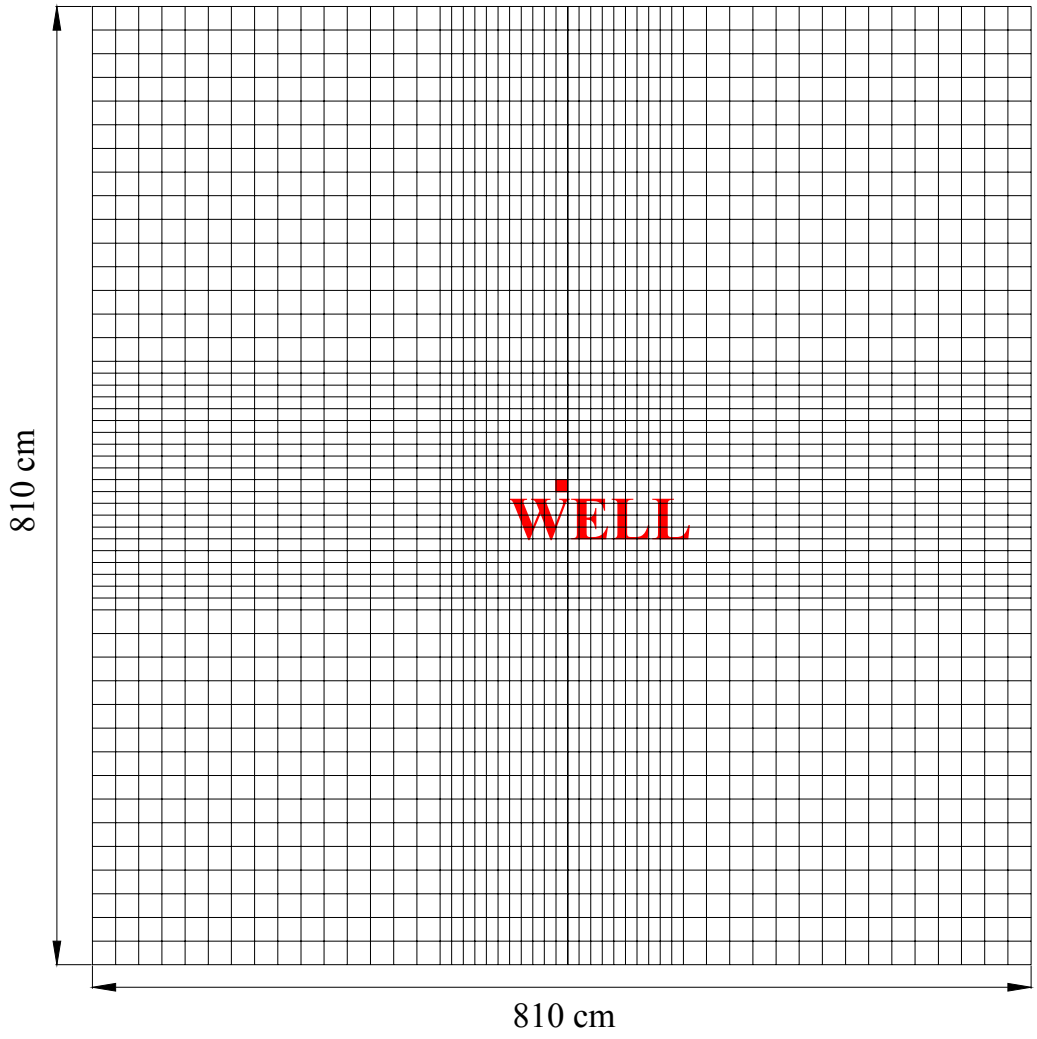

Figure 3.6. Plan view of the model grid

The domain is vertically divided into equally spaced 15 layers. Since well screen is positioned between 60 cm and 120 cm below land surface, the cells representing the well are found between 7^{th} and 12^{th} layers.

The curves in Figure 3.7 represent the steady state pressure distribution at 55 cm below ground surface.

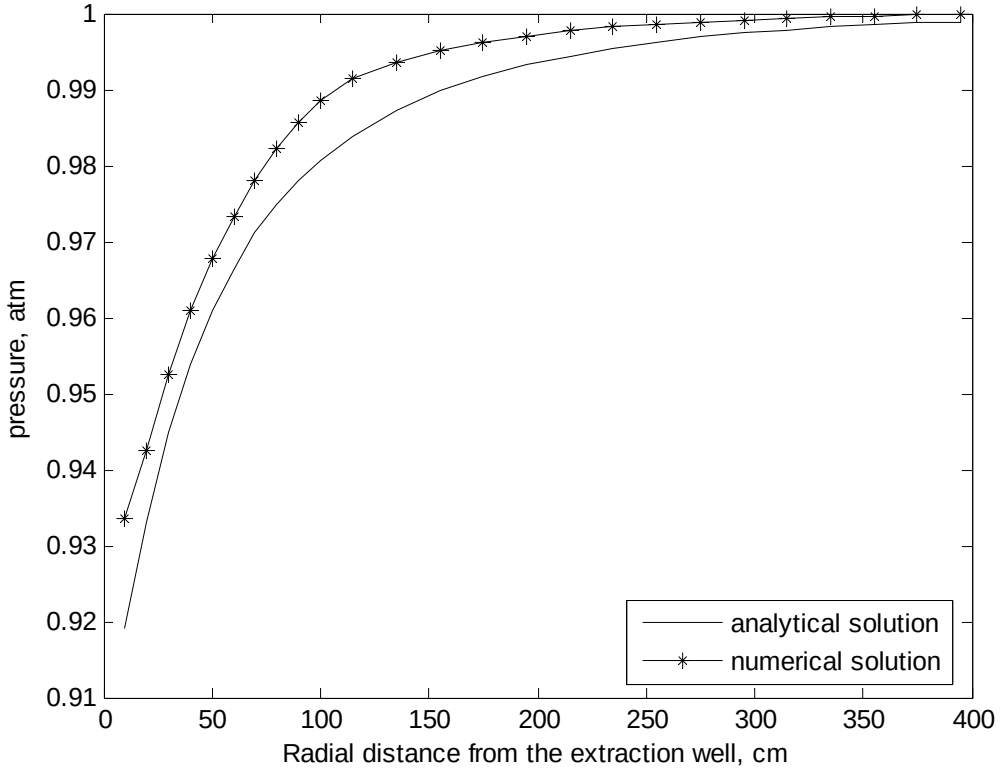

Figure 3.7. Steady state pressure distribution at 55 cm below ground surface

The MAE and RMSE values for the numerically and analytically obtained pressure distribution curves are calculated as 0.003 and 0.0035 atm respectively. The gap between the curves given in Figure 3.7 is primarily due to the specified boundary conditions for the numerical model, whereas, the utilized analytical solution was developed for a domain of infinite extent.

3.3.3. Testing the Vapor Transport Model

The transient advection-diffusion equation for instantaneously released point source can be solved analytically via the following expression.

$$C(x,y,z,t) = \frac{m}{(4\pi t)^{3/2}\left(D_{xx}D_{yy}D_{zz}\right)^{0.5}} e^{\left(-\frac{(x-v_x t)^2}{4D_{xx}t} - \frac{(y-v_y t)^2}{4D_{yy}t} - \frac{(z-v_z t)^2}{4D_{zz}t}\right)} \tag{3.73}$$

where m is the mass of the point source (Baetslé, 1969).

A simple scenario is developed in order to apply both the analytical solution given in Eq.(3.73) and the proposed numerical model. A chemical substance having a mass of 100 mg is released to a porous system, where specific discharge of the flow in longitudinal (x) direction is known to be $5\times10^{-2}\,\mathrm{cm/sec}$, while it is $10^{-2}\,\mathrm{cm/sec}$ in transverse (y) direction and $10^{-4}\,\mathrm{cm/sec}$ in vertical (z) direction. The porosity of the system is found to be 0.3. The dispersivity values in x, y and z directions are taken as 2 cm, 1 cm and 0.5 cm respectively. The diffusion coefficient of the substance is $0.4\,\mathrm{cm^2/sec}$.

For the numerical simulation, the horizontal plane of the domain is divided into 61 rows and 61 columns and vertically divided into 41 layers. Figure 3.8 and Figure 3.9 show the planar and cross sectional views of the grid respectively. The point source is released from the origin.

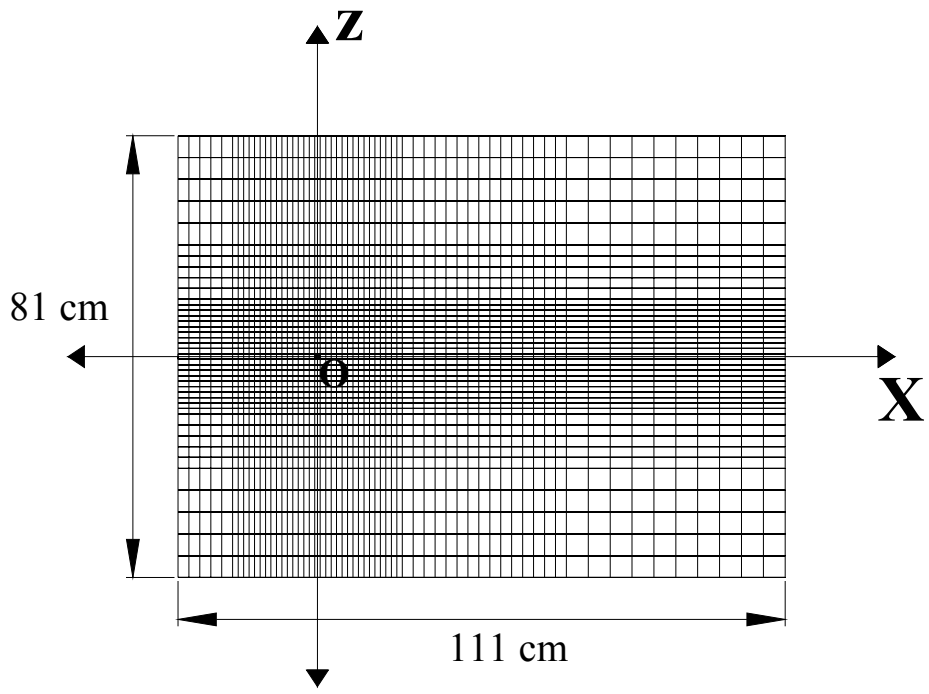

Figure 3.8. The cross sectional view of the model grid

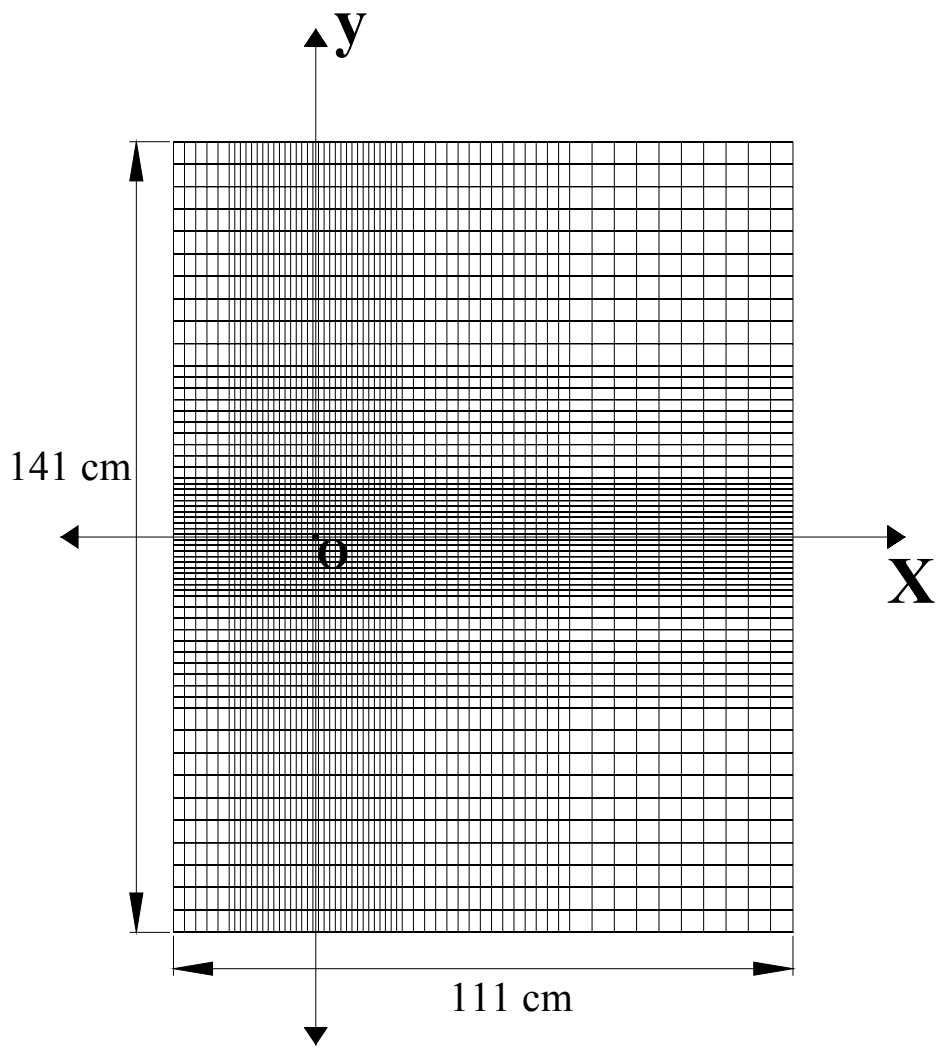

Figure 3.9. The plan view of the model grid

The simulation is performed for a time period of 100 seconds and the time interval is taken as 1 second.

In Figure 3.10 simulation results are compared to the results obtained by the analytical solution. As seen in this figure, the analytically and numerically attained concentration curves are quite close to each other, therefore the proposed numerical solution can be considered satisfactory. The error analysis results, based on these curves, are tabulated in Table 3.2.

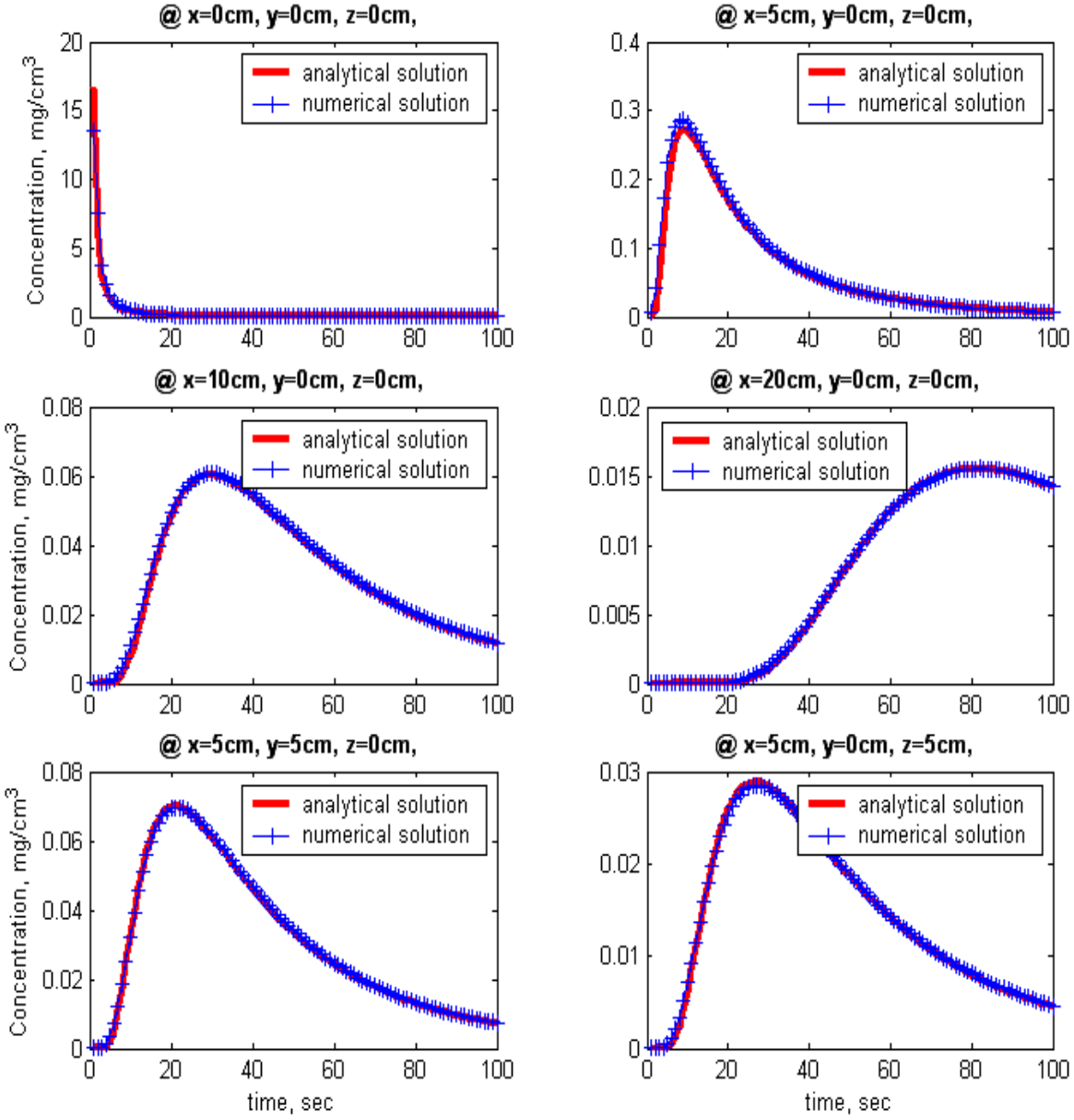

Figure 3.10. The change in concentration with time at 6 different locations.

Table 3.2. MAE and RMSE values for the concentration vs. time curves at six dfferent locations

	x: 0 cm y: 0 cm z: 0 cm	x: 5 cm y: 0 cm z: 0 cm	x: 10 cm y: 0 cm z: 0 cm	x: 20 cm y: 0 cm z: 0 cm	x: 5 cm y: 5 cm z: 0 cm	x: 5 cm y: 0 cm z: 5 cm	Unit
MAE	0.0691	0.0042	0.0006	0.0001	0.0004	0.0002	g/cm^3
RMSE	0.3723	0.0099	0.0009	0.0001	0.0005	0.0003	g/cm^3

4. IMPLEMENTATION OF THE MODEL FOR THE GASOLINE STATION SITE

4.1. The Grid Properties

The gas station site is represented by a rectangular domain extending over an area of 34000 m^2 as illustrated in Figure 1.1. The model domain has a length of 230 m in East-West direction and a length of 145 m in North-South direction, with a depth of 48 m. The domain is divided into 230 columns in East-West direction, represented by the *x*-axis, and divided into 145 rows along y axis which accounts for the North-South direction. The grid spacings both in x and y directions are taken as 1 m. The domain is vertically divided into 18 layers with variable grid spacings as shown in Figure 4.1.

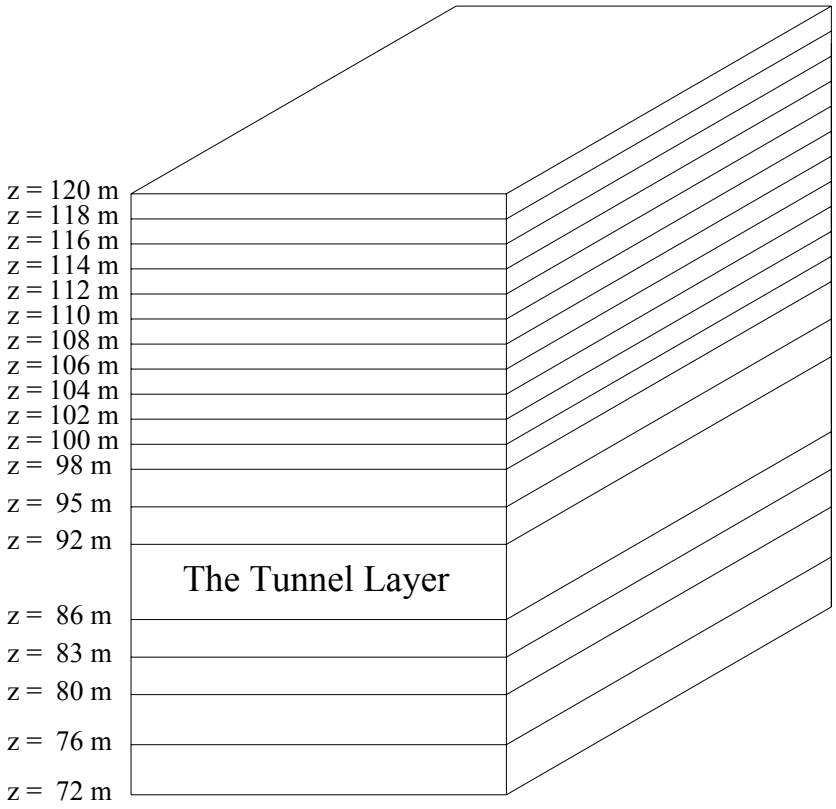

Figure 4.1. Illustration of the model layers

4.2. The Boundary Conditions

During the groundwater flow simulation, the hydraulic head values on the lateral surfaces of the domain are assumed to remain constant. Also the cells which represent the tunnels are constant–head cells, at each of which the head is equal to the bottom elevation of the tunnel. Due to the ongoing construction work, the tunnel progressively gets longer with time, thus an ordinary active cell becomes a constant-head cell in case the construction work reaches that cell. The groundwater is assumed to be underlain by an impervious layer, therefore the head gradient along the vertical direction at the bottom layer is taken as zero. Due to the impervious formation to the North-West of the domain, the cells at this zone are no-flow cells with zero head gradient along all directions.

During vapor extraction simulation, the pressure at a vapor extraction cell is constant throughout the simulation. The cells on the lateral surfaces are constant-pressure cells as per the assumption that these cells are not subject to the influence by the extraction well. The vapor concentration values are assumed to be zero on the lateral surfaces of the domain. Since groundwater acts as a barrier, the pressure and concentration gradients along the vertical direction at the groundwater table are assumed to be zero. Similarly the gradients along the vertical direction at the ground surface can also be considered zero, based on the assumption that the surface is paved with an impervious material.

For vapor flow simulation, the saturated cells are taken into account as no-flow cells, however when a saturated cell gets dry due to the dewatering of the aquifer, it is converted to an active cell.

Two and three-dimensional illustrations of the boundary conditions are presented in Figure 4.2 and Figure 4.3.

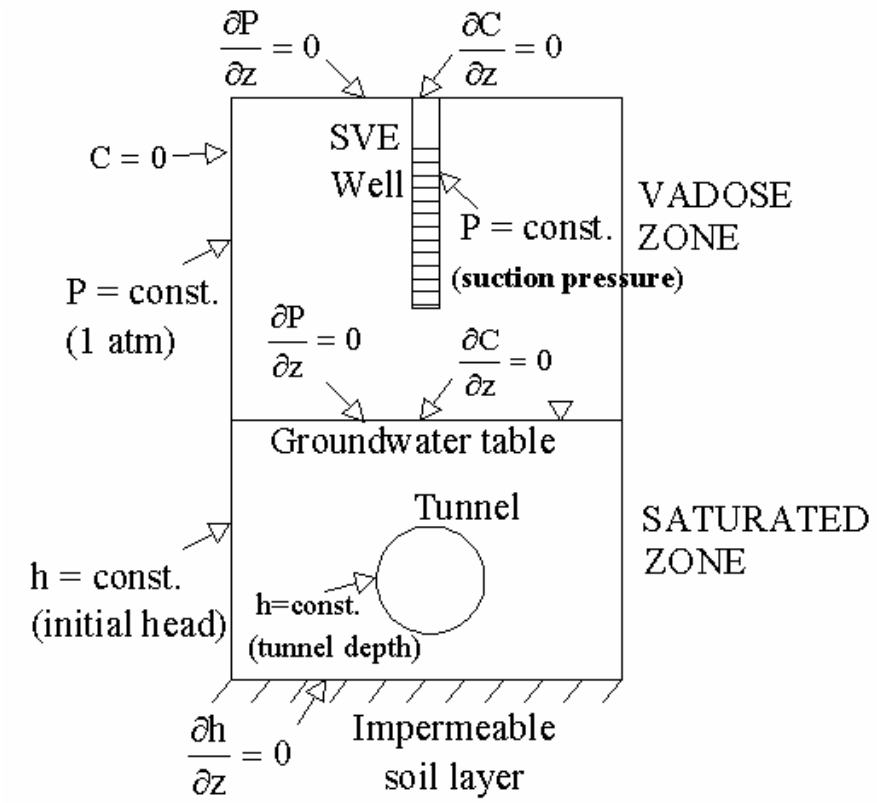

Figure 4.2. Two-dimensional illustration of the boundary conditions (*x*-*z* plane)

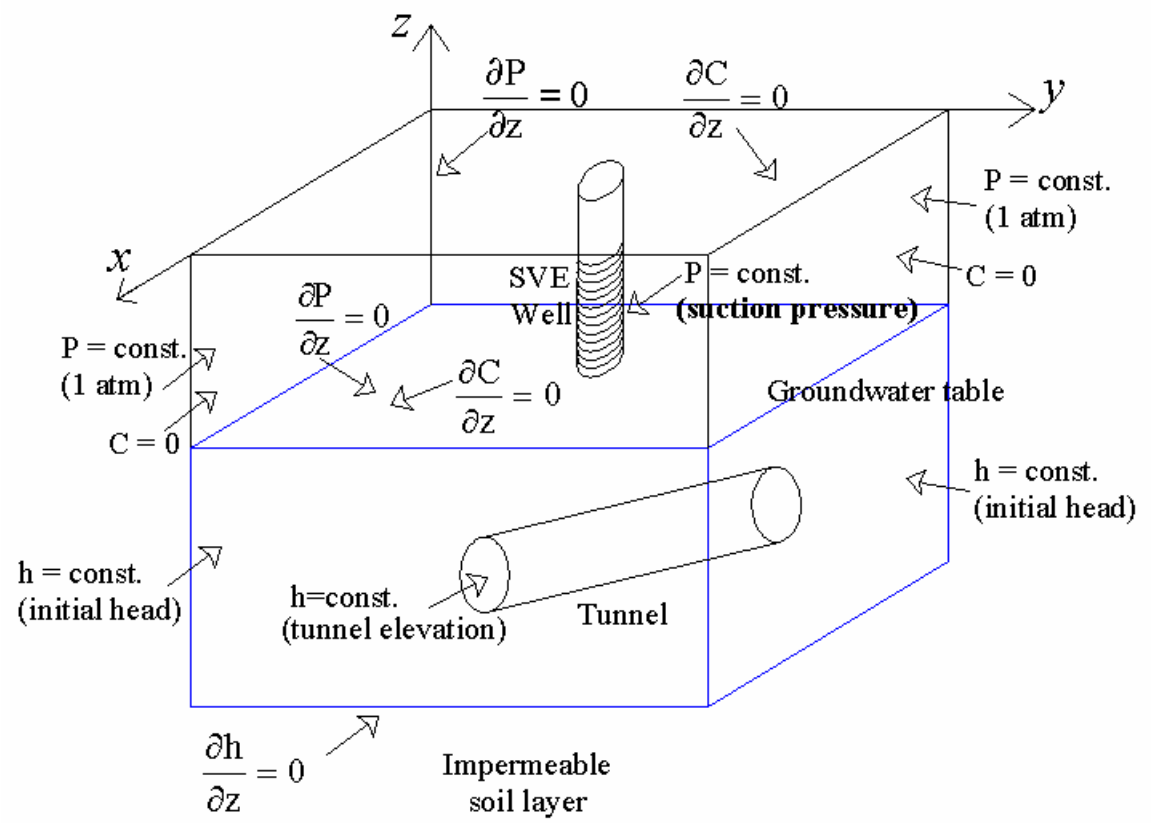

Figure 4.3. Three-dimensional illustration of the boundary conditions

4.3. The Initial Conditions

The initial head values to be used in groundwater flow simulation are specified by utilizing past site data. The initial groundwater table is illustrated in Figure 1.2.

Initially all of the cells in the vadose zone are assumed to be under atmospheric pressure.

The initial vapor concentrations of each organic constituent are estimated on the assumption that the gas and the liquid phases of the organic compounds are in equilibrium.

Initial residual organic concentrations in the vadose zone at different soil depths, defined by interpolating the site data, are presented in Figure 4.4 through Figure 4.19.

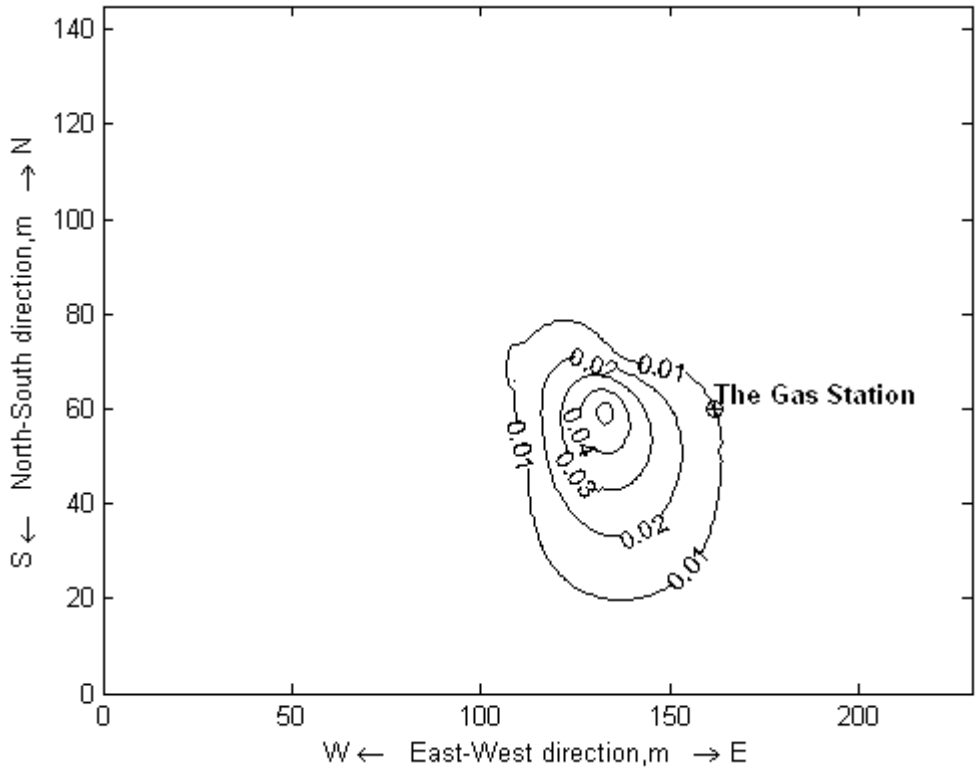

Figure 4.4. Residual benzene concentration at 3 m below ground surface (mg/kg)

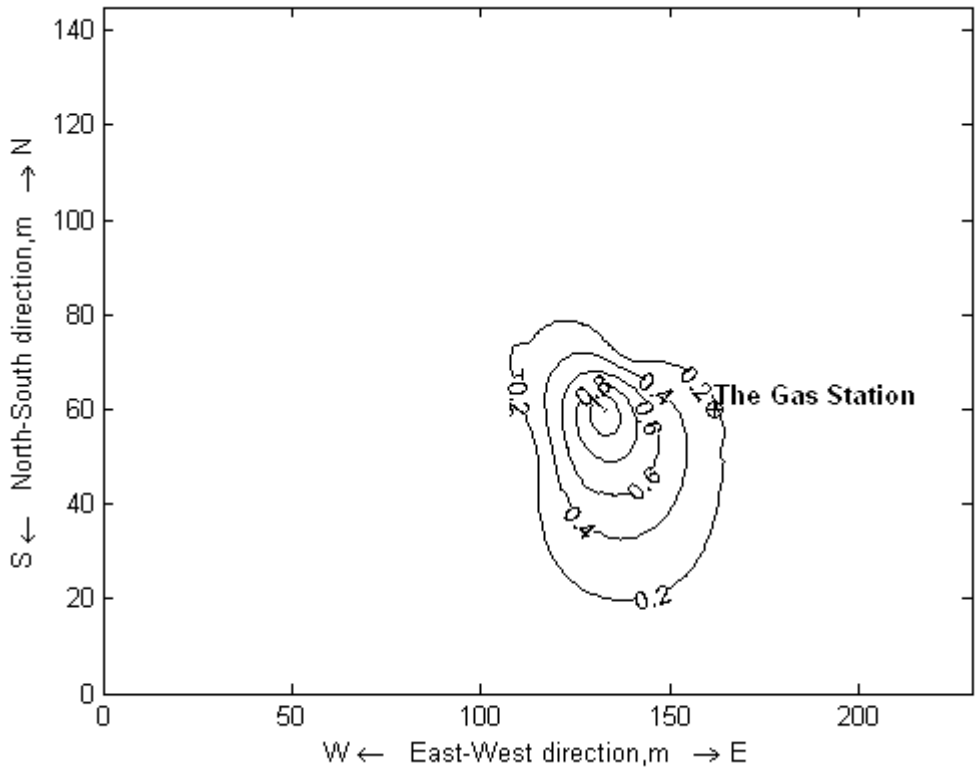

Figure 4.5. Residual benzene concentration at 5 m below ground surface (mg/kg)

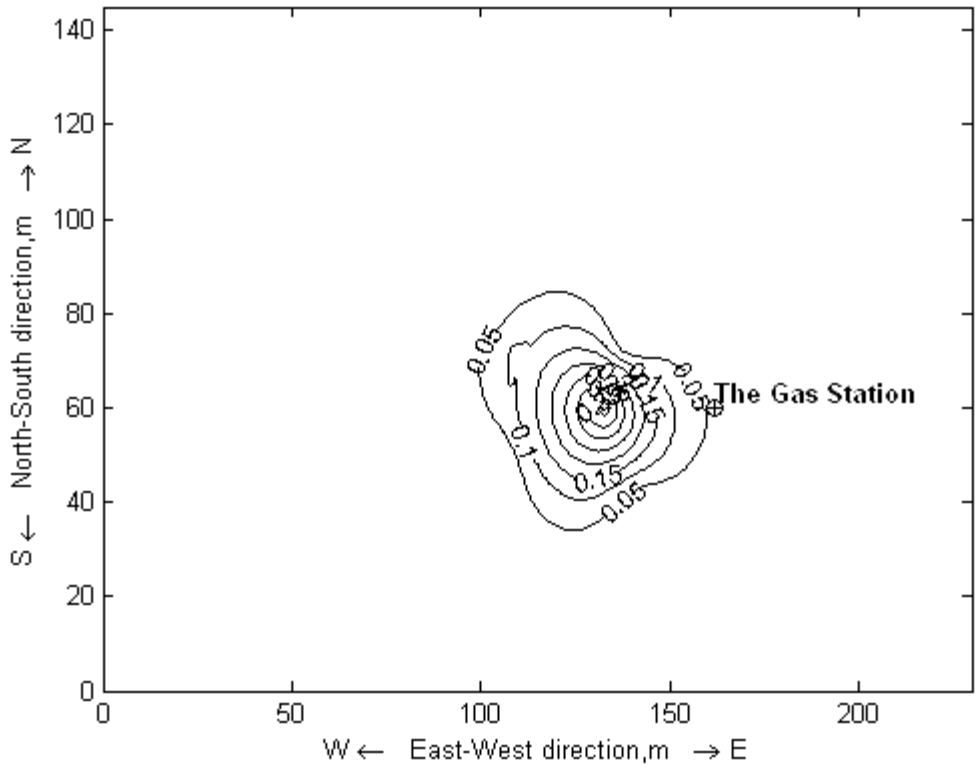

Figure 4.6. Residual benzene concentration at 7 m below ground surface (mg/kg)

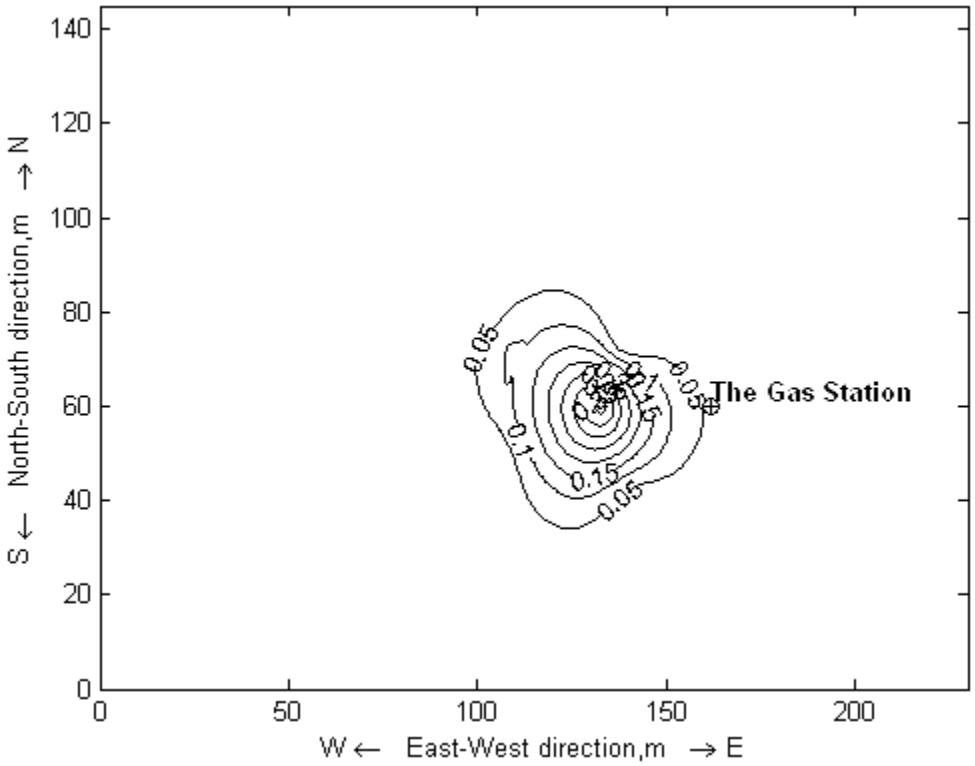

Figure 4.7. Residual benzene concentration at 9 m below ground surface (mg/kg)

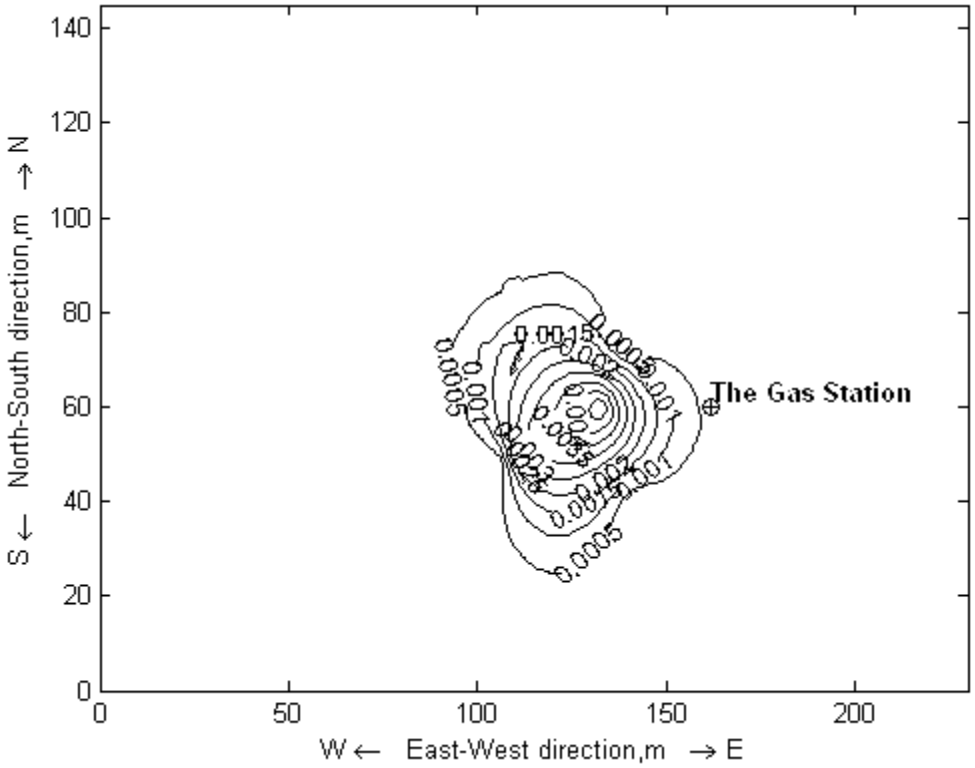

Figure 4.8. Residual toulene concentration at 3 m below ground surface (mg/kg)

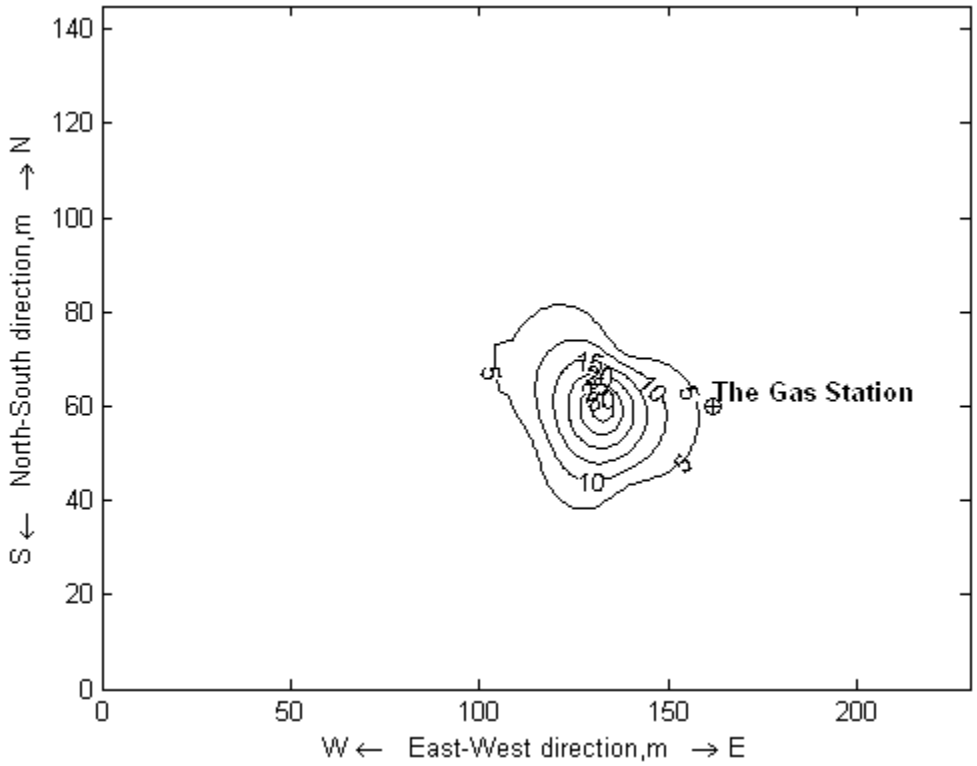

Figure 4.9. Residual toulene concentration at 5 m below ground surface (mg/kg)

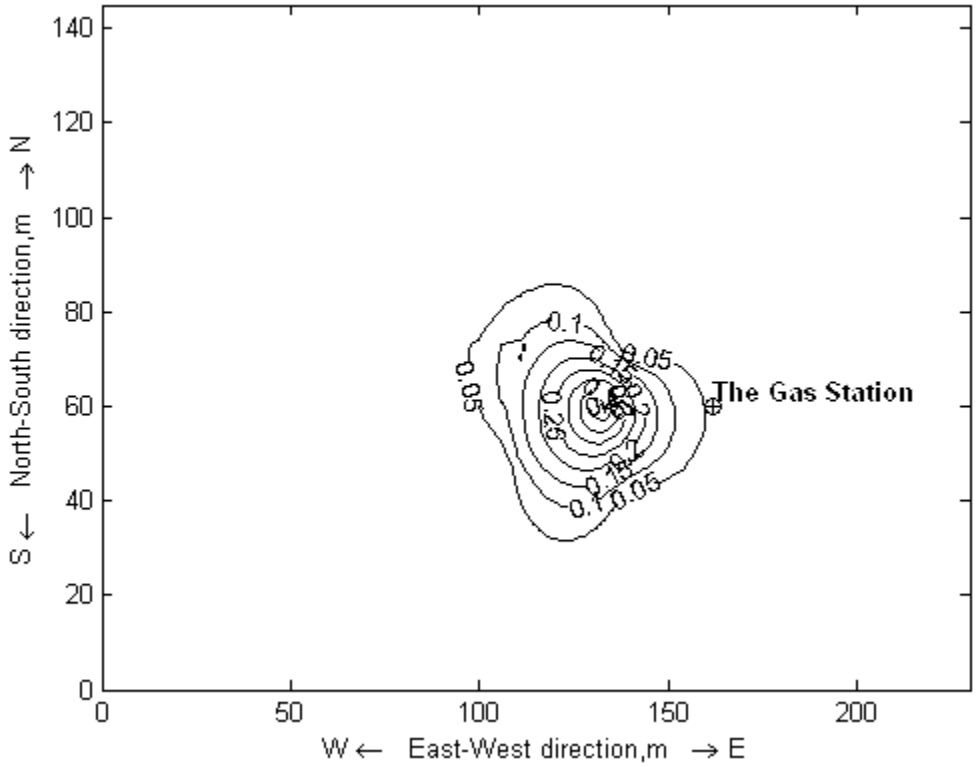

Figure 4.10. Residual toulene concentration at 7 m below ground surface (mg/kg)

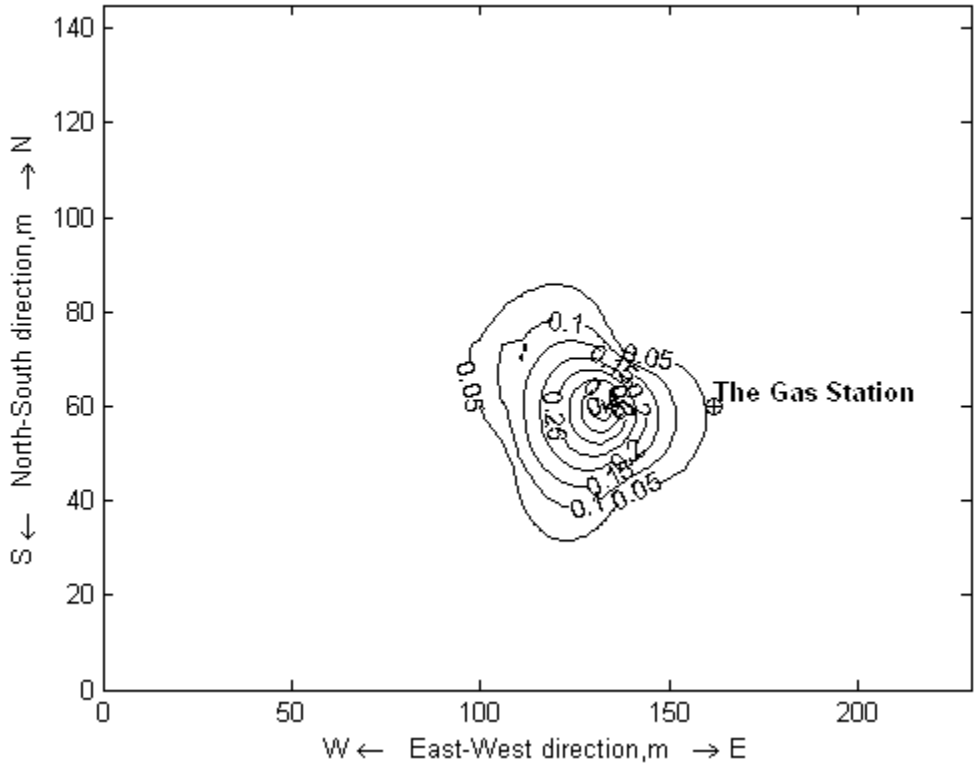

Figure 4.11. Residual toulene concentration at 9 m below ground surface (mg/kg)

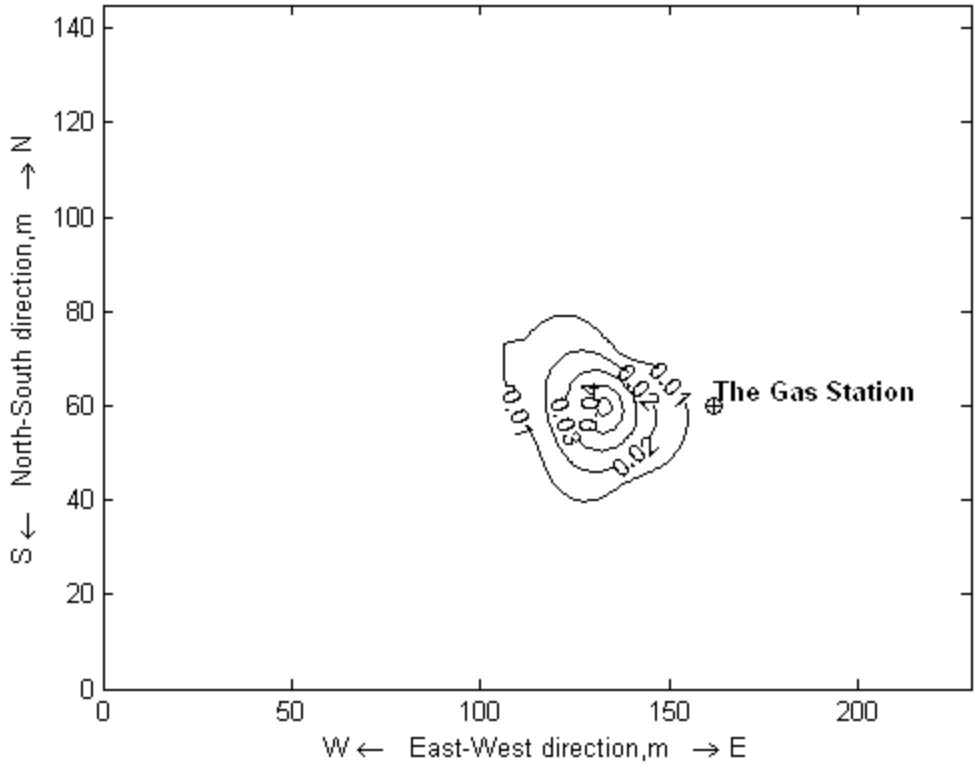

Figure 4.12. Residual ethylbenzene concentration at 3 m below ground surface (mg/kg)

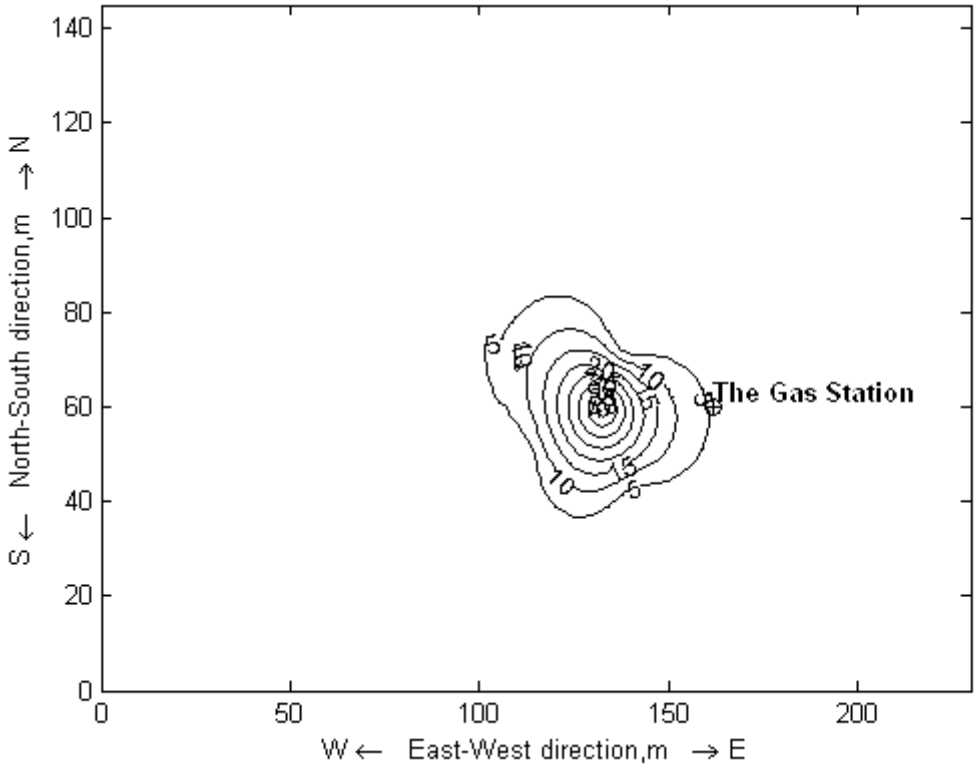

Figure 4.13. Residual ethylbenzene concentration at 5 m below ground surface (mg/kg)

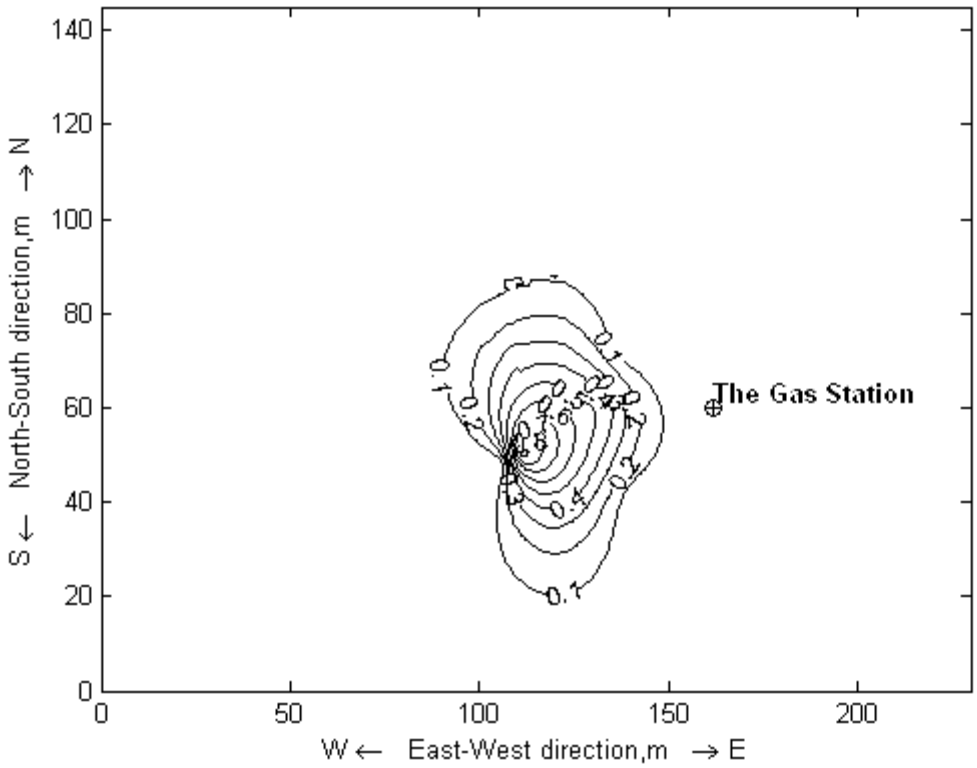

Figure 4.14. Residual ethylbenzene concentration at 7 m below ground surface (mg/kg)

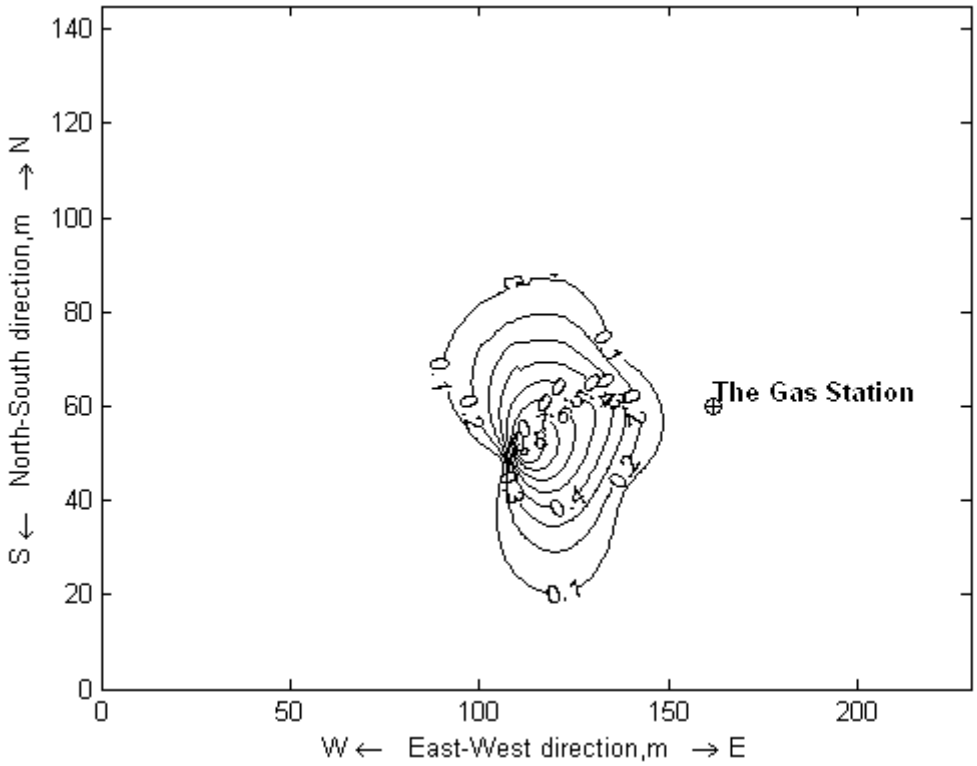

Figure 4.15. Residual ethylbenzene concentration at 9 m below ground surface (mg/kg)

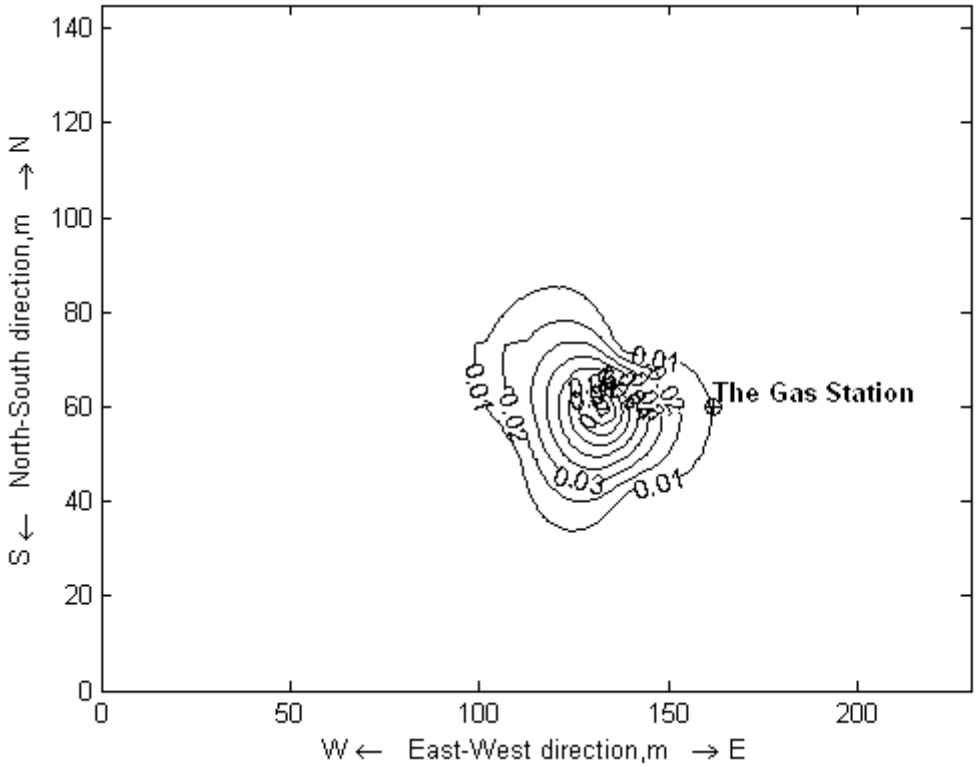

Figure 4.16. Residual xylene concentration at 3 m below ground surface (mg/kg)

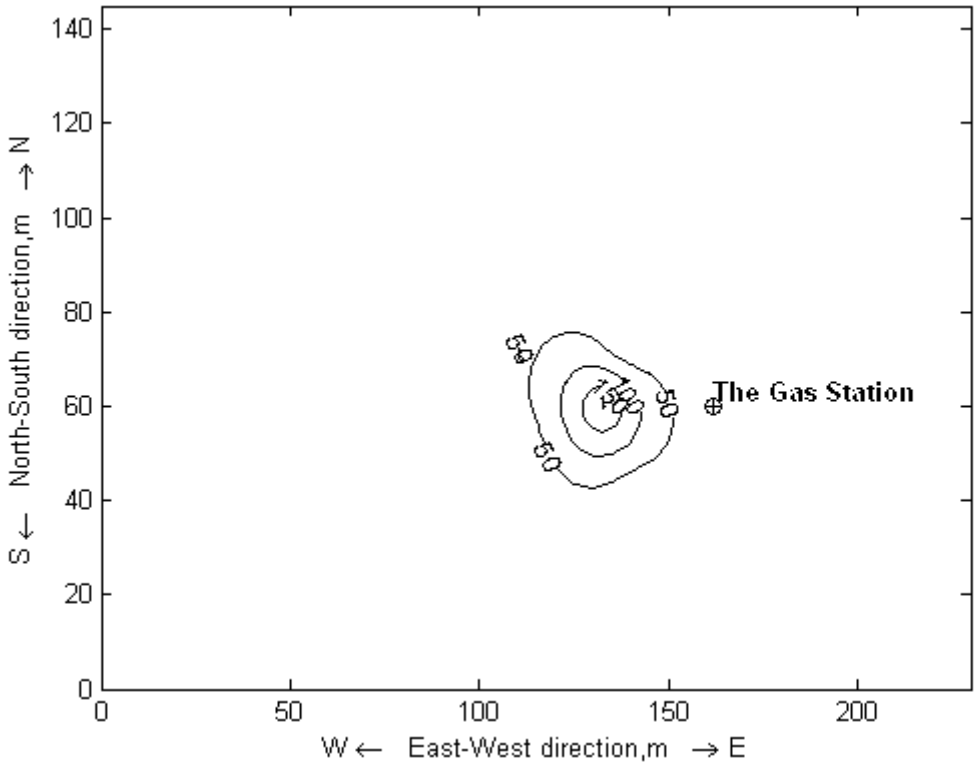

Figure 4.17. Residual xylene concentration at 5 m below ground surface (mg/kg)

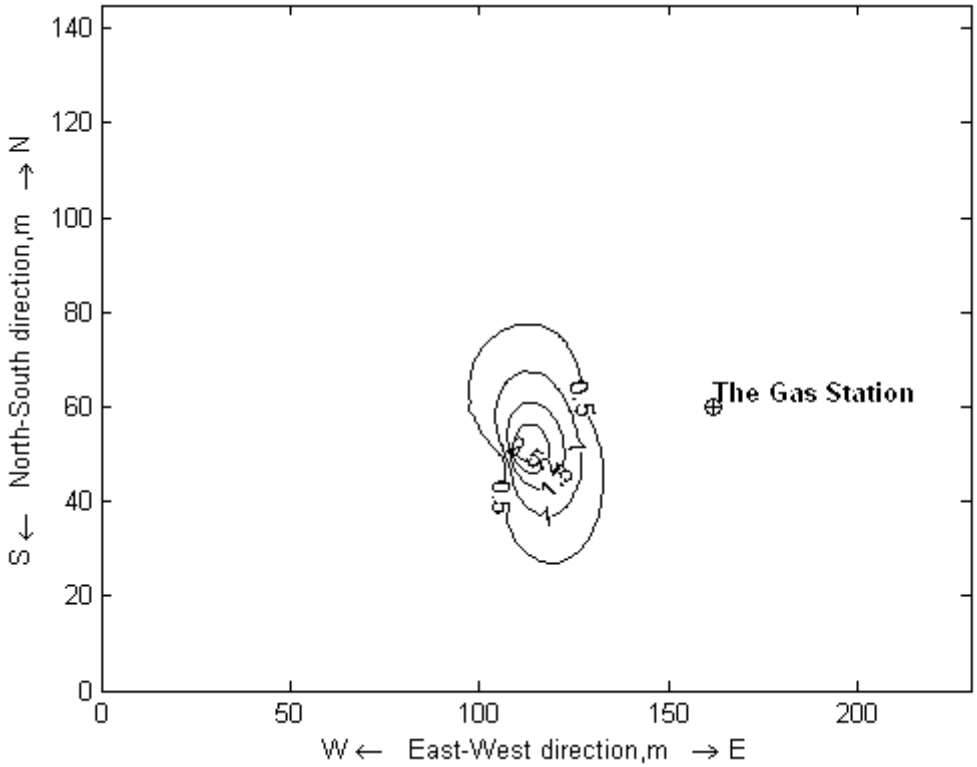

Figure 4.18. Residual xylene concentration at 7 m below ground surface (mg/kg)

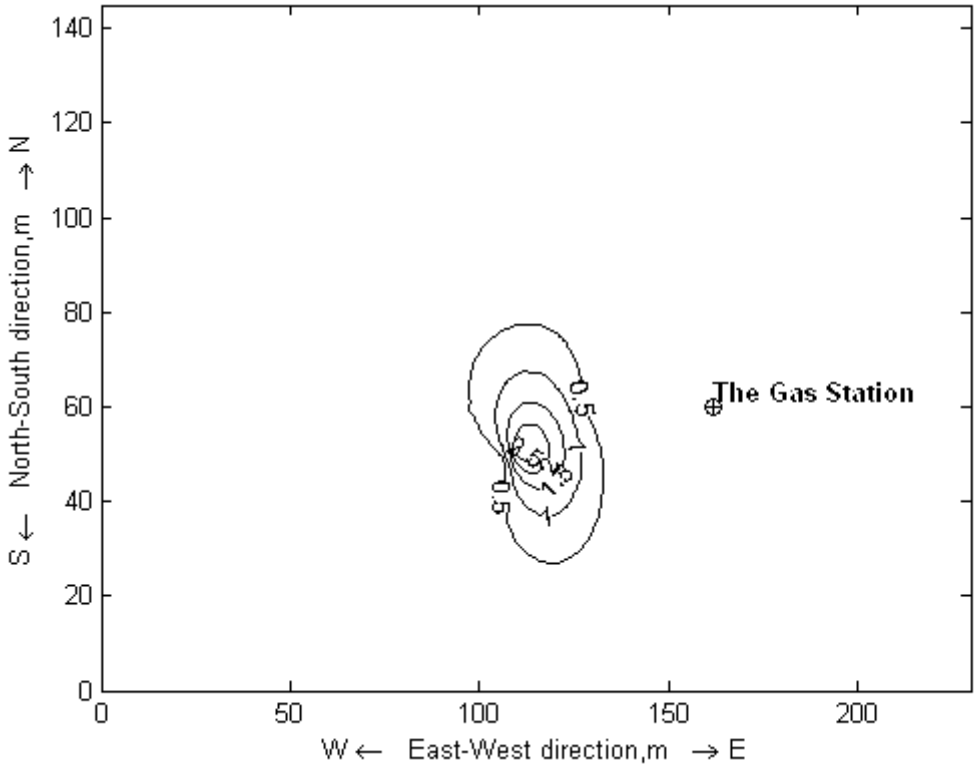

Figure 4.19. Residual xylene concentration at 9 m below ground surface (mg/kg)

4.4. The Model Parameters

Based on the geological and hydrogeological information gathered from the site, the model parameters are specified. These parameters are presented in Table 4.1 and Table 4.2.

Six soil vapor extraction wells, of which locations are displayed in Figure 1.1, are operating at the site. The top and the bottom levels of the well screens are known to be located at 4 m and 12 m respectively below ground surface.

Table 4.1. The Model Parameters

Molecular weight of the air, M_{air}		29	g/mole
Viscosity of the air, μ_{air}		1.84E-04	g/cm-sec
Density of the air, ρ_{air}		1.24E-03	g/cm^3
The atmospheric pressure		1	atm
The suction pressure		0.5	atm
Temperature of the air, T		300	^oK
The gas constant, R		8.31E-07	cm^2-gm/sec^2-mole-^oK
Intrinsic air permeability in x dir., k_{xx}		1.00E-09	cm^2
k_{xx}/k_{yy}		1	-
k_{xx}/k_{zz}		2	-
Longitudinal dispersivity, α_L		0.02	m
Transverse dispersivity, α_{TH}		0.02	m
Vertical dispersivity, α_{TV}		0.002	m
Soil bulk density, ρ_b		1.6	g/cm^3
Irreducible moisture content, θ_r		1.00E-06	cm^3/cm^3
Particle size index, λ		2	-
Porosity, θ		0.2	-
Specific storage, S_s		0.0001	m^{-1}
Specific yield, S_y		0.025	-
Hydraulic Conductivity along x direction, K_{xx}	1st layer -6th layer	0.025	m/day
	7th layer	0.02	m/day
	8th layer	0.015	m/day
	9th layer	0.01	m/day
	10th layer	0.005	m/day
	11th layer	0.0025	m/day
	12th layer	0.002	m/day
	13th layer - 18th layer	0.001	m/day
K_{xx}/K_{yy}		1	-
K_{xx}/K_{zz}		1	-

Table 4.2. The properties of the VOCs detected at the site

		Benzene	**Toulene**	**Ethylbenzene**	**Xylene**	Unit
Density, ρ		0.879	0.867	0.867	0.864	g/cm^3
Mass transfer coefficient, $\alpha/\theta_l^{0.67}$		6.00E-04	5.50E-04	4.50E-04	4.50E-04	1/sec
Diffusion coefficient in air, D_m		9.23E-06	8.30E-06	7.07E-06	7.60E-06	m^2/sec
Molecular weight, M		78.12	92.13	106.18	106.18	g/mole
Antoine's vapor pressure constants	A_1	6.89272	6.95805	6.9565	7.00646	-
	A_2	1203.531	1346.773	1423.543	1460.183	-
	A_3	219.888	219.693	213.091	214.827	-

4.5. The Utilized Assumptions

In this study the groundwater flow model is developed by utilizing the governing equations valid for porous systems. However some fractures have been detected at the deeper sections of the site. For such systems, Berkowitz et al.(1988) propose *the equivalent porous media approach* in which, rather than using the parameters of the fractured system, parameters of an equivalent non-fractured porous system are used. The equivalent porous system parameters are specified so that the flow pattern in the equivalent porous medium shows similarity with the flow pattern in the fractured system. *The equivalent porous media approach* is implemented in this study.

Movement of the organic liquid contaminants, is neglected in this work. Vapor sorption on soil matrix and the chemical reactions among the organic constituents are also assumed to be negligible.

The advective vapor movement is only due to the externally induced suction pressure. Other factors, such as gravitational force, are presumed to have no effect on the vapor flow.

The groundwater is assumed to be free of organic contaminants. It is presumed that there exists no interaction between the groundwater and the soil air in terms of contaminant mass transfer.

In the developed model, the residual water content in the unsaturated zone is not taken into account. While liquid content is defined, only the non-aqueous volatile organic liquid is considered.

5. RESULTS AND DISCUSSION

5.1. Results From Groundwater Dewatering Simulation

A simulation is performed in order to investigate the movement of the free groundwater surface within a period of four months. The contour lines in Figure 5.1 stand for the equipotential lines for the groundwater flow at the end of 4 months. Since the flow is unconfined, these lines also represent the groundwater table.

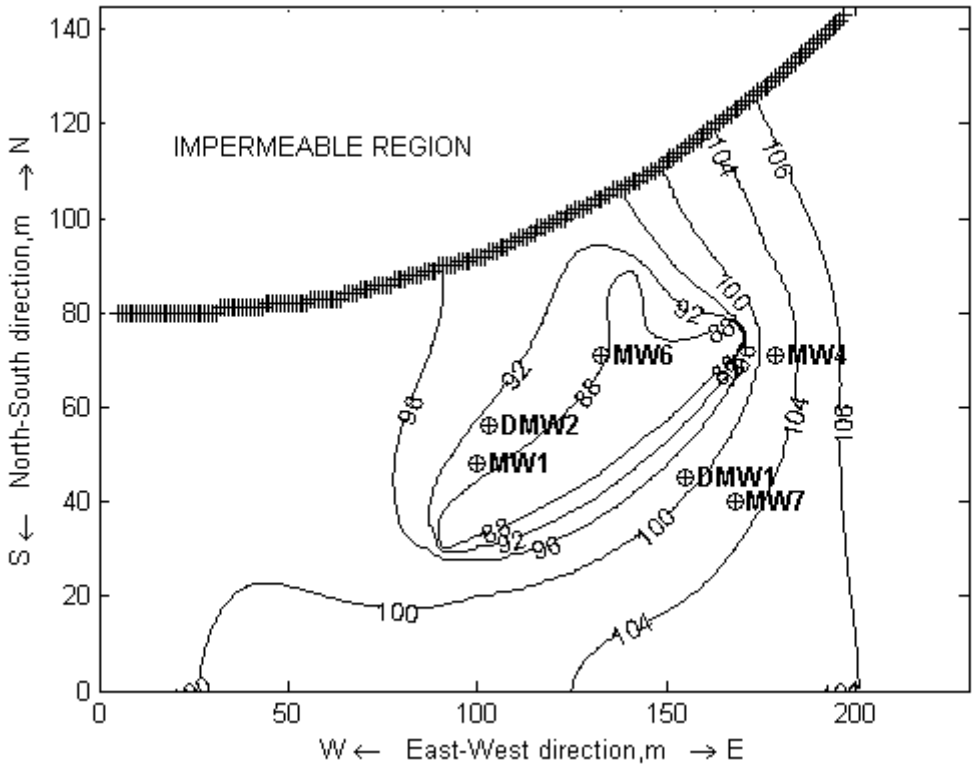

Figure 5.1. Equipotential lines for the groundwater flow at the end of 4 months

The radius of influence created by the tunnels is detected to be small on account of the low hydraulic conductivity of the geological formation. As a consequence of this, a deep cone of depression develops in the vicinity of the tunnels, where the groundwater table drops to the depth of the tunnels. In Figure 5.2 the three-dimensional view of the groundwater table is presented.

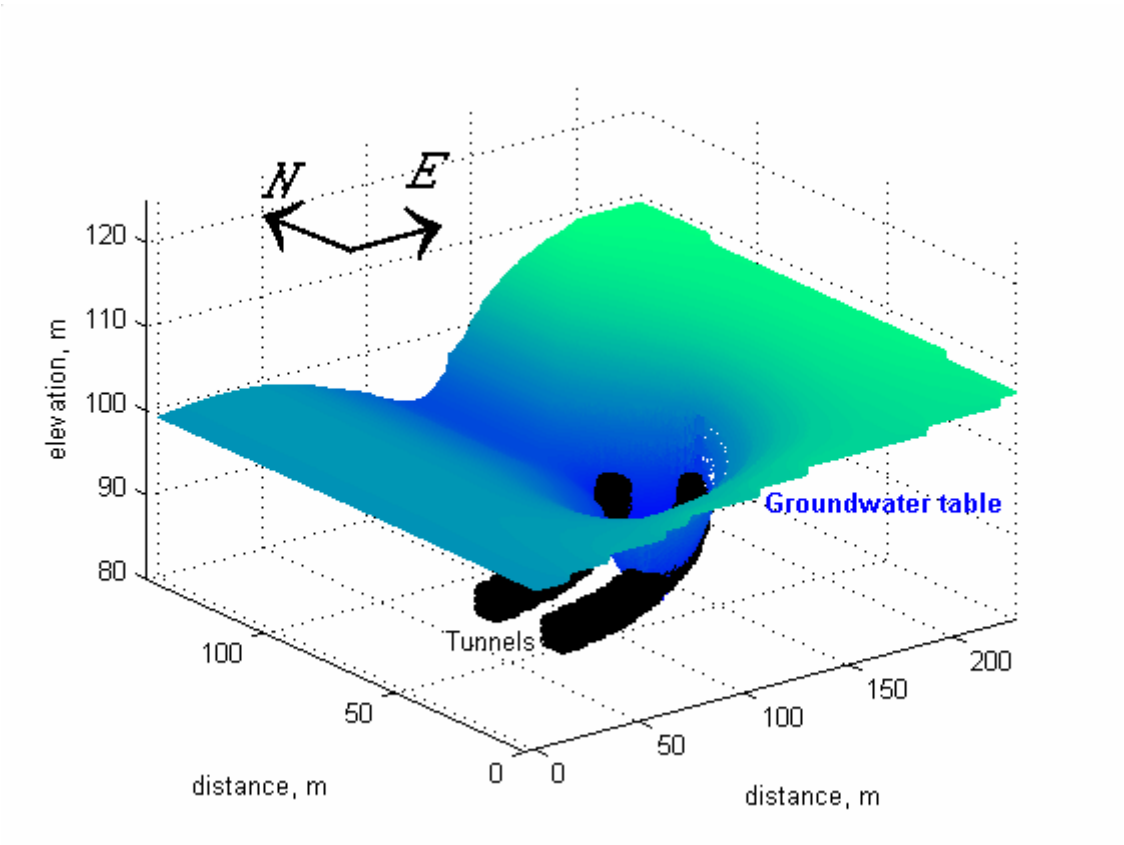

Figure 5.2. Three-dimensional illustration of the water table

The figures from Figure 5.3 through Figure 5.6 display the variation of groundwater levels with time at 4 different locations. For the early period of the simulation, no drawdown is observed at MW1 and DMW2. As tunnels come closer to these points, the groundwater levels at both locations begin to drop rapidly.

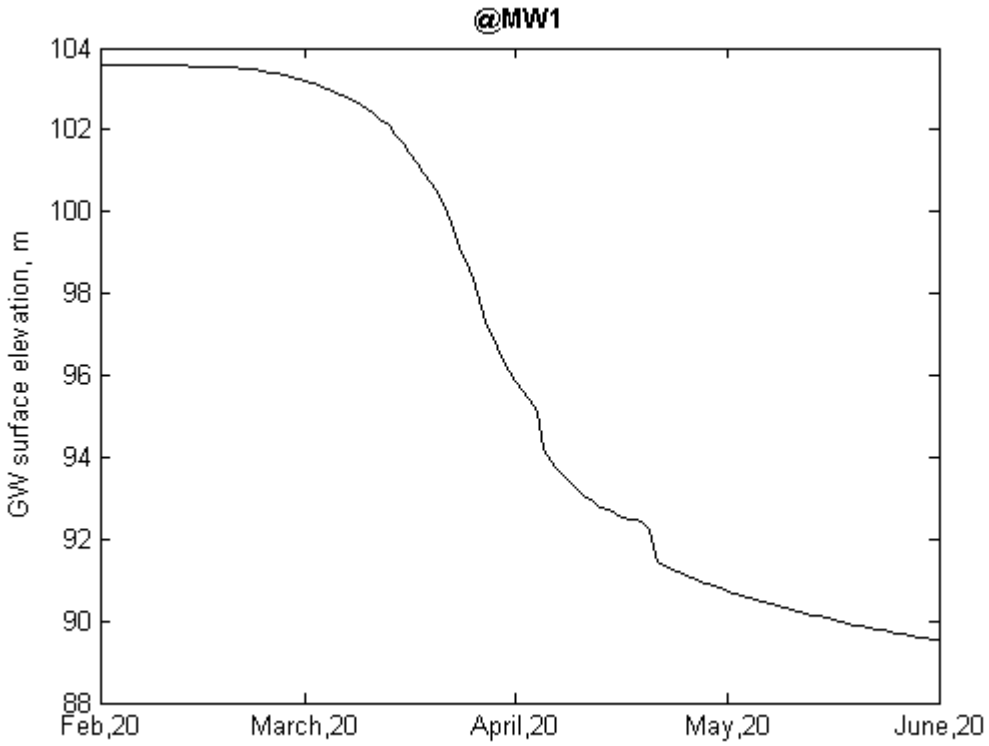

Figure 5.3. The variation of groundwater level with time at MW1

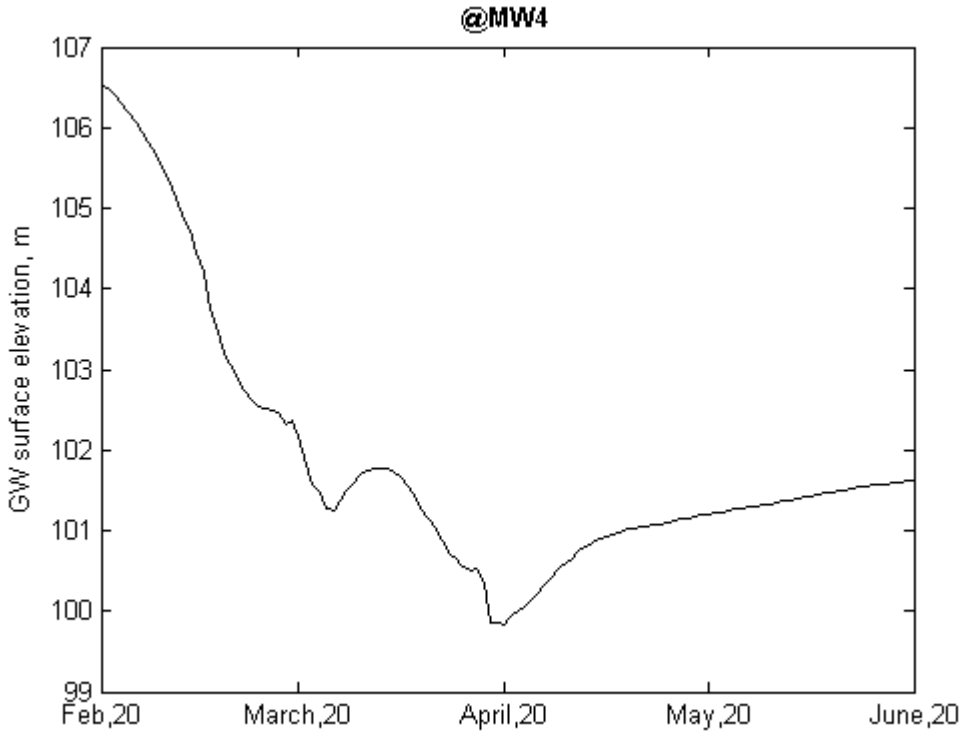

Figure 5.4. The variation of groundwater level with time at MW4

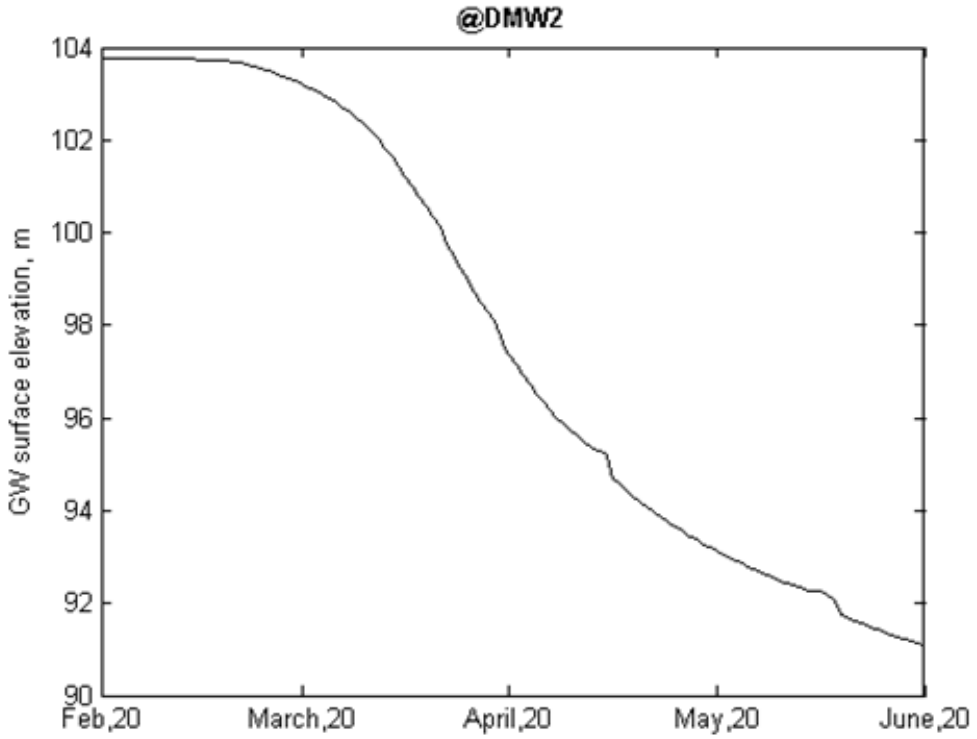

Figure 5.5. The variation of groundwater level with time at DMW2

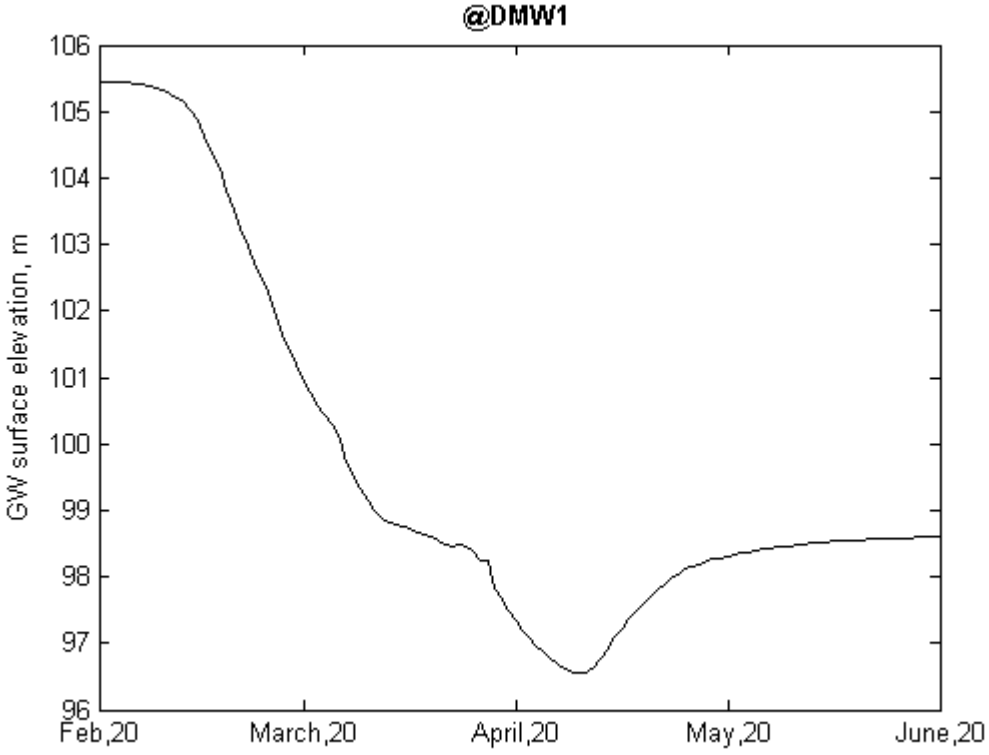

Figure 5.6. The variation of groundwater level with time at DMW1

The comparison between the numerical solution at DMW2 and the site data collected from the 20th of February to the 14thof May is given in Figure 5.7.

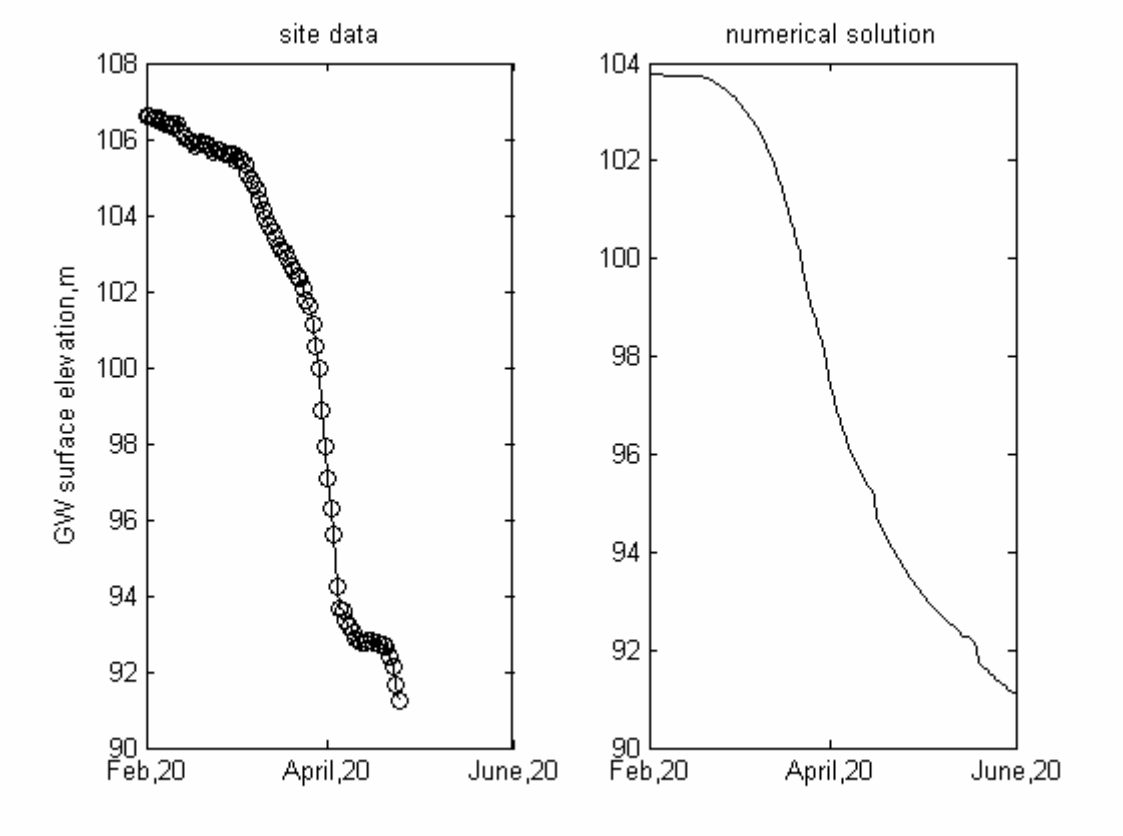

Figure 5.7. The comparison between the numerical solution at DMW2 and the site data

As illustrated in the above figure the drawdown patterns obtained from the numerical simulation and from the site data show similarities. However, in the real case, the tunnel construction processes may lead to the occurrence of some soil fractures, the influence of which is not taken into account for the numerical model, therefore the two drawdown curves do not match exactly. One way to cope with this problem is to utilize time dependent hydraulic conductivity values, but, since it is almost impossible to estimate fracture formation resulting from construction work, how to modify the conductivity values with time is a matter of question.

5.2. Results from Soil Vapor Extraction Simulation

The soil vapor extraction simulation is exercised for calculating the amount of VOCs removed from the soil in 1 month. The time step for the simulation is specified as 600 seconds.

The pressure distribution at 5 m below ground surface at the end of 1 month is illustrated in Figure 5.8.

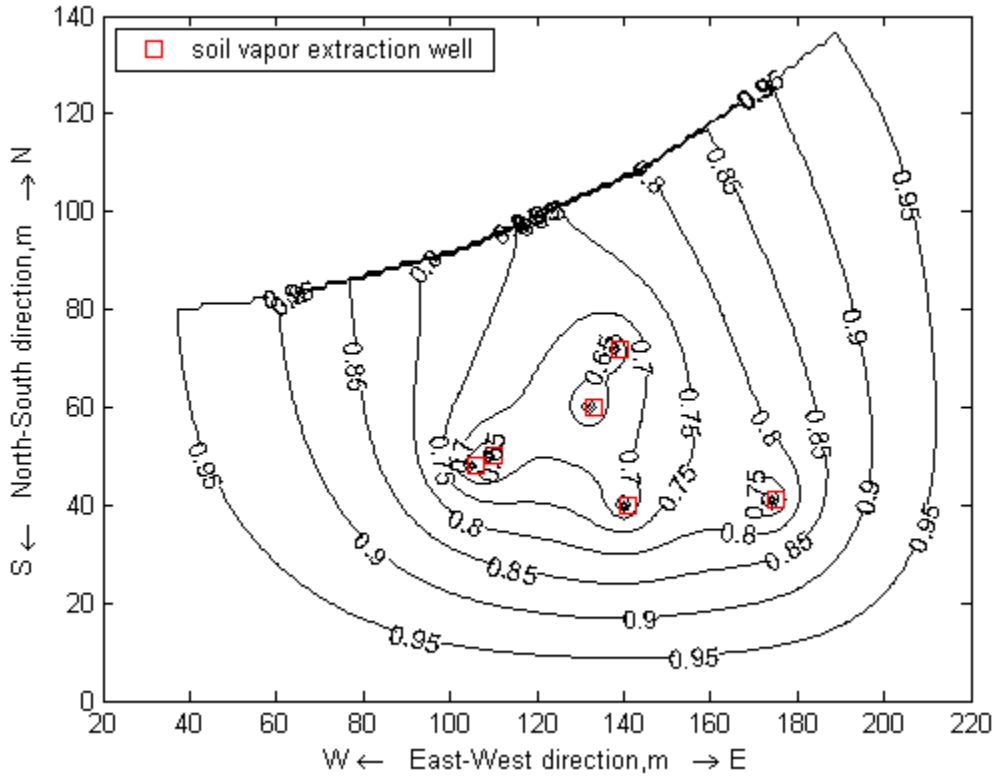

Figure 5.8. The pressure distribution at 5 m below ground surface at the end of 30 days of pumping (atm)

The cumulative mass removal of different volatile organic liquids from the soil with time is displayed from Figure 5.9 through Figure 5.12. The mass values of the residual VOCs before and after the application of soil vapor extraction are tabulated in Table 5.1. As illustrated in Figure 5.13. totally 27.92 kg of residual VOCs is removed from the soil which constitutes 4.5 % of the total mass of VOCs detected before the soil vapor extraction begins.

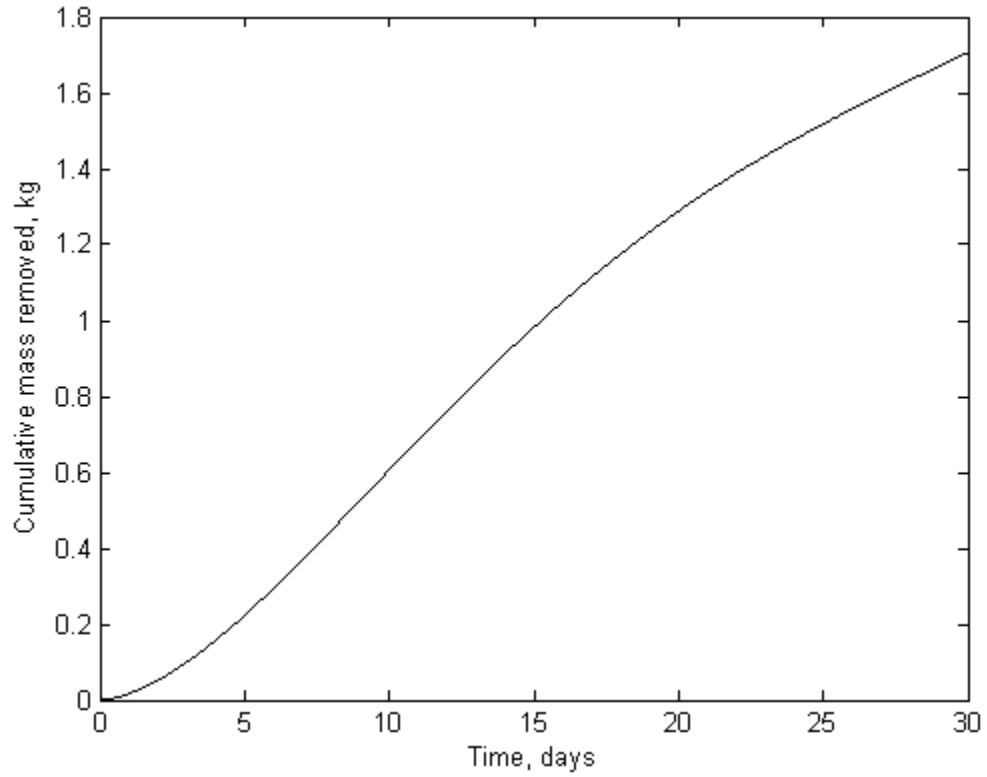

Figure 5.9. The cumulative mass removal of residual benzene

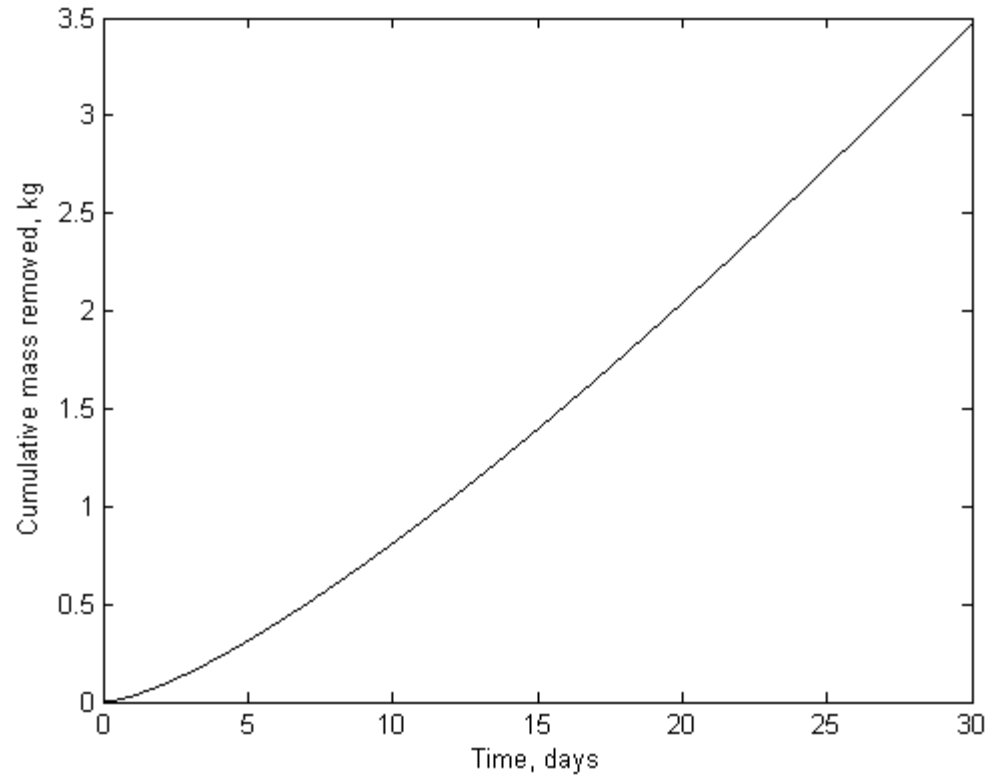

Figure 5.10. The cumulative mass removal of residual toulene

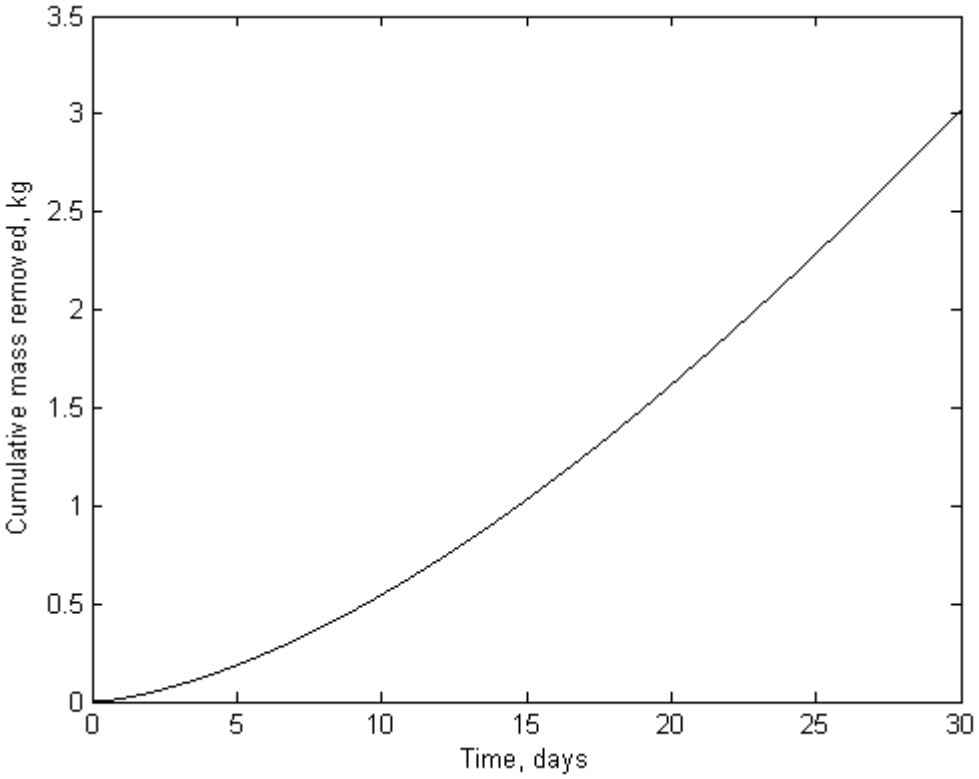

Figure 5.11. The cumulative mass removal of residual ethylbenzene

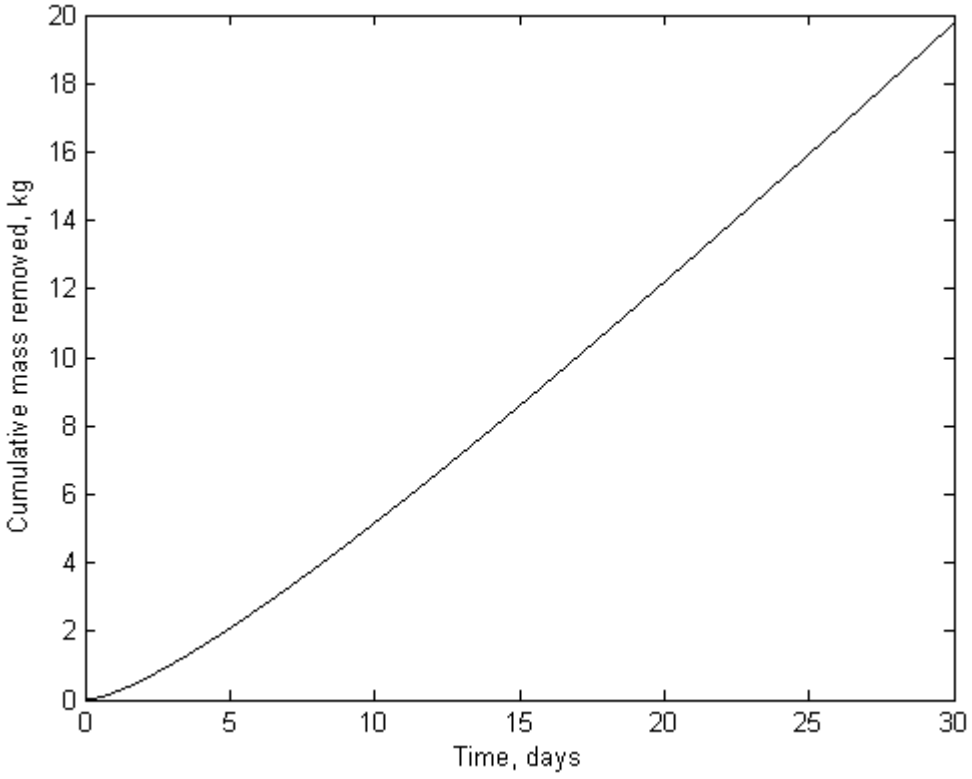

Figure 5.12. The cumulative mass removal of residual xylene

Table 5.1. The mass values of the residual VOCs before and after the application of SVE

	Residual liquid mass before the vapor extraction begins (kg)	Remaining residual mass after 100 days of vapor extraction. (kg)	Removed mass at the end of 100 days (kg)
Benzene	6.59	4.89	1.71
Toulene	76.39	72.92	3.46
Ethylbenzene	97.08	94.07	3.02
Xylene	439.24	419.50	19.73
TOTAL	619.30	591.38	27.92

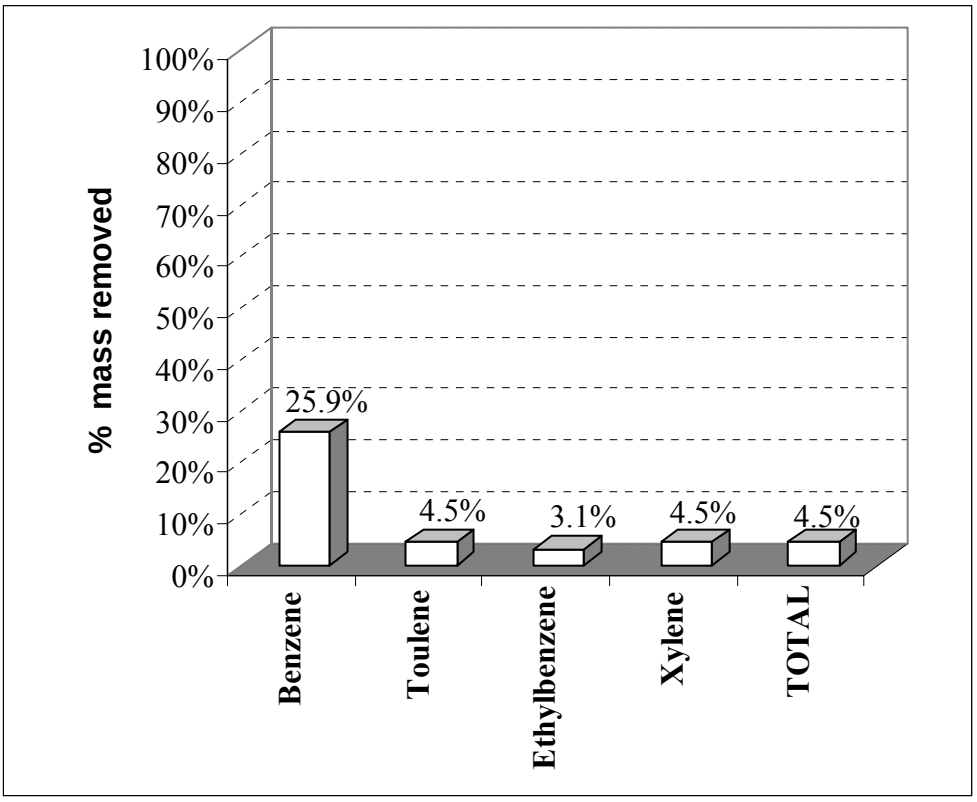

Figure 5.13. The removed percent of each residual organic constituent

The concentration distributions of the organic vapors at the end of the 1 month-long soil vapor extraction are presented in Figure 5.14 through Figure 5.17.

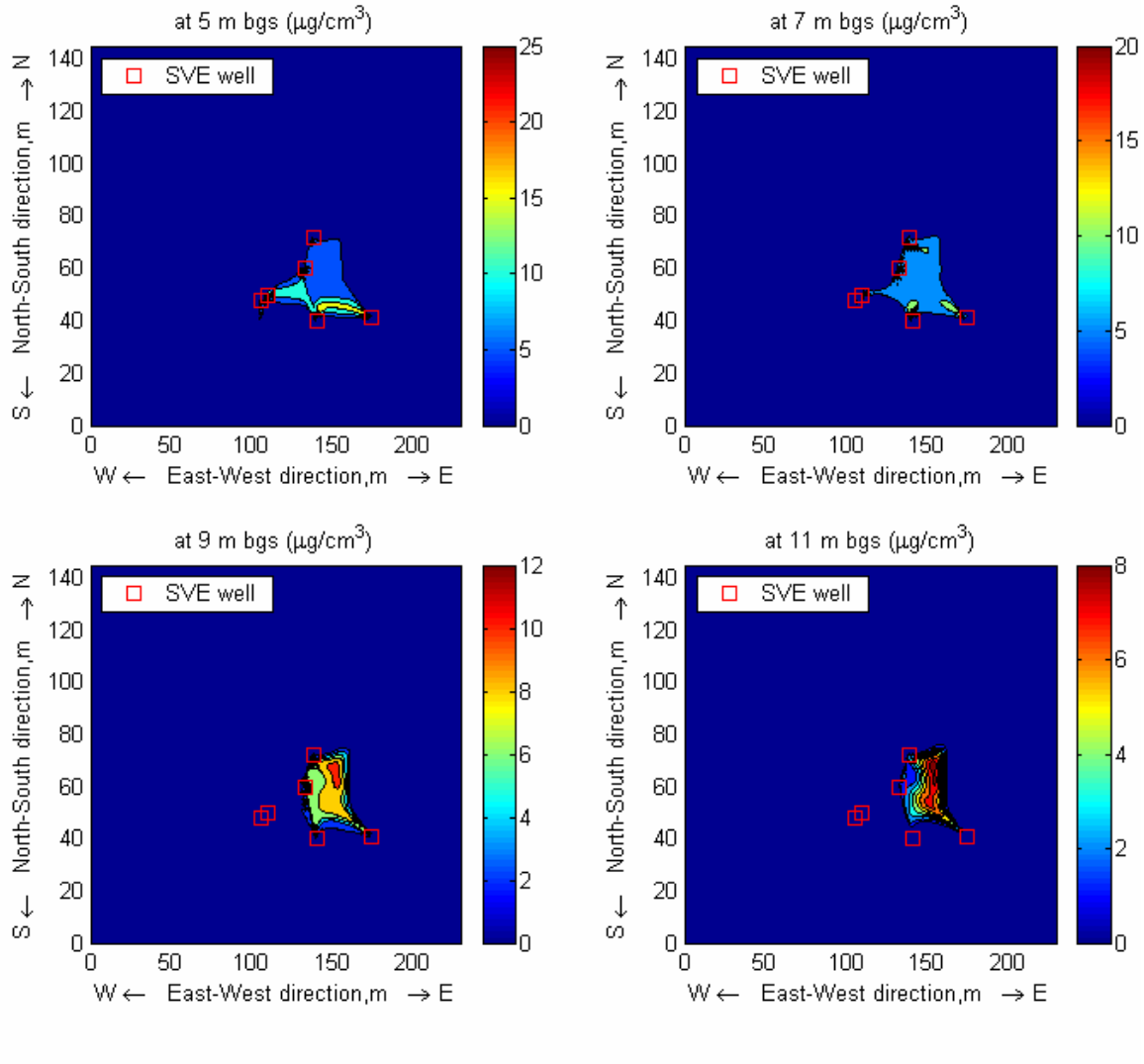

Figure 5.14. Concentration distribution of benzene vapor at different soil depths

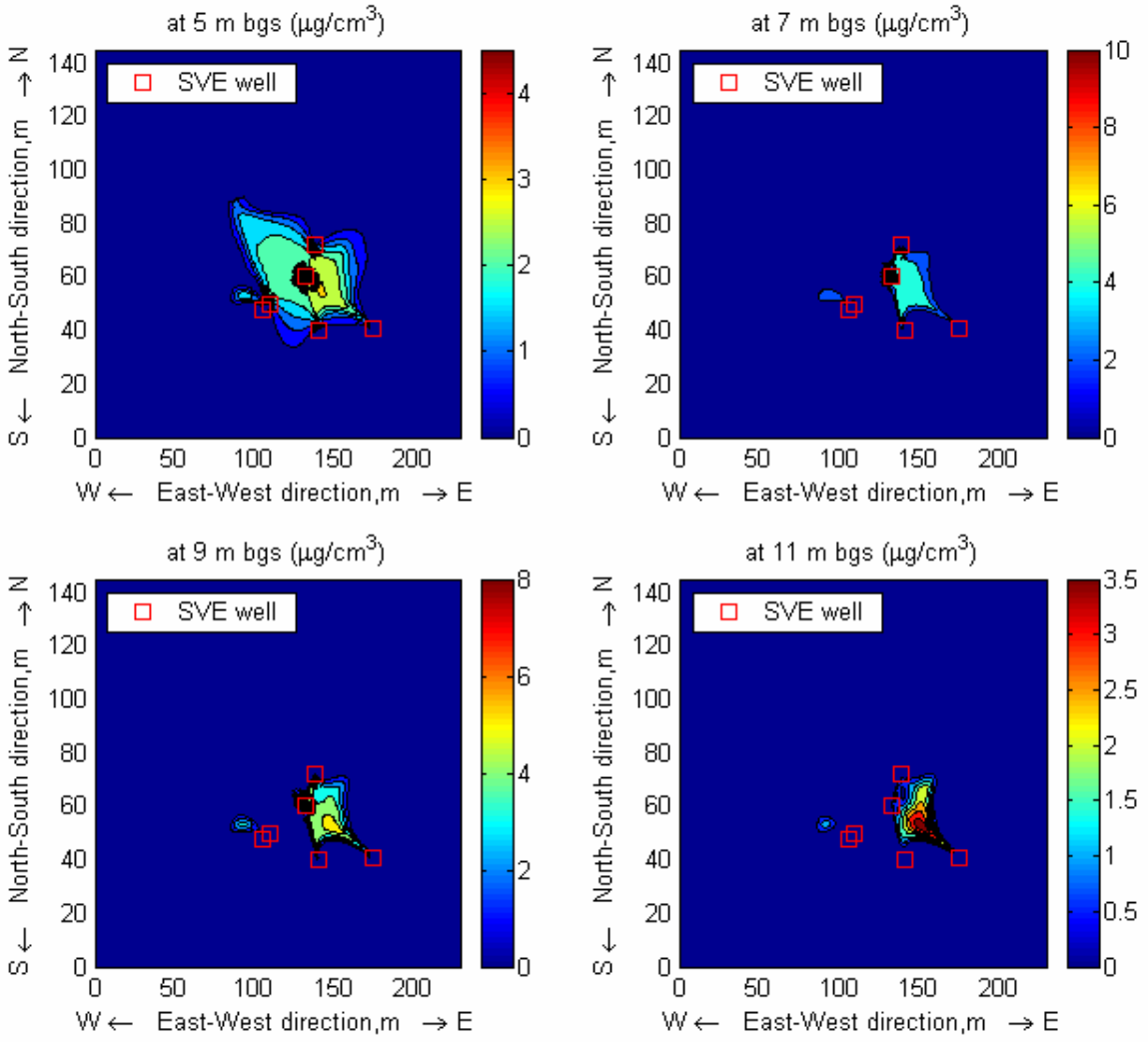

Figure 5.15. Concentration distribution of toulene vapor at different soil depths

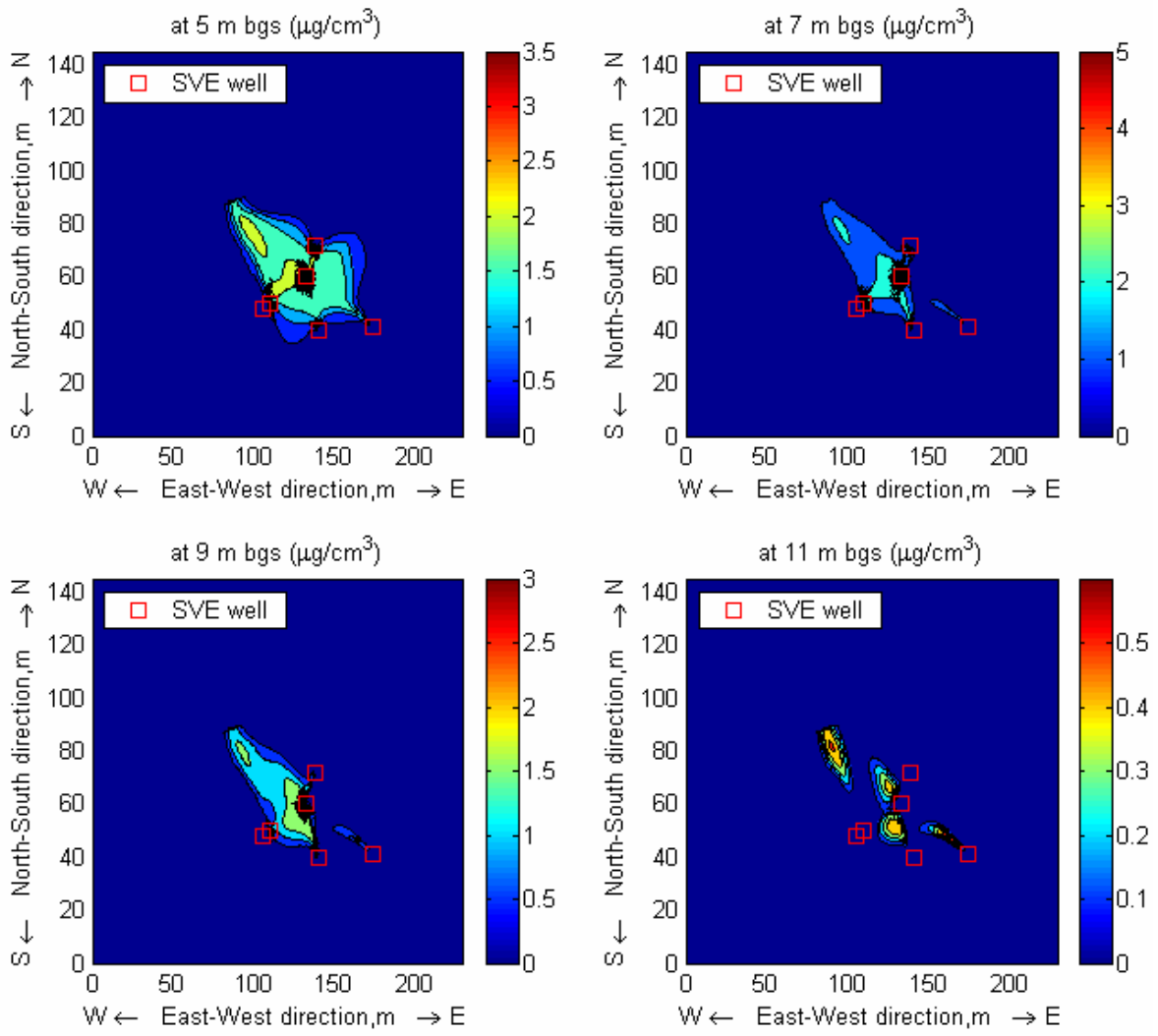

Figure 5.16. Concentration distribution of ethylbenzene vapor at different soil depths

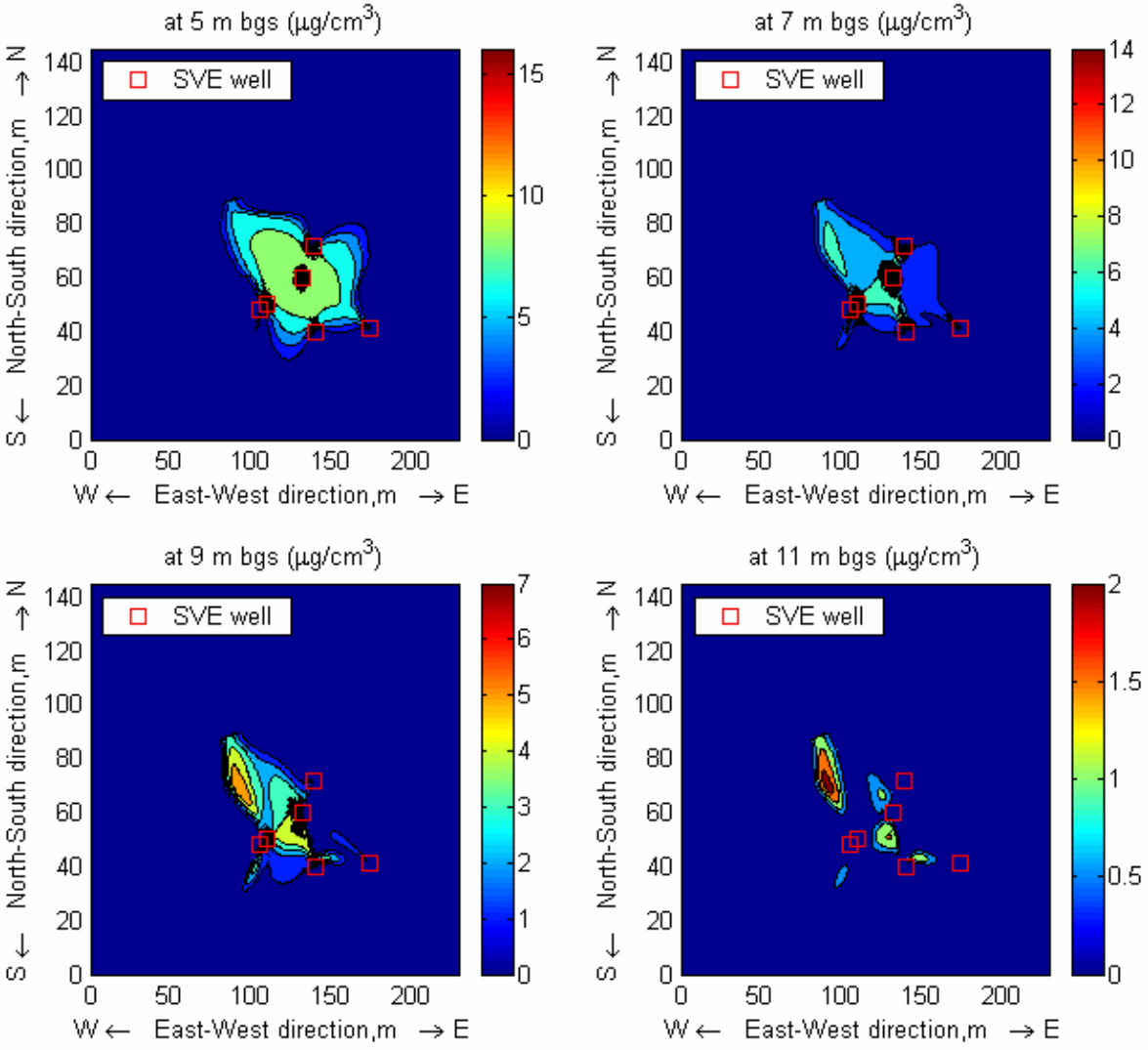

Figure 5.17. Concentration distribution of xylene vapor at different depths

6. CONCLUSIONS

In this study, a soil vapor extraction system was modeled over a domain where the specified boundary conditions change with time due to the ongoing tunnel construction work and the consequent dewatering of the aquifer.

A soil vapor extraction system operates under the influence of many physical and chemical processes, such as volatilization, diffusion or multiphase transport of organic contaminants. In this study the equations which govern these processes were numerically solved by utilizing finite difference techniques.

As demonstrated by the groundwater flow simulation, groundwater table along the metro lines drops to the level of the tunnels, corresponding to a drawdown of approximately 10 meters, at the end of the 4 month-long construction work. The groundwater measurements taken from the site support this finding.

The results acquired from the soil vapor extraction simulation have shown that, approximately 5% of residual organic liquid was removed at the end of an extraction period lasting 1 month. Xylene was found to constitute the largest portion of the organic mass removed from the soil. This finding demonstrates the dependence of mass transfer rate on residual organic content.

Unstable response of the model, particularly when large time steps were used, was the major problem encountered during the simulations. To overcome this problem smaller time steps had to be utilized which, in turn, led to longer simulation durations. Thus the model might imply some limitations in terms of time consideration when a long-lasting vapor extraction process is simulated over a large domain. With the use of more powerful computers this problem can be solved to a certain extent.

Taking the limitations of the model into consideration, some improvements can be implemented for the model through future studies.

The model was developed on the assumption that the groundwater is free of organic contaminants. The model might be further extended to incorporate the presence of contaminants in the groundwater, so that the contaminant mass transfer between the groundwater and the soil air is taken into account.

The residual water content in the unsaturated zone was neglected in this model. The incorporation of this parameter may provide more realistic estimates of permeabilities.

The predictive capability of the model might be improved by incorporating the effect of the temperature on the physco-chemical processes involved in the model.

REFERENCES

Anderson, M. P. and W. W. Woessner, 1992, *Applied Groundwater Modelig*, Academic Press, San Diego.

Baehr, A. L. and C. J. Bruell, 1990, "Application of the Stefan-Maxwell Equations to Determine Limitations of Frick's Law When Modeling Organic Vapor Transport in Sand Columns", *Water Resources Research*, Vol. 26, No. 6, pp. 1155-1163.

Baehr, A. L. and M. F. Hult, 1991, "Evaluation of unsaturated zone air permeability through pneumatic tests", *Water Resources Researc,* Vol. 27, No. 10, pp. 2605-2617.

Baetslé, L. H., 1969, "Migration of Radionuclides in Porous Media", A. M. F. Duhamel (ed), *Progress in Nuclear Energy, Series XII, Health Physics,* pp. 707-730, Pergamon Press, Elmsford, New York.

Bear, J., 1972, *Dynamics of Fluids in Porous Media*, American Elsevier, New York.

Berkowitz, B., J. Bear and C. Braester, 1988, "Continuum Models for Contaminant Transport in Fractured Porous Formations", *Water Resources Research*, Vol. 24, No. 8, pp. 1225-1236.

Boulton, N. S., 1963, "Analysis of Data from Nonequilibrium Pumping Test Allowing for Delayed Yield From Storage", *Proceedings of the. Institute of Civil Engineers*, London, Vol. 26, pp. 469-482.

Brooks, R. H., and A. T. Corey, 1964, *Hydraulic Properties of Porous Media*, Colorado State University, Hydrology Paper No. 3, Fort Collins, CO.

Burnett, R. D. and E. O. Frind, 1987, "An Alternative Direction Galerkin Technique for Simulation of Groundwater Contamination Transport in Three Dimensions, 2 Dimensionality Effects", *Water Resources Research*, Vol. 23, No. 4, pp. 695-705.

Coats, K. H. and B. D. Smith, 1964, "Dead-end pore volume and dispersion in porous media", *Society of Petroleum Engineering Journal*, Vol. 4, No. 3, pp. 73-84.

Darcy, H. P. G., 1856, *Les Fountaines Publiques de la Ville de Dijon*, Victor Dalmont, Paris.

Dragun, J., 1988, *The Soil Chemistry of Hazardous Materials*, Hazardous Materials Control Research Institute, Silver Springs, MD.

Dupuit, J., 1863, *Etudes Théoriques et Pratiques Sur Le Mouvement Des Eaux Dans Les Canaux Découverts et à Travers Les Tterrains Perméables*, Dunod, Paris

Ferris, J. G., D. B. Knowles, R. H. Brown and R. W. Stallman, 1962, *Theory of Aquifer Tests*, Geological Survey Water Supply Paper, 1536-E, United States Government Printing Office, Washington.

Grathwohl, P., 1998, *Diffusion in Natural Porous Media: Contaminant Transport, Sorption/desorption and Dissolution Kinetics*. University of Tübingen, Germany, Kluwer Academic Publishers, Dordrecht, The Netherlands.

Hutzler, N. F., B. E. Murphy and J. S. Gierke, 1989, *State of Technology Review of Soil Vapor Extraction Systems*, USEPA Report 600/2–89/024, USEPA, Washington DC.

Hunt, J. R., N. Sitar, and K. S. Udell, 1988, "Nonaqueous Phase Liquid Transport and Cleanup, 2. Experimental Studies", *Water Resources Research*, Vol. 24, No. 8, pp. 1259-1267.

Istok, J., 1989, *Groundwater Modeling by the Finite Element Method*, American Geophysical Union, Water Resources Monograph 13.

Jacob, C. E., 1950, "Flow of Groundwater", in H. Rouse (ed),. *Engineering Hydraulics*, pp. 321–385, John Wiley, New York.

Joss, C. J. and A. L. Baehr, 1995, *Documentation of AIR3D, an Adaptation of the Ground-Water-Flow Code Modflow to Simulate Three Dimensional Air Flow in the Unsaturated Zone*, U.S. Geological Survey, Open-File Report 94-533, West Trenton, New Jersey.

Jury, W. A., A. M. Winer, W. F. Spencer and D. D. Focht, 1987, "Transport and Transformations of Organic Chemicals in the Organic chemicals in the Soil-Air-Water Ecosystem." *Reviews of Environmental Contamination and Toxicology,* Vol. 99, pp. 119-164.

Karlsrud, K., 2002, "Control of Water Leakage When Tunnelling under Urban Areas in the Oslo Region," *Norwegian Tunnelling Society,* Publication No.12, Oslo.

Kim, Y. Y. and K. K. Lee, 2003, "Disturbance of Groundwater Table by Subway Construction in the Seoul Area, Korea", *Geosciences Journal,* Vol. 7, No. 1, pp. 37-46.

McDonald, M. G., and A. W. Harbaugh, 1988, *A Modular Three-Dimensional Finite-Difference Groundwater Flow Model: Techniques of Water Resource Investigations*, Investigations of the United States Geological Survey, Book 6, Chapter A1.

Marshall, T. J., 1959, "The Diffusion of Gases Through Porous Media", *Journal of Soil Science*, Vol. 10, pp. 79–82.

Millington, R. J. and J. P. Quirk, 1961, "Permeability of. Porous Solids", *Transactions of the Faraday Society*, Vol. 57, pp. 1200-1207.

Moench A. F., 1996. "Flow to a Well in a Water-Table Aquifer: An Improved Laplace Transform Solution", *Ground Water*, Vol. 34, No. 4, pp. 593–596.

Moldrup, P., T. Olesen, D. E. Rolston and T. Yamaguchi, 1997, "Modeling Diffusion and Reaction in Soil: VII. Predicting Gas and Ion Diffusivity in Undisturbed and Sieved Soil", *Soil Science,* Vol. 162, No. 9, pp. 632–640

Neuman, S. P., 1975. "Analysis of Pumping Test Data from Anisotropic Unconfined Aquifers Considering Delayed Gravity Response", *Water Resources Research,* Vol. 11, No. 2, pp. 329-342.

Penman, H. L., 1940, “Gas and Vapor Movement in the Soil: I. The Diffusion of Vapors through Porous Solids”, *Journal of Agricultural Science*, Vol. 30, pp. 570–581.

Prickett, T. A., 1965, “Type-Curve Solution to Aquifer Tests Under Water-table Conditions”, *Ground Water*, Vol. 3, No. 3, pp. 5-14.

Rathfelder, K., J.R. Lang, and L.M. Abriola. 1995. “Soil Vapor Extraction and Bioventing: Applications,. Limitations, and Future Research Directions”, *Reviews of Geophysics*, Vol. 33, pp. 1067-1082.

Reid, R. C., J. M. Prausnitz and B. E. Poling, 1987, *The Properties of Gases and Liquids*, 4th ed., McGraw-Hill, New York.

Rhodes, D. Jr., G. K. Burke, N. Smith, and D. Clark, 1995, “In-situ Diesel Fuel Bioremediation: A Case History”, R. E. Hinchee, R. N. Miller and P. C. Johnson (eds), *In-situ Aeration: Air sparging, Bioventing, and Related Remediation Processes*, pp. 441-446, Battelle Press, Columbus, Ohio.

Schwartz, F. W., and H. Zhang, 2002, *Fundamentals of Ground Water*, Wiley Publishers, Alameda, California.

Theis, C. V., 1935, “The Relation Between the Lowering of the Piezometric Surface and the Rate and Duration of Discharge of a Well Using Ground-Water Storage”, *American Geophysical Union Transcript*, Vol. 2, No.16, pp. 519-524.

Weast, R. C. (editor), 1981, *Handbook* of *Chemistry and Physics,* 62nd ed., CRC Press, Cleveland.

Zaman, M. R., 1993, *Subsurface Remediation by Vacuum Extraction for Volatile Organic Chemicals: A Finite Element Model,* Ph.D. Dissertation, Department of Civil Engineering, Texas Tech University, Lubbock, Texas.